THE UNIVERSITY *of* EDINBURGH

This thesis has been submitted in fulfilment of the requirements for a postgraduate degree (e.g. PhD, MPhil, DClinPsychol) at the University of Edinburgh. Please note the following terms and conditions of use:

- This work is protected by copyright and other intellectual property rights, which are retained by the thesis author, unless otherwise stated.
- A copy can be downloaded for personal non-commercial research or study, without prior permission or charge.
- This thesis cannot be reproduced or quoted extensively from without first obtaining permission in writing from the author.
- The content must not be changed in any way or sold commercially in any format or medium without the formal permission of the author.
- When referring to this work, full bibliographic details including the author, title, awarding institution and date of the thesis must be given.

Development and application of a thermal analysis framework in OpenSees for structures in fire

YAQIANG JIANG

Doctor of Philosophy

The University of Edinburgh

2012

Declaration

This thesis and the research described and reported within has been completed solely by Yaqiang Jiang under the supervision of Professor Asif Usmani and Dr. Stephen Welch. Where other sources are quoted, full references are given. This work has not been submitted for any other degree or professional qualification.

Yaqiang Jiang

December 2012

Abstract

The last two decades have witnessed the shift of structural fire design from prescriptive approaches to performance-based approaches in order to build more advanced structures while reducing costs. However, it is recognised that the implementation of performance-based approaches requires several key elements that are currently not fully developed or understood. This research set out to address some of these issues by focusing on the development, validation and application of methodologies for accurate predictions of thermal responses of structures in fire using numerical methods.

This research firstly proposed a numerical approach with the finite element and the discrete ordinates method to quantify the fire imposed radiative heat fluxes to structural members with cavity geometry. With satisfactory results from the verification and validation tests, it is used to simulate heat transfer to unprotected steel I-sections with symmetrical cavities exposed to post-flashover fires. Results show that the cavity geometry could strongly attenuate the radiative energy, while the presence of hot smoke enhances radiative transfer by emission. Average radiative fluxes for the inner surfaces of the I-sections are seen to increase with smoke opacity. In addition, the net radiative fluxes are observed to decrease faster

for I-sections with higher section factors. This work also shows that the self-radiating mechanism of I-sections is important in the optically thin region, and existing methodologies neglecting these physics could significantly underpredict steel temperatures.

The next focus of this work is to develop a thermal analysis framework dedicated to structures-in-fire modelling in the OpenSees (Open System for Earthquake Engineering Simulation) platform which has been developed towards a highly robust, extensible and flexible numerical analysis framework for the structural fire engineering community. The thermal analysis framework, which is developed with object-oriented programming paradigm, consists of a fire module which has incorporated a range of conventional empirical models as well as the travelling fire model recently developed elsewhere to quantify the fire imposed boundary conditions, and a heat transfer module which addresses non-linear heat conduction in structural members with the finite element method. The developed work has demonstrated good performance from benchmark problems where analytical solutions are available and from full scale tests with measured data.

With the thermal analysis capability developed in this work together with the work by other colleagues to quantify the mechanical response at elevated temperatures, the extended OpenSees framework can be used to predict structural performances subjected to a wide range of fire scenarios. This work uses OpenSees for a case study of a generic composite structure subjected to travelling fires. The latest work on traveling fire methodology for structural fire design has been implemented in the OpenSees framework. The work presented in this thesis is the first effort to examine both the thermal and structural responses of a composite tall building in travelling fires using OpenSess. Results from the thermal analysis

show that traveling fires of larger sizes (e.g. burning area equal to 50% of the floor area) are more detrimental to steel beams in terms of more rapid heating rate, while those of smaller sizes (e.g. burning area equal to 4% of the floor area) burn for longer duration and thus are more detrimental to concrete slabs in light of higher peak temperatures. The results also show that fires of large sizes tends to produce higher through-depth thermal gradients in the steel beam sections particularly in neighbouring regions with the concrete slab. Due to less rapid heating rates but prolonged burning durations, smaller fires produce lower thermal gradients but with higher temperatures in the concrete slab particularly at locations far from the fire origin. The subsequent structural analysis suggests that travelling fires produce higher deflections and higher plastic deformations in comparison with the uniform parametric fires, particularly with smaller fire sizes producing more onerous results. The results seem to be more physically convincing and they challenge the conventional assumption that the post-flashover fires are always more conservative for structural performance.

Publications

Journal papers

Yaqiang Jiang, Guillermo Rein, Stephen Welch, Asif Usmani. Modeling fire-induced radiative heat transfer in smoke-filled structural cavities, International Journal of Thermal Sciences (2012).

Yaqiang Jiang, Panagiotis Kotsovinos, Asif Usmani, Guillermo Rein, Jamie Stern-Gottfried. Numerical investigation of thermal responses of a composite structure in horizontally travelling fires using OpenSees, Procedia Engineering (in press).
Note: The above paper was also presented at The 9th Asia-Oceania Symposium on Fire Science and Technology, Hefei, China, 2012

Panagiotis Kotsovinos, **Yaqiang Jiang**, Asif Usmani. Effect of vertically travelling fires on the collapse of tall buildings, International Journal of High-Rise Building (invited submission).

A. Usmani, J. Zhang, J. Jiang, **Y. Jiang**, I. May. Using OpenSees for structures in fire, Journal of Structural Fire Engineering, 2012, 3(1):57-70.

Conference papers

Asif Usmani, **Yaqiang Jiang**, *et al.* Adapting OpenSees to simulate bridge structures in fire, in Proceedings of the 6th International Conference on Bridge Maintenance, Safety and Management, 2012, pp. 315-319.

Yaqiang Jiang, Asif Usmani, Stephen Welch. Development of heat transfer modelling capability in OpenSees for structures in fire, in Proceedings of Application of Structural Fire Design, 2011, pp. 324-330.

Acknowledgements

I wish to express my sincere gratitude to my supervisors Professor Asif Usmani and Dr. Stephen Welch for their expert guidance, support and encouragement over the last three years. I would also like to thank Dr. Guillermo Rein for providing insightful comments and valuable suggestions. I want to thank my colleague and friend, Panagiotis Kotsovinos, for the enjoyable discussions and collaborations. I would also like to express my appreciation to other colleagues, Praveen Kamath (from IIT Roorkee), Dominic Ahiaga-Dagbui, Jian Zhang, Liming Jiang, Mariyana Ab-Kadir and Payam Khazaeinejad and many others from the Fire Group who helped me at different stages of my PhD work.

Additional thanks go to Dr. Frank McKenna from UC Berkeley for the help of code implementations in OpenSees.

This research is jointly funded by the China Scholarship Council and The University of Edinburgh and is gratefully acknowledged.

Finally, I must thank my family for their understanding and unreserved support. I am extremely grateful to my wife Wurong who was always willing to listen and offered me tremendous support throughout this work.

Contents

List of Tables

List of Figures

Chapter 1

Introduction

1.1 Background

A major concern of structural fire safety engineering is to prevent the catastrophic collapse of buildings due to fires. The principal aim of structural design for fire safety is to ensure structural stability to allow safe evacuation and safe intervention by first responders. Traditional prescriptive design approaches are based on fire resistance testing, where the resulting fire resistance rating is expressed as the time that the structural member is able to withstand exposure to the standard fire before reaching a specified failure criteria (e.g. 550 ℃). This has led to extensive use of passive fire protection to limit the heating of structural members and it is accepted that the current prescriptive approaches of structural fire design are overly conservative and not based on rational principles [1]. Furthermore, the seemingly conservative design approaches do not necessarily ensure even adequate levels of safety, as shown by the collapse of the WTC towers

on 11 September 2001. Unlike the Twin Towers which had sustained considerable structural damage, the WTC 7 with insignificant structural damage also collapsed which was the first recorded instance of such a structure failed entirely by fire [2].

The collapse of WTC towers provided an impetus for structural fire engineering research and development in many research organisations worldwide. As a result, there is an increasing international consensus that structural fire safety should be achieved by following performance-based design approaches, which require a deeper understanding of the fire conditions, heat transfer to structure, and whole frame structural behaviour. However, it is recognised that the implementation of performance-based approaches requires several key elements that are currently not fully developed or understood [3, 4]. These include improved methodologies to predict fire imposed boundary conditions to structural members with complicated geometry, and more realistic representation of fire development in large spaces and understanding of the thermal and structural responses of structures under these more realistic situations. Furthermore, there is also a need of advanced numerical analysis framework for modelling "structures in fire" in order to incorporate the rapid advancements in this field. For instance, the recently developed methodology on travelling fires [5, 6] represents a paradigm shift of structural design for fire safety in large spaces but such a methodology imposes spatially and temporally varying boundary conditions for the subsequent heat transfer modelling thus it clearly requires greater effort on the thermal analysis than the usual assumption of uniform post-flashover fires. It is believed that with further advancement of design fires as well as innovative construction materials used in the future, performing an integrated thermal and structural analysis will become more challenging and it naturally requires a more flexible and extensible modelling

framework which benefits the whole structural fire research community and also allows contributions from the community to further improve the framework itself.

1.2 Objectives and originality

This project sets out to address some of the issues discussed in the foregoing section with particular focus on the thermal input to structural members for modelling "structures in fire". The objectives of this research are as follows:

- Propose a general methodology to determine fire imposed radiative heat flux to structural members with cavity geometry.
- Develop and validate a general, flexible and extensible thermal analysis framework for "structures in fire" modelling.
- Investigate the effects of travelling fires on the thermal and structural responses of a composite structure using the developed framework.

1.3 Layout of thesis

Chapter 2 includes a literature review of fire and heat transfer modelling within the scope of structural fire engineering. A review of research in methodologies for evaluating fire imposed boundary conditions is also presented. Finite element formulation and the solution algorithms for the heat conduction equation which are used in subsequent chapters is derived.

Chapter 3 presents a general methodology to predict fire imposed radiative heat fluxes in structural cavities. Finite element method and discrete ordinates method are used to solve the coupled conduction and radiation heat transfer. Effect of cavity geometry and participating medium on radaitive heat transfer to steel I-setions exposed to post-flashover fires are investigated. A comparative analysis is presented for the temperature development in the steel members using the proposed methodology and the conventional one-way calculation methodology.

Chapter 4 presents the work of developing an object-oriented thermal analysis software framework. This is done by adding fire and heat transfer modules in an existing structural analysis platform, Open System for Earthquake Engineering Simulation (OpenSees). The fire module incorporates some of the fire models discussed in Chapter 2 in order to determine the fire imposed thermal environment. The heat transfer module is based on the finite element method for accurate resolution of the temperature distribution in structural members. The software architecture and interaction mechanisms between different modules are discussed. A number of verification and validation tests are carried out to examine the performance of the developed work. Along with other fire models, the methodology developed in Chapter 3 can also be included into this framework as a method for accurate prediction of fire imposed heat fluxes to structural members with complicated geometry and located in a radiation dominated environment. The work of modifying the structural module of OpenSees to include the thermal effect in structural analysis is addressed by other colleagues [7] and is not presented in this thesis.

Chapter 5 presents an application of the extended OpenSees framework to examine the thermal and structural behaviour of a generic composite tall building

subjected to horizontally travelling fires. This is a collaborative research effort with structural engineers to study both the thermal and structural responses using the newly developed capabilities in OpenSees.

Chapter 6 is a summary of the work undertaken and the outcomes from this project. Recommendations for future work are also highlighted in this chapter.

Chapter 2

Thermal analysis of structures in fire

2.1 Introduction

Thermal analysis, which covers the processes of selecting appropriate design fires and predicting temperature rise in structures based on fundamental heat transfer principles, is essential to quantify the structural behaviour in fire from a performance-based design point of view. This chapter presents a review of research in thermal analysis relevant to the field of structural fire engineering. The complexities in heat transfer modelling as well as available modelling approaches are discussed. A review is also presented of a range of fire models used to determine fire imposed boundary conditions.

2.2 Heat transfer in structural members

Heat transfer in structures is governed by the following second order diffusion equation

$$\rho c_p \frac{\partial T}{\partial t} = \nabla \cdot (k \nabla T) \tag{2.1}$$

where ρ is the density of the structural member, c_p is the specific heat capacity, and k is the thermal conductivity. The solution of this transient heat conduction equation requires the specification of initial condition and boundary conditions, which are given as

Initial condition

$$T(t_0) = T_0 \qquad \text{in} \quad \Omega \tag{2.2}$$

Dirichlet boundary condition

$$T(t) = T_b \qquad \text{on} \quad \Gamma_T \tag{2.3}$$

Neumann boundary condition

$$-\mathbf{k}\nabla T = \overline{q} \qquad \text{on} \quad \Gamma_q \tag{2.4}$$

$$\Gamma_T \cup \Gamma_q = \Gamma$$

$$\Gamma_T \cap \Gamma_q = \emptyset$$

where $\overline{q} = q_c + q_r + q_{pr}$, q_c is the convective heat flux, q_r is the radiation boundary flux, and q_{pr} is the prescribed flux at boundaries. Accurate prescription of fire

imposed heat fluxes is not trivial and it is still under active research within the structural fire community as will be discussed in Section 2.5. Note that Eqs. (2.1)-(2.4) are given for heat transfer in solids that are opaque, e.g. concrete and steel. For translucent solids such as glass, an extra source term accounting for divergence of the radiative heat flux, due to absorption and emission of thermal radiation by glass, should be included on the right hand side of Eq. (2.1) in order to predict glazing breakage [8, 9]. However, this mechanism is not considered here as the current work focuses on heat transfer in opaque structural materials.

For most construction materials, such as steel and concrete, their thermal properties (mainly k and c_p for heat transfer) normally demonstrate strong temperature dependence. As concrete consists of several other materials, e.g. cement paste, aggregates and moisture, information on each individual constituent as well as the mass fractions are needed to evaluate the thermal properties of the mixture [10]. However, a lot of complexity would be involved in the estimation of thermal properties for each single constituent [10]. Instead, empirical models, such as those given in Eurocode [11] and ASCE manual [12], are normally used in practice. Figure 2.1 shows the variations of thermal properties of normal weight concrete with temperatures as given in [11, 12]. As shown in Figure 2.1(a), the thermal conductivity given by both models tends to decrease with increasing temperature. In fact, the value and change of thermal conductivity also depends on the degree of crystallinity of the aggregate. Higher thermal conductivity is expected for higher degree of crystallinity [12]. Figure 2.1(b) shows the variations of specific heat with temperatures, where there are some clear differences between the EC 2 and ASCE models. The EC 2 model presents sharp spikes around 100 ℃ for concrete with moisture, which is attributed to the phase change of moisture content in that temperature region. In contrast, the ASCE model presents a peak

value around 500 ℃ and this is believed to be caused by the thermal properties of cement paste at about 500 ℃ [10, 12].

Thermal properties of carbon steel at elevated temperatures are shown in Figure 2.2. The change of thermal conductivity of carbon steel is similar to that of concrete, i.e. tending to decrease with increasing temperatures but reaching a constant value when the temperatures are above 800 ℃. The values given be the EC 3 model [13] and the ASCE model [12] are relative close, which are also found to agree well with measured values [14]. The thermal conductivity is high compared with that of concrete, and this fact has lead to a common assumption that heat conduction is rapid in steel and the temperature distribution is uniform across a steel section [12, 13]. As shown in Figure 2.2(b), the specific heat of steel gradually increases with temperature but reaches a peak value around 750 ℃. The spike of specific heat within such a narrow temperature range is due to the phase change of steel where the atoms transition from a face centered cubic to a body centered cubic structure [14]. Although the EC 3 model presents a much higher peak value than the ASCE model, only minor variations are found between the predicted temperatures using the two models [14].

As seen in Figure 2.1(b) and 2.2(b), the specific heat of some materials may undergo severe changes within a rather narrow temperature band. This could lead to potential difficulties for numerical solutions when a temperature increment is too large. To remedy this problem, the so called *apparent heat capacity method* [15] or *enthalpy method* [16] may be used in the numerical solution procedures

$$C^A = \left(\frac{\nabla H \nabla H}{\nabla T \nabla T} \right)^{0.5} \tag{2.5}$$

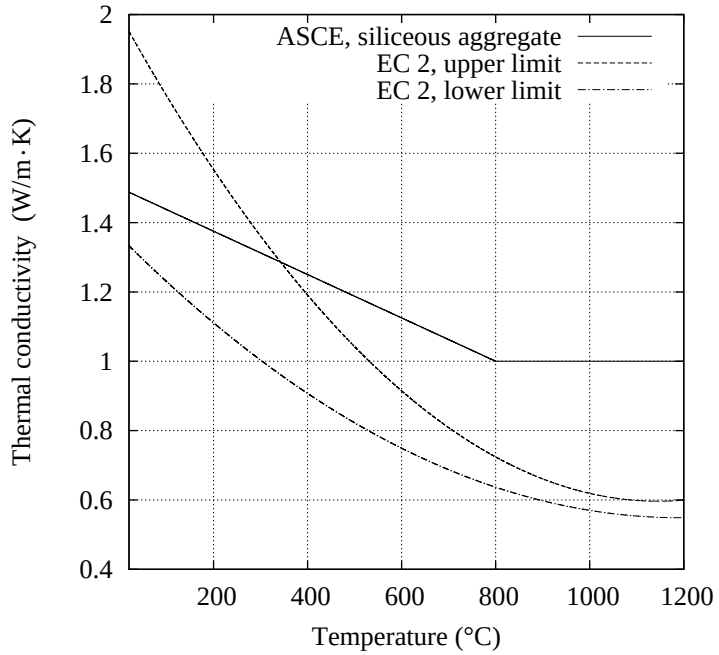

(a) Thermal conductivity

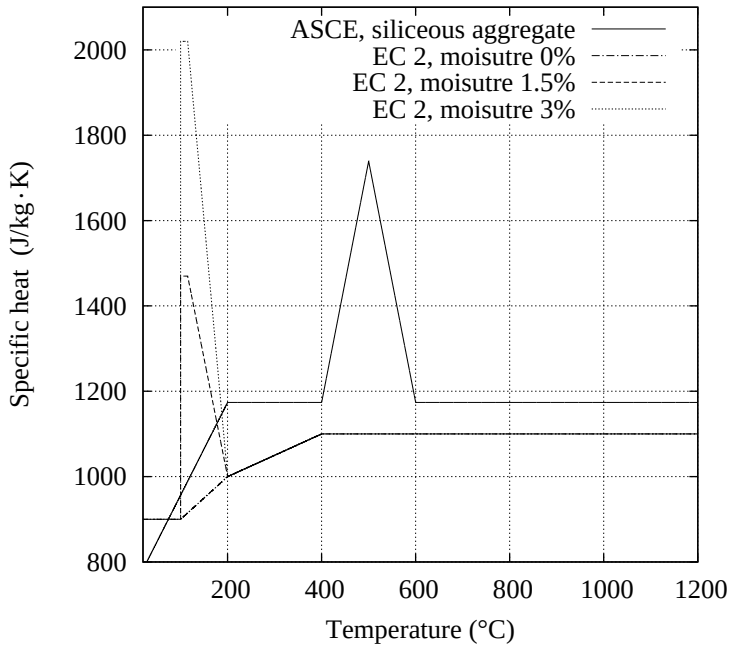

(b) Specific heat

Figure 2.1: Thermal properties of normal weight concrete at elevated temperatures

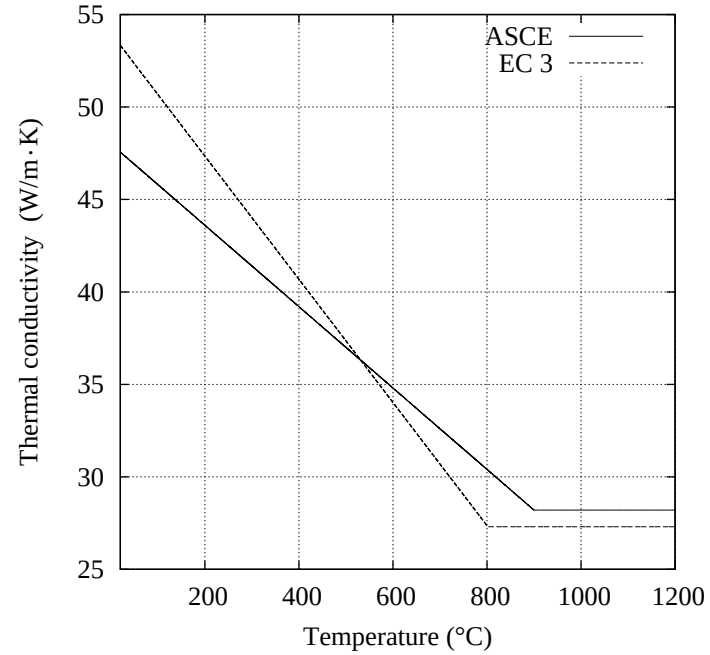

(a) Thermal conductivity

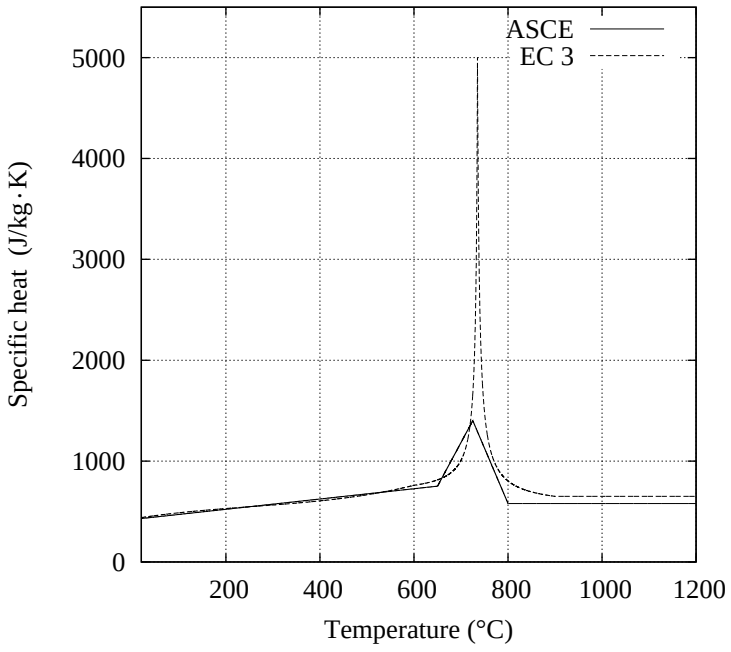

(b) Specific heat

Figure 2.2: Thermal properties of carbon steel at elevated temperatures

where the enthalpy within a temperature range is given as $H = \int_{T_r}^{T} \rho c_p dT$, T_r is a reference temperature lower than T.

The above method is a space averaging technique originally proposed by Lemmon [17], and it is widely used to address phase change problems. This approach enables the heat capacity to be defined as a smooth function of temperature and the numerical difficulties presented by the original heat capacity are bypassed. A detailed discussion of numerical methods to treat phase change problems and their implementations in finite element code can be found in [16]. Figure 2.3 shows the subsequent enthalpy of carbon steel obtained by integrating the heat capacity as shown in Figure 2.2(b) (taking $\rho = 7850$ kg/m^3 and $T_r = 20$ ℃). Generally speaking, use of numerical approximations akin to Eq. (2.5) will lead to efficient and accurate solutions [15], and this will be sufficient for most situations concerning heat transfer in structures.

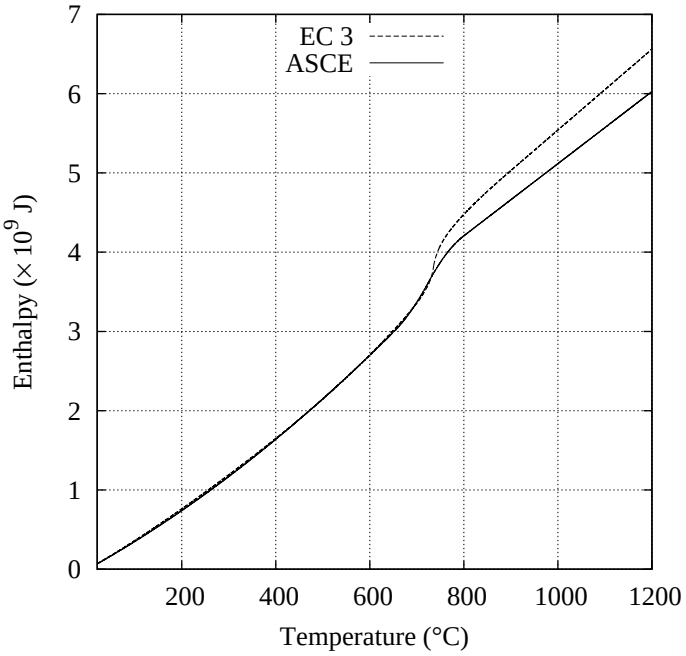

Figure 2.3: Enthalpy of carbon steel at elevated temperatures

2.3 Heat transfer modelling approaches

Heat transfer modelling is an essential component of analysing fire resistance because the load capacity or the containment capability of a fire-exposed element or structure depends on its temperature history [18]. The temperature distribution from the heat transfer modelling is essential input to a subsequent structural model for calculating load-bearing capacity.

The first thing one need to consider for heat transfer calculation are the material properties of a structural member. For thermally thin members (e.g. steel sections [19]), a simplified approach with lumped heat capacity method may be used for temperature predictions [20, 18]. However, the limitations of this approach are obvious as it is unable to naturally address heat transfer in structural members in the most general fashion, e.g. different correction procedures have to be applied when considering heat conduction in multi-directions [21]. For a more accurate thermal analysis, Eq. (2.1) should be solved with numerical methods such as the finite element method which is perhaps the most widely used numerical method within structural fire engineering. A good review of the strengths and limitations for a range of commercial and specialist FE packages is presented in [22]. Fire protection materials such as intumescent coatings bring more complexities in the heat transfer modelling due to the geometric expansion and chemical degradation of the materials [23]. It is not practical to model this process directly from structural fire engineering point view, but a lumped effective thermal conductivity may be incorporated into a general heat transfer model [24, 21, 25].

The other complexity involved in heat transfer modelling is to determine the fire imposed boundary conditions. This is affected by the fire models used in order

to establish the thermal field of the gas phase which will be discussed in detail in Section 2.5. The geometry of the structural member itself can also require greatly increased effort for an accurate imposition of boundary conditions (for radiation in particular). For example, radiative heat transfer from surrounding fire environment to an unprotected steel I-section is a complicated issue due to the presence of two open cavities formed in this geometry, where the inner surfaces of the I-section receive less intensive radiative heating due to the *shadow effect* [26] or *geometric effect* [27]. This has drawn many researchers' attention but most of the work provides very approximate solutions such as using a lumped shadow factor to reduce the overall radiative heat fluxes for the whole section boundaries or assume a uniform temperature for the whole steel section using the lumped heat capacity method [26, 28, 29, 27]. A recent work proposed by Jiang *et al.* used the finite element method and discrete ordinates method to address this coupled heat transfer phenomenon (by conduction and radiation) more rigorously [30]. It is revealed that quantitatively stronger shadow effect comes with steel-I sections with larger aspect ratios, while the presence of hot smoke in the cavities is found to augment radiative transfer by emission. It is also found that cavity radiation can be important so that neglect of this coupled process when linking fire modelling and thermal modelling could lead to significant underpredictions of steel temperatures.

Incorporating the above mentioned issues into thermal modelling is within the scope of performance-based design for structural fire safety which requires a robust software framework with integrated fire, heat transfer and structural models [31, 4]. While many commercial FE packages (such as ABAQUS, ANSYS) can be used for heat transfer by conduction, great limitations still exist for modelling structures in fire in a seamless, efficient and appropriate way, e.g. the

links between fire, thermal and structural model are not advanced [4, 32]. For instance, a sequentially coupled thermo-mechanical analysis in ABAQUS requires to use the same meshes in the two analyses with continuum solid elements which however are not commonly accepted for structural modelling as more efficient and accurate beam-column elements are normally used instead. Transferring computed temperature data from thermal analysis using continuum elements to structural analysis would be a particularly daunting task for a large structural model if complicated fire scenarios are considered, say traveling fires (see Section 2.5.5). Moreover, it is also recognized that these general purpose commercial programs are overly complex to use for fire applications, expensive and perhaps too cost prohibitive [4]. SAFIR is one of the very few specialist FE programs that incorporates both thermal and structural models and facilitates data transmission from a 2D thermal model to a structural model [32]. However, as any other in-house specialist programs, it only allows limited access within the community and is restrictive for a field that is growing at a rapid pace (as the field of structures and fire is, with increasing interest and development in both research and industry).

Researchers at The University of Edinburgh have chosen the Open System for Earthquake Engineering Simulation (OpenSees) platform as a different route to develop a robust, extensible and flexible software framework for the structural fire engineering community [7]. A thermal analysis framework with fire and heat transfer modules have been developed for the this platform based on the object-oriented programming paradigm [33, 7] (also see Chapter 4). The heat transfer module is based on the finite element method and both 2D and 3D modelling capabilities have been made available. The extended framework has been validated against benchmark problems with analytical solutions as well as full-scale experimental data, and its application has demonstrated interesting

results in investigating the thermal and structural responses of a composite tall building to travelling fires [34].

2.4 Finite element formulation and solution algorithms

2.4.1 FE spatial discretization

The finite element method will be used in this work as a general numerical approach to solve heat conduction in structures exposed to fires. Finite element approximation consists of dividing the entire domain of interest into non-overlapping sub-domains or finite elements. The approximation is built upon the nodal function values within each element domain, while ensuring certain conditions of the global approximation on the whole domain. Converting the governing equations from strong form (Eqs. (2.1)-(2.4)) to weak form is the first step in the finite element derivation. This is achieved by multiplying Eq. (2.1) with the weighting function W and integrating over the element, integrating by parts those terms with higher-order derivatives, which yields

$$\int_{\Omega^e} \left[W \rho c_p \frac{\partial T}{\partial t} + k_x \frac{\partial W}{\partial x} \frac{\partial T}{\partial x} + k_y \frac{\partial W}{\partial y} \frac{\partial T}{\partial y} + k_z \frac{\partial W}{\partial z} \frac{\partial T}{\partial z} \right] d\Omega - \oint_{\Gamma_q^e} W \overline{q} \, d\Gamma = 0 \quad (2.6)$$

The semidiscrete finite element model is obtained from Eq. (2.6) by substituting

a finite element approximation for the field variable T(within an element domain),

$$T(\mathbf{r},t) \approx \sum_{i=1}^{n} N_i(\mathbf{r}) T_i(\mathbf{r},t) \tag{2.7}$$

where $\mathbf{r}$ a position vector indicating the location of a point in space, n is the number of DOFs(in our case it is the number of nodes of the element), N_i is a set of interpolation functions of the element Ω^e.

Substituting $W = N_i$ $(i = 1, 2, \cdots, n)$ and replacing T by the approximation in Eq. (2.7), the semidiscrete, weak-form finite element model is obtained in matrix form

$$\mathbf{C}^e\dot{\mathbf{T}}^e + \mathbf{K}^e\mathbf{T}^e = \mathbf{Q}^e \tag{2.8}$$

where the entries of the matrices and vectors are given as

$$\begin{aligned} K_{ij}^e &= \int_{\Omega^e} \left[k_x(T)\frac{\partial N_i}{\partial x}\frac{\partial N_j}{\partial x} + k_y(T)\frac{\partial N_i}{\partial y}\frac{\partial N_j}{\partial y} + k_z(T)\frac{\partial N_i}{\partial z}\frac{\partial N_j}{\partial z} \right] d\Omega \\ C_{ij}^e &= \int_{\Omega^e} N_i \rho c_p(T) N_j \, d\Omega \,, \quad Q_i^e = -\int_{\Gamma_q^e} N_i \overline{q}(T) \, d\Gamma \end{aligned} \tag{2.9}$$

The above procedures for the finite element discretisation is generally referred to as the *Galerkin Weighted Residual Method* [16]. Once the form of element interpolation function N_i is known and the geometry is specified, the integrals in Eq. (2.9) can be evaluated numerically. The global system of equations can be constructed following the assembling procedures as given in [35]

$$\mathbf{C}\dot{\mathbf{T}} + \mathbf{K}\mathbf{T} = \mathbf{Q} \tag{2.10}$$

Note Eq. (2.10) is a semidiscrete finite element model as it contains the first order

time derivative ($\dot{T} = \frac{\partial T}{\partial t}$). The temporal discretisation can be achieved using the direct time integration scheme with the following formula

$$(1-\alpha)\dot{T}(t_n) + \alpha\dot{T}(t_{n+1}) = \frac{T(t_{n+1}) - T(t_n)}{\Delta t} \tag{2.11}$$

where $t_n = t,\ t_{n+1} = t + \Delta t,\ n \in \{0, 1, \cdots, nTimeSteps\},\ 0 \leq \alpha \leq 1$. The subscripts are used to indicate the location within a time interval in the following context.

Eq. (2.11) is the widely used general trapezoidal rule, which approximates the derivative within a time interval as a weighted mean of the values at the beginning and the end of that interval. The fully discrete finite element model can be obtained by evaluating each term in equation (2.10) at t_{n+1} and reorganising terms following Eq. (2.11)

$$\mathbf{C}_{n+1}\dot{\mathbf{T}}_{n+1} + \mathbf{K}_{n+1}\mathbf{T}_{n+1} = \mathbf{Q}_{n+1} \tag{2.12}$$

where $\dot{\mathbf{T}}_{n+1} = \frac{1}{\alpha\Delta t}\left[\mathbf{T}_{n+1} - \mathbf{T}_n - (1-\alpha)\Delta t\dot{\mathbf{T}}_n\right]$.

2.4.2 Solution algorithms

As discussed in Section 2.2, thermal properties of most construction materials generally vary with temperature, which means the matrices $\mathbf{C}$ and $\mathbf{K}$ in Eq. (2.12) are temperature dependent. In addition, due to the specification of radiation boundary condition, the load vector $\mathbf{Q}$ is also temperature dependent. As a result, a residual vector $\mathbf{R}(\mathbf{T})$ is introduced in Eq. (2.12) when $\mathbf{T}$ is replaced by a trial solution. Iterative procedures such as Newton-Raphson method should be

used in order to cancel the residual, i.e. finding a solution $\mathbf{T}_{n+1}$ which satisfies the following equation

$$\mathbf{R}_{n+1}(\mathbf{T}_{n+1}) = 0 \tag{2.13}$$

The left hand side of the above equation can be expanded using the first order *Taylor Series* expansion at $\mathbf{T}^{ir}_{n+1}$ (ir is iteration number)

$$\mathbf{R}_{n+1}(\mathbf{T}_{n+1}) = \mathbf{R}_{n+1}(\mathbf{T}^{ir}_{n+1}) + \left.\frac{\partial \mathbf{R}(\mathbf{T})}{\partial \mathbf{T}}\right|_{\mathbf{T}=\mathbf{T}^{ir}_{n+1}} (\mathbf{T}_{n+1} - \mathbf{T}^{ir}_{n+1}) \tag{2.14}$$

Defining the difference between "exact solution" and the irth iterative solution as $\Delta\mathbf{T}^{ir}_{n+1} = \mathbf{T}_{n+1} - \mathbf{T}^{ir}_{n+1}$, and the tangent matrix $\mathbf{M} = \left.\frac{\partial \mathbf{R}(\mathbf{T})}{\partial \mathbf{T}}\right|_{\mathbf{T}=\mathbf{T}^{ir}_{n+1}}$, the following predictor-corrector algorithm can be obtained by combining Eqs. (2.13) and (2.14)

$$\mathbf{M}\Delta\mathbf{T}^{ir}_{n+1} = -\mathbf{R}_{n+1}(\mathbf{T}^{ir}_{n+1}) \tag{2.15}$$

The above equation computes the incremental of temperature solution at the $n+1$ time step, and ensures that the residual vanishes (Eq. (2.13)) after a number of iterations.

It is beneficial to regroup the terms in the residual vector and tangent matrix considering different sources of nonlinearities, i.e. specific heat, thermal conductivity, and flux boundary condition [36, 37]. In this way, the residual vector may be expressed as

$$\mathbf{R} = \mathbf{R}^{c_p} + \mathbf{R}^{k} + \mathbf{R}^{q} \tag{2.16}$$

where $\mathbf{R}^{c_p} = \mathbf{C}_{n+1}\dot{\mathbf{T}}_{n+1}$, $\mathbf{R}^{k} = \mathbf{K}_{n+1}\mathbf{T}_{n+1}$, $\mathbf{R}^{q} = -\mathbf{Q}_{n+1}$, the superscripts c_p, k

and q are used as indicators for specific heat, thermal conductivity and boundary heat flux, respectively.

Accordingly, the tangent matrix may be given as

$$\mathbf{M} = \frac{\partial \mathbf{R}(\mathbf{T})}{\partial \mathbf{T}} = \mathbf{M}^{c_p} + \mathbf{M}^{k} + \mathbf{M}^{q} \tag{2.17}$$

The entries for $\mathbf{M}^{c_p}$, $\mathbf{M}^{k}$ and $\mathbf{M}^{q}$ are given in the following text at element level,

$$\mathbf{M}_{ij}^{e,c_p} = \sum_{m=1}^{n} \dot{T}_m \int_{\Omega^e} N_i N_j N_m \, d\Omega + \frac{1}{\alpha \Delta t} \int_{\Omega^e} \rho c_p N_i N_j \, d\Omega \tag{2.18}$$

$$\begin{aligned} \mathbf{M}_{ij}^{e,k} = \sum_{m=1}^{n} T_m \int_{\Omega^e} \Big(\frac{\partial k_x}{\partial T} \frac{\partial N_i}{\partial x} \frac{\partial N_m}{\partial x} N_j + \frac{\partial k_y}{\partial T} \frac{\partial N_i}{\partial y} \frac{\partial N_m}{\partial y} N_j + \frac{\partial k_z}{\partial T} \frac{\partial N_i}{\partial z} \frac{\partial N_m}{\partial z} N_j \Big) \, d\Omega \\ + \int_{\Omega^e} \Big(k_x \frac{\partial N_i}{\partial x} \frac{\partial N_j}{\partial x} + k_y \frac{\partial N_i}{\partial y} \frac{\partial N_j}{\partial y} + k_z \frac{\partial N_i}{\partial z} \frac{\partial N_j}{\partial z} \Big) \, d\Omega \end{aligned} \tag{2.19}$$

$$\mathbf{M}_{ij}^{e,q} = - \int_{\Gamma_q^e} (h_c + 4\varepsilon\sigma T^3) N_i N_j \, d\Gamma \tag{2.20}$$

It is usually a common practice to retain only the symmetric entries as given in Eqs. (2.18) and (2.19) in order to achieve higher computational efficiency

$$\mathbf{M}^{c_p} = \mathbf{C} = \int_{\Omega} \mathbf{N}^T \rho c_p \mathbf{N} \, d\Omega \tag{2.21}$$

$$\mathbf{M}^{k} = \mathbf{K} = \int_{\Omega} \mathbf{B}^T D \mathbf{B} \, d\Omega \tag{2.22}$$

where $\mathbf{B} = \nabla \mathbf{N}$. This suggests that the tangent matrices $\mathbf{M}^{c_p}$ and $\mathbf{M}^{k}$ may be approximated with the capacitance and conductance matrices respectively.

With the tangent matrix known, the predictor-corrector solution algorithm may

be given as

Solution predictor(given $\mathbf{T}_n$, $\dot{\mathbf{T}}_n$, $ir = 0$)

$$\mathbf{T}^{ir}_{n+1} = \tilde{\mathbf{T}}_{n+1} = \mathbf{T}_n + \Delta t(1-\alpha)\dot{\mathbf{T}}_n \tag{2.23}$$

$$\dot{\mathbf{T}}^{ir}_{n+1} = \tilde{\dot{\mathbf{T}}}_{n+1} = 0 \tag{2.24}$$

Solution corrector (iterating until converged)

$$\mathbf{M}^{*ir}_{n+1}\Delta\mathbf{T}^{ir}_{n+1} = -\mathbf{R}^{ir}_{n+1} \tag{2.25}$$

$$\mathbf{T}^{ir+1}_{n+1} = \mathbf{T}^{ir}_{n+1} + \Delta\mathbf{T}^{ir}_{n+1} \tag{2.26}$$

$$\dot{\mathbf{T}}^{ir+1}_{n+1} = \frac{1}{\alpha\Delta t}(\mathbf{T}^{ir+1}_{n+1} - \tilde{\mathbf{T}}_{n+1}) \tag{2.27}$$

$$ir = ir + 1 \tag{2.28}$$

where $\mathbf{M}^{*ir}_{n+1} = \frac{1}{\alpha\Delta t}\mathbf{C}(\mathbf{T}^{ir}_{n+1}, t_{n+1}) + \mathbf{K}(\mathbf{T}^{ir}_{n+1}, t_{n+1}) + \mathbf{M}^q(\mathbf{T}^{ir}_{n+1}, t_{n+1})$. The residual (unbalanced force) is evaluated as

$$\mathbf{R}^{ir}_{n+1} = \mathbf{C}(\mathbf{T}^{ir}_{n+1}, t_{n+1})\dot{\mathbf{T}}^{ir}_{n+1} + \mathbf{K}(\mathbf{T}^{ir}_{n+1}, t_{n+1})\mathbf{T}^{ir}_{n+1} - \mathbf{Q}(\mathbf{T}^{ir}_{n+1}, t_{n+1}) \tag{2.29}$$

Alternatively, Winget and Hughes [36] proposed the solution algorithm by solving the system of equations for the increment of the temperature derivative ($\Delta\dot{\mathbf{T}}$). Then Eqs. (2.25) - (2.27) may be replaced with the following equations [36]

Solution corrector (iterating until converged)

$$\mathbf{M}^{*ir}_{n+1}\Delta\dot{\mathbf{T}}^{ir}_{n+1} = -\mathbf{R}^{ir}_{n+1} \tag{2.30}$$

$$\dot{\mathbf{T}}^{ir+1}_{n+1} = \dot{\mathbf{T}}^{ir}_{n+1} + \Delta\dot{\mathbf{T}}^{ir}_{n+1} \tag{2.31}$$

$$\mathbf{T}^{ir}_{n+1} = \tilde{\mathbf{T}}_{n+1} + \alpha\Delta t\dot{\mathbf{T}}^{ir+1}_{n+1} \tag{2.32}$$

where $\mathbf{M}^{*ir}_{n+1} = \mathbf{C}(\mathbf{T}^{ir}_{n+1}, t_{n+1}) + \alpha\Delta t\left[\mathbf{K}(\mathbf{T}^{ir}_{n+1}, t_{n+1}) + \mathbf{M}^q(\mathbf{T}^{ir}_{n+1}, t_{n+1})\right]$.

Figure 2.4 shows the flow chart for the algorithms discussed in the forgoing text. These solution algorithms will be used in the work presented in Chapter 3 and 4.

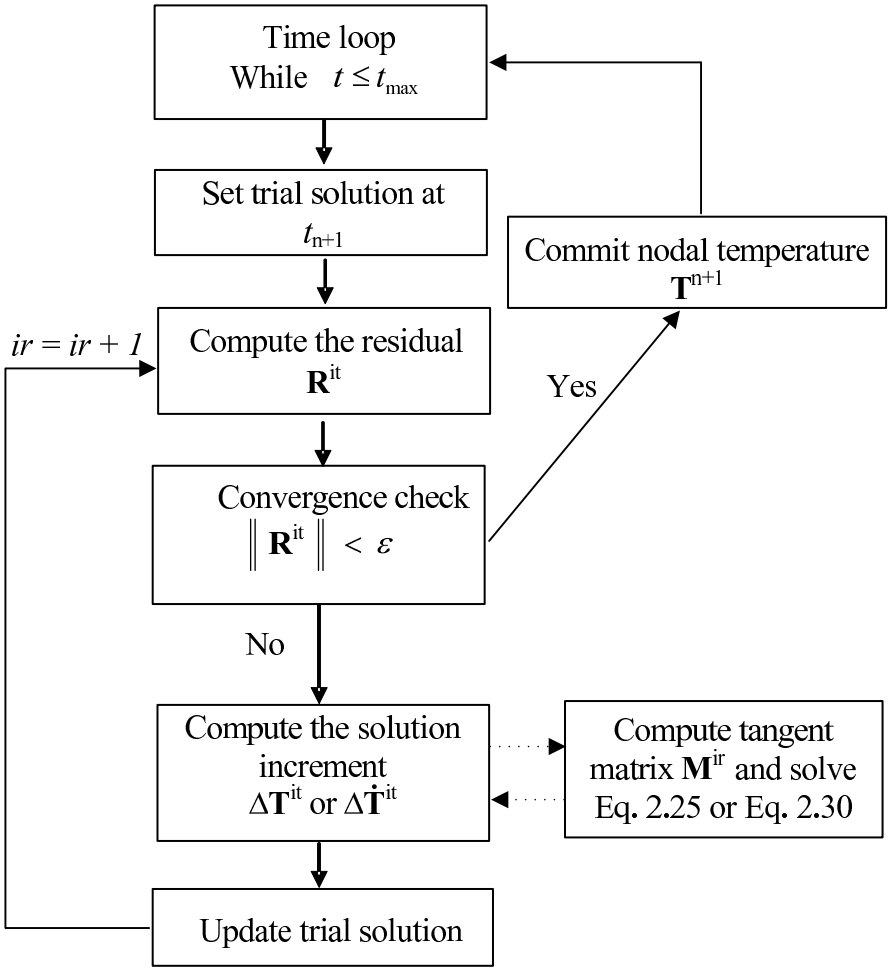

Figure 2.4: Flow chart of the solution algorithms for the non-linear heat conduction problem

2.5 Determining fire imposed boundary conditions

2.5.1 Temperature-time relationships

Post-flashover fire models have been generally used to represent the worst possible fire scenarios for structural analysis and the growth phase of the fire development is normally neglected within the context of structural fire engineering [38]. Due to very high gas phase temperatures in post-flashover fires, heat transfer from fire to structural members is usually dominated by radiation, e.g. the convective component is much less than 10% of the total heat flux when the compartment temperatures exceed 1000 ℃ [20, 39]. The simplest representation of a post-flashover fire is to use the "standard fire" which is defined by a temperature-time curve. This concept was initially introduced based on the observations of the gas phase temperatures of wood fires used in early tests and it has been widely used to test the fire resistance of structural members [38, 12, 18]. Although standard fires have some limitations (e.g. important factors such as fuel load and ventilation conditions are not considered), they are still considered useful as they provide a relatively simple way of comparing different fire resistive assemblies, and also provide experimental data for verifying complicated computer models [40].

The "parametric fires", which represent real compartment fires (post-flashover) better by incorporating the effects of fuel load, ventilation condition and thermal properties of the wall linings, are widely used nowadays for fire safety in structural design. In EC 1 [19], a set of equations are given to generate the gas phase temperature curves which are divided into a heating phase and a cooling phase.

Discussions on the origin and development of the parametric fire curves used in EC 1 can be found in a number of publications [22, 18, 3, 41, 42, 43]. The mathematical formulations given in EC 1 is not straightforward in application and a procedure with better clarity is given in [44]. It should be noted that a number of limitations exist with this parametric fire model, i.e. the height of the compartment should be less than 4 m and the floor area should not exceed 500 m^2, the thermal inertia of lining material should be in the range of $100 \sim 2200$ $J/m^2 \cdot s^{0.5} \cdot K$ and the opeing factor should fall in $0.02 \sim 0.20$ $m^{0.5}$.

In addition to the EC 1 model, a variety of other parametric fire models were proposed in [45, 46, 47]. One of these is the BFD curve which is obtained by applying the curve fitting process to the results from a large number of full-scale fire tests. A recent study shows that the predictions using the BFD curve demonstrate better agreement with the test data than the EC 1 model [48]. However, the generality of this parametric fire model still remains unclear as the effect of thermal inertia of lining materials was not taken into account during the curve fitting process [46].

2.5.2 Localised fire models

The foregoing discussion of post-flashover fire models is based on the assumption that a fully developed fire occurs in a compartment. In some circumstances, if the compartment or its opening is large enough, the development of fire would be of fuel-controlled type and the effect of heating on structural members could be localised [49, 50]. These situations may be found in parking buildings, atria, airports, metro stations, and even bridges [51]. If a load bearing member is heated

by a loalised fire, a more rational approach should be established to evaluate the fire imposed thermal boundary conditions which can then be used to accurately predict the temperature rise of the component. This led to the work initially carried out by Hasemi *et al.* [49, 52], who correlated the heat flux (at ceiling level and at surfaces of a beam beneath the ceiling) with other factors (heat release rate, fire size, radial distance from the fire source and the height of the compartment) using measured data from small scale fire tests with porous propane burners [49]. This work was followed with a series of larger scale tests where similar correlations with different coefficients were proposed for different surfaces of the steel I-beam located just below the ceiling [52, 50]. The Hasemi model has been adopted in the EC 1 [19] after comprehensive validation work with large scale fire tests [53]. According to [53], this model gave very good predictions of steel temperatures at locations just above the fire source but underpredicted the temperatures (due to lower heat fluxes) at locations away from the fire origin, which was believed to be caused by the presence of hot smoke layer in the test while the original work by Hasemi *et al.* was conducted in an open environment and there was almost no accumulation smoke under the ceiling. The validity range of the Hasemi model is that the flame impinges ceiling, the diameter of fire source is less than 10 m and the heat release rate of a single fire is under 50 MW [19].

For situations where the flame does not impact the ceiling, the EC 1 [19, 44] suggests the use of Heskestad correlation [54] for estimating the centre line plume temperature but no specifications are given on how to calculate the resulting heat fluxes. In fact, if the fire is at a stage when the flame does not reach the ceiling, the locally heating effect to the structural member may be not so important and thus it may be simply neglected in the calculation [44].

In addition to the Hasemi model, the Alpert ceiling jet model may also be used to examine the localised heating effect [55, 56, 57]. It should be noted that this model was originally developed for weak plume-driven flow field and it may produce overly high temperatures in some cases (e.g. with relatively low ceiling height but large heat release rate) around the domain just above the fire source. In that case, a cap value of the ceiling jet temperature in that domain may be used to overcome the potential non-physical predictions. It is also found in this work (not presented here) that the Alpert correlation always produces more conservative predictions than the Hasemi model in the field far from the fire source which is consistent with the findings in [53] that suggested under-predictions from the Hasemi model compared to the measured values.

2.5.3 Zone models

As a widely used mathematical model to predict the development of compartment fires, the zone modelling approach normally treats a compartment with two distinct zones, i.e. an upper zone of hot combustion products and a lower zone of cold air. This approach is based on experimental observations of compartment fires, where a distinct "two-layer" was formed and relatively uniform temperature and composition were found in the upper and lower layers (zones) [58]. Therefore, the assumption of homogeneous temperature and composition in the two layers is used in the zone modelling. The transient change of smoke layer height and temperature can be obtained by considering conservation of mass and energy in each of the layers, which are linked together by the *fire plume* that "pumps" mass from the lower layer to the upper layer.

A comprehensive survey of zone model programs is given in [59]. In most its applications, a two-zone fire model deals with a localised fire and predicts the temperature development in the hot layer and the layer height which are important for the design of smoke control systems and egress analysis. However, owing to global averaging on the variables of interest over the two zones, zone models are generally unable to predict the local physical phenomenon such as more intense heating above the fire source which could cause local damage to the structural members (Section 2.5.2). Some researchers have attempted to improve this by embedding an empirical localised fire model (such as the Hasemi model) within a two-zone model [53, 60, 61, 62]. Only a very few computer programs have considered the transition from two-zone phase to one-zone phase due to the occurrence of flashover which is deemed more detrimental to structural integrity [60, 63, 64]. However, the switching criteria used in these models seem to be very crude approximation of actual conditions necessary for flashover [38]. Moreover, due to the limitations of many empirical correlations used in zone modeling, its application to complicated geometries is still questionable [65].

2.5.4 CFD models

The development of Computational Fluid Dynamics (CFD) modelling made it possible to model fire phenomena from first principles via solution of the fundamental conservation equations (mass, momentum and energy). CFD modelling of compartment fires is able to give high resolution of the field variables such as gas temperature and radiative heat intensity (or flux). The application of CFD is gaining in popularity and usage for the studies of fire behaviours and

for the performance-based fire safety design. However, using CFD modelling for structural fire safety is still a new area which is under active research [4, 66].

The major difficulty in the application of CFD for structural fire analysis is always associated with significant differences in time and length scales, and spatial discretisation schemes used in fire and thermal modelling [67], e.g. it is not practical to include a steel beam (or column) into a CFD model for a large compartment as the length scale for the former can be an order of magnitude smaller than the spatial scale used for the latter. Therefore, it is more desirable to develop a range of coupling strategies between CFD modelling for fire development and FEM modelling for thermal responses of structural members [67].

A systematic examination of possible coupling methodologies between CFD and FEM modelling is presented in [67]. The authors proposed to divide the methodologies into two high-level categories, i.e. *one-way* coupling where no feedback from the thermal modelling is taken into account in the fire modelling, and *two-way* coupling where data exchange between the thermal and fire modelling is treated in a two-way fashion. It was found that *one-way* coupling, with obvious advantage in computational efficiency, produced satisfactory results if structural members are small enough and do not interfere strongly with the flow field. For situations where the presence of structural members has a significant impact on the flow field, it is necessary to include their boundaries in the fire model, at least approximately through adiabatic assumption or one-dimensional heat conduction treatment [67]. The *two-way* strategy requires simultaneous CFD modelling for the fire environment and FEM thermal modelling for the structural member therefore it is very costly in terms of computational resources. The *one-way* coupling strategy seems to be a more practical approach, and it was used by most of the

existing works [20, 21, 68, 69, 70], where different implementation methods were used to handle the results from CFD computations.

2.5.5 Travelling fires

As discussed in Section 2.5.1, post-flashover fires have been of major interest within the structural fire community because these type of fires were always thought to represent the worst scenarios for structural safety. However, in large compartments (e.g. with floor area larger than 1000 m^2) like open plan offices or industrial buildings, it seems unrealistic to assume uniformly burning post-flashover fires. It is more likely that fires burn progressively from one location to the next in these large compartments. This travelling nature of fires in large spaces has been observed in both fire tests and accidental fires (e.g. the One Meridian Plaza fire burnt for almost 19 hrs from the 22nd to the 30th floor) [5]. Fires travelling horizontally across a single large floor area were observed in the reconstruction of the WTC fires using CFD modelling [71].

The major distinctions between travelling fires and post-flashover fires are the prolonged burning time and the spatially non-uniform heating nature within the whole compartment [5]. It is only very recently that the effects of travelling fires have drawn the attention of researchers who raised questions on the application of conventional design fires on modern structures with large spaces [72, 3]. Rein and Stern-Gottfried *et al.* [72, 73, 74, 5, 6] have developed a novel methodology which represents traveling fires more realistically by considering key aspects of fire dynamics in large enclosures. By horizontally dividing the whole fire environment into two regions, i.e. "near field" and "far field", this methodology

is able to generate spatially non-uniform and transient thermal environment for the whole floor. The near field temperature is usually approximated with a constant value (e.g. 1200 ℃) while the far field temperatures are produced with an empirical correlation (the Alpert ceiling jet model) which possesses the advantage of rapid resolution of the thermal environment with sufficient accuracy for engineering applications [5, 6]. The authors of [75] implemented the travelling fire methodology in a CFD program (Fire Dynamics Simulator [76]) by turning on/off specified burning areas but the key characteristic of non-homogeneous heating was not discussed in that work. It was found in a recent work that travelling fires would produce a more severe impact on the structural performance in comparison with the EC 1 parametric fires [77]. This methodology has also been implemented in the extended OpenSees framework and was used to study both the thermal and structural behaviours of a composite tall building [34] (also see Chapter 5). Results from thermal analysis show that travelling fires with larger burning areas are more detrimental to the steel beams while fires with small burning areas produce a more severe impact on the concrete slabs. Results from structural analysis show that, when compared to the conventional parametric fires, travelling fires with smaller sizes causes higher midspan deflections of the floor and higher plastic deformations of the steel beam.

The discussions above are mainly focused on horizontally travelling fires across a single floor. It should be noted that vertical travelling which may lead to multiple floor fires is also possible in high-rise buildings [5]. Perhaps due to the complexities involved in fire spread between floors, only a very limited number of works have studied the effects of vertically travelling fires on structural performance [78, 79]. A global time delay was introduced in [78] to simulate the vertically travelling nature and the results indicated that possible connection failure may take place

because of the cyclic column movements. The authors of [79] further discussed the mechanisms of fire spread from one floor to another and a range of vertically travelling speeds (time delays) were considered for the parametric studies. The extended OpenSees framework was used in that work for both the thermal and structural calculations. The results showed that simultaneous multifloor fires were found to be more conservative than vertically travelling fires in terms of global structural behaviour therefore vertical fire compartmentation is very important in securing structural integrity. It was also found that travelling fires produced higher tensile axial forces in the floors and thus the likelihood of connection failure was increased.

2.6 Conclusions

A review of heat transfer in structural members including sources of non-linearities, and relevant modelling approaches have been discussed. Finite element formulation of heat transfer in solids and the solution algorithms are presented, which will be used in later work presented in Chapter 3 and Chapter 4. A review of design fires involving different level of complexities to establish the thermal boundary conditions is presented. The discussions on the validity and limits of different fire models provides a guideline on selecting the appropriate one in order to maintain a consistent level of crudeness between thermal and structural analyses for a specific problem. The review work in this chapter forms the theoretical foundation for the development of an advanced thermal analysis framework as will be presented in Chapter 4.

Chapter 3

Modelling fire-induced radiative heat transfer in smoke-filled structural cavities

3.1 Introduction

Structural members with cavity geometry, such as I-sections, H-sections and hollow sections, are commonly found in the building industry. In the case of natural fires (especially during the post-flashover phase), these members may be exposed to a severe thermal environment which is dominantly controlled by radiation heat transfer [38, 39]. However, calculation of radiative fluxes in a cavity is often complicated by two mechanisms. The first complication arises from its geometry [26, 27]. The inner cavity surfaces experience different levels of thermal exposure from the fire environment, which generally can not be readily quantified.

Besides, those surfaces also heat each other by emission and the radiative intensity is reflected many times within the cavity with partial absorption at each reflection. Secondly, fire smoke normally consists of strong participating media (such as soot particles) and its presence in cavities further complicates radiative heat exchange [80, 81]. Current engineering calculation methods for structural fire engineering (e.g. those in EC 3 [13]) do not provide sufficient guidelines in calculating radiative fluxes for these type of structural members. Inaccurate calculations of the heat flux could potentially compromise the subsequent predictions of thermo-mechanical behaviors.

On the geometric effect, Wickstrom [26] noticed that the inner surfaces of an I-section receive different radiant energy even in a uniformly heating environment. A shadow effect factor was then introduced and the results were claimed to be equivalent to those obtained from view-factor based calculations. The concept has been adopted by the recently developed performance-based design code [13]. More recently, Wang [27] opted for an analytical solution to the problem of radiative transfer within I-section cavities. It was found that, in comparison with the analytical solution, the EC 3 approach over-predicts heat fluxes received by the section surfaces. These approaches are limited to I-sections with radiatively transparent medium, which is valid for the thermally-thin heating conditions such as some furnace fire tests, but may be not for soot laden environment as seen in natural fires.

Efforts have been made in other works to incorporate the effect of participating media in the heat flux calculation. Ghojel [82] introduced a total gas emissivity and a surface absorptivity into the blackbody radiation exchange equation. On that basis, Ghojel and Wong [83] improved the empirical resultant emissivity by

including those two parameters and the gas temperature. Wang and Tan [80] tackled the problem more rigorously by solving the radiative transfer equation following the two flux method. An analytical solution was obtained to include the non-isothermal, absorbing-emitting behavior of the participating media. Nevertheless, all these methods can not deal with multidimensional radiative heat transfer in structural cavities where the geometric effect can be important [26, 27].

In addition to the works mentioned above, a variety of methodologies have been established for quantifying the fire imposed heat fluxes by utilizing results from Computational Fluid Dynamics (CFD) simulations of the fire environment. For example, Prasad and Baum [68] used an approach by solving the 1D radiative transport equation with medium properties from CFD calculations. Similar work is found in [20], where the calculations rely on detailed resolutions of the radiative properties of the local smoke. Duthinh *et al.* [69] proposed a fire-thermal interface using the "adiabatic surface temperature" concept. Welch *et al.* [67] examined more systematically the strategies to link fire modeling (gas phase) and thermal modeling (solid phase). However, a common limitation of many of these approaches is that unless full two-way analysis is performed with sufficient grid resolutions then the coupling physics between radiation in structural cavities and conduction in structures is not correctly modeled. This is likely to yield inaccurate results for typical structural members as will be discussed in this chapter.

In order to address the aforementioned limitations of previous investigations, this work proposes a numerical approach to simulate the fire induced radiative heat transfer in structural cavities. The discrete ordinates method and the finite element method are used to model the coupled heat transfer by radiation and conduction. The proposed model is validated with benchmark tests and

experimental data. Unprotected steel I-sections exposed to post-flashover fires are studied using this approach. Effects of section geometry and participating media on the net radiative heat fluxes and steel temperatures are systematically investigated. Performance of other methodologies is also examined through comparative analyses with the proposed model.

3.2 Mathematical model

3.2.1 Radiative heat transfer in generic structural cavities

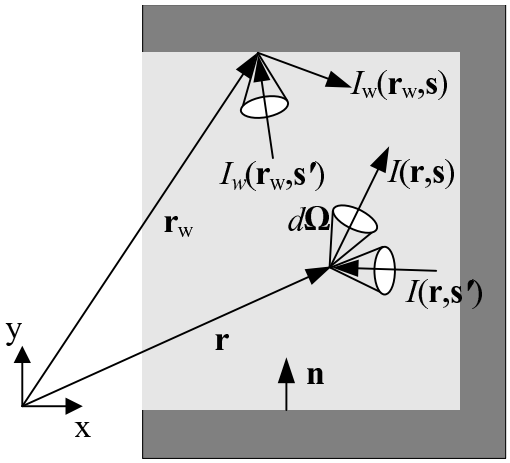

Figure 3.1: Radiation in a generic cavity for a typical structural member

To illustrate the nature of the problem, radiative heat transfer in a generic cavity for a typical structural member is shown in Figure 3.1. The governing equation for multidimensional radiant exchange in a cavity with participating (emitting-absorbing and isotropically scattering) medium is,

$$\mathbf{s} \cdot \nabla I(\mathbf{r}, \mathbf{s}) = -\beta I(\mathbf{r}, \mathbf{s}) + \kappa I_b(\mathbf{r}) + \frac{\sigma_s}{4\pi} \int_{4\pi} I(\mathbf{r}, \mathbf{s}') d\Omega \tag{3.1}$$

where I is the radiative intensity, $\mathbf{s}$ is the direction of radiation propagation path, $\mathbf{r}$ is a position vector indicating the location of a point in space, κ and σ_s are the absorption coefficient and the scattering coefficient of the medium respectively, β is the extinction coefficient ($\beta = \kappa + \sigma_s$), I_b is the local blackbody intensity of the medium, $\mathbf{s}'$ is the incoming radiation direction, $d\Omega$ represents a differential solid angle. This equation is called the radiative transfer equation (RTE), which states the radiant energy conservation for a differential volume in the participating medium.

For a gray medium at temperature T_m, the local blackbody intensity is normally evaluated as [81]

$$I_b(\mathbf{r}) = \frac{\sigma T_m^4}{\pi} \tag{3.2}$$

where σ is the Stefan-Boltzmann constant.

If the boundary of the domain is assumed gray and diffuse, then the radiative boundary condition for Eq. (3.1) is expressed as

$$I_w(\mathbf{r}_w, \mathbf{s}) = \varepsilon I_{bw}(\mathbf{r}_w) + \frac{\rho}{\pi} \int_{\mathbf{n}\cdot\mathbf{s}'<0} |\mathbf{n} \cdot \ \mathbf{s}'| I(\mathbf{r}_w, \mathbf{s}') d\Omega \tag{3.3}$$

where $I_w(\mathbf{r}_w, \mathbf{s})$ is the leaving intensity at the boundary wall, $\mathbf{n}$ is the unit inward normal vector at the boundary location, ε is the surface emissivity, ρ is the surface reflectivity, I_{bw} is the surface blackbody emission intensity, determined by $I_{bw} = \sigma T_s^4/\pi$, where T_s is the surface temperature of the boundary. The physical meaning of the above boundary condition is that the leaving intensity at the boundary is the sum of the emitted radiation and the reflected irradiation.

According to Kirchhoff's law, the surface emissivity is equal to the surface absorptivity [84]. Thus the net heat flux penetrating into the boundary may

be evaluated with the following equation

$$q_{rad}(\mathbf{r}_w) = \varepsilon \left(\int_{\mathbf{n}\cdot\mathbf{s}'<0} |\mathbf{n} \cdot \ \mathbf{s}'| I(\mathbf{r}_w, \mathbf{s}') d\Omega - \pi I_{bw}(\mathbf{r}_w) \right) \tag{3.4}$$

3.2.2 Heat conduction in structural members

Radiant energy propagates into the solid material of the cavity walls by conduction, and causes temperature rise in the structural member. The governing equation for heat conduction in the solid is shown below:

$$\rho c_p \frac{\partial T}{\partial t} = \nabla \cdot (k \nabla T) \tag{2.1}$$

where c_p is the specific heat of the structural member, ρ is its density, and k is the thermal conductivity. Depending on the nature of the solid material, heat conduction may be evaluated with different methods involving different levels of complexity [20]. A dimensionless Biot number can be introduced to quantify the nature of the problem [20, 84],

$$Bi = \frac{hL_c}{k} \tag{3.5}$$

where h is the total heat transfer coefficient, L_c is the characteristic length of the solid which is customarily defined as the ratio of its volume to surface area, $L_c = V/A$.

The above dimensionless number represents the ratio of thermal resistance inside the solid and at its surface. If $Bi > 0.1$, the material is thermally-thick, and the temperature gradients within the solid can be significant. In this case, Eq. (2.1) has to be solved numerically with proper boundary conditions imposed. If

$Bi < 0.1$, the material is thermally-thin, and the temperature distribution can be considered to be uniform throughout the solid [20]. The lumped capacitance method can be used to calculate the temperature rise in this case [84],

$$\rho c_p V \frac{dT_s}{dt} = \int q_{net} dA \tag{3.6}$$

where V is the volume of the solid material, and A is the surface area exposed to the fire, q_{net} is the net heat flux (including contributions from both convection and radiation) received by the structural member.

Eq. (3.6) is suggested in [13] for the use of calculating temperature development of steel structural members. Note that if heat flux distribution were spatially uniform, the section factor, A/V, would appear explicitly in Eq. (3.6). It relates the exposed surface area of the member to its volume, and its reciprocal indicates the equivalent thickness of the structural member. Structural members with larger section factors would be heated up faster due to their smaller equivalent thickness.

3.2.3 Coupled heat transfer mode

For structural members with cavity geometry, coupled heat transfer by radiation and conduction should be addressed. This is because that the boundary emission intensity I_{bw} in Eq. (3.3) is completely controlled by the surface temperature T_s. High heat fluxes from the fire environment could create very high temperatures, and the boundary conditions for the radiative heat transfer would change rapidly in typical transient situations. This is particularly true for unprotected structural members made of steel and aluminum due to their high conductivity. In the

current work, the radiative heat transfer and heat conduction are calculated separately, and the coupling process is addressed by exchanging computed data (heat fluxes and temperatures) at the cavity boundaries at each time step.

However, this inherent coupling nature has not been considered in many of the recent works towards more accurate predictions of thermal responses of structural members [68, 20, 69]. As opposed to our proposed model, the existing works normally adopt completely separate calculation processes, i.e. first calculating the radiative heat flux history by assuming cold cavity boundaries, then performing thermal modeling with the pre-calculated heat fluxes and including the radiation heat loss with the simple formula $q_{loss} = \varepsilon\sigma T_s^4$. While approaches like this are appropriate for flat or convex structural members, they fail to capture the important physics of re-radiation occurring in the structural cavities, that is, the contribution (due to both reflection and emission) from hot cavity walls is lost. Therefore, the results would be lower heat fluxes and lower temperature values. Following the notations used in [67], these approaches are denoted "one-way" methodology in general and their inaccuracy is quantitatively studied by comparing with the proposed model.

3.3 Solution strategies

As Eq. (3.1) (RTE) is a first order radiative equation, and if no special treatment is applied when solving it numerically, it often produces non-physical oscillating results. In this work, a recent method presented by Zhao *et al.* [85] is used so that the problem of oscillation can be overcome. With this approach, the first order RTE is transformed into second order governing equation and intrinsically

stable property is achieved. After substitution and rearrangement, the second order RTE can be written as

$$-\mathbf{s}\cdot\nabla(\mathbf{s}\cdot\nabla I(\mathbf{r},\mathbf{s}))+\mathbf{s}\cdot\nabla S=-\beta I(\mathbf{r},\mathbf{s})+S \tag{3.7}$$

where the source term is $S=\kappa I_b(\mathbf{r})+\frac{\sigma}{4\pi}\int_{4\pi} I(\mathbf{r},\mathbf{s}')d\Omega$.

The boundary conditions [85] for equation (3.7) are given bellow

$$I(\mathbf{r},\mathbf{s})=I_0(\mathbf{r},\mathbf{s}) \qquad \mathbf{n}\cdot\mathbf{s}>0 \quad \text{on} \quad \Gamma_D \tag{3.8}$$

$$\mathbf{s}\cdot\nabla I+\beta I=S \qquad \mathbf{n}\cdot\mathbf{s}\leq 0 \quad \text{on} \quad \Gamma_N \tag{3.9}$$

where Γ_D is the Dirichlet boundary and Γ_N is the Neumann boundary. Eqs. (3.7)-(3.9) are solved by combining the finite element method and discrete ordinates method (FEDOM). Finite element method is chosen because it has the advantage in dealing with irregular geometry [16], and radiative transfer in any structural cavity can be readily tackled. Discrete ordinates method has now been widely used to solve many radiative heat transfer problems with high accuracy and moderate computational resources [81, 85, 86].

Eqs. (3.7)-(3.9) are written for each ordinate direction. By using the standard Galerkin weighted residual method [16] and rearranging terms, the following matrix equation evaluated at elemental level can be obtained

$$K_{ij}^m I_j^m=B_j^m \qquad i,j=1,2,\ldots,n \tag{3.10}$$

where m represents the m_{th} angular direction for which the solution is sought, n is the number of nodes for each element. The left hand side matrix and the right

hand side vector are the expressed as follows

$$K_{ij}^m = \int \mathbf{s}^m \cdot \nabla N_i \, \mathbf{s}^m \cdot \nabla N_j \, dV + \int \beta^2 N_i N_j \, dV - \int_{\Gamma_N} \beta N_i N_j \, \mathbf{s}^m \cdot \mathbf{n} \, d\Gamma \quad (3.11)$$

$$B_j^m = \int \beta S^m N_j \, dV - \int \mathbf{s}^m \cdot \nabla S^m N_j \, dV - \int_{\Gamma_N} S^m N_j \, \mathbf{s}^m \cdot \mathbf{n} \, d\Gamma \quad (3.12)$$

where N is the nodal interpolation function.

Summing the contribution from each element, the global matrix system can be written as

$$\mathbf{K}^m \mathbf{I}^m = \mathbf{B}^m \quad (3.13)$$

where $\mathbf{K}$ is the "stiffness matrix", $\mathbf{I}$ is the intensity vector, $\mathbf{B}$ is the "load vector". The system of equations is then solved for each direction separately. Global iteration is necessary in order to include the source term and boundary conditions. The surface heat flux is calculated based on the solution from the previous global iteration using Eq. (3.4). Iterations are continued until convergence is obtained, that is, the norm of change in incident energy is less than 10^{-4}. The readers are referred to other publications [81, 86] for more details on the algorithms specific to the discrete ordinates method.

Once converged solutions are obtained, angular integrals over a range of solid angles are replaced by numerical quadratures within that range. This may produce inaccurate results when there are discontinuous boundary conditions, which is identified as *ray effects* [81]. In this work, the piecewise constant angular (PCA) [87, 88] approximation is used for the numerical quadrature, which mitigates the *ray effects* more effectively compared to other quadrature

sets including the conventional S_N sets [87, 88]. The total solid angle is divided uniformly in the zenith (θ) and azimuthal (ϕ) directions, producing N_θ and N_ϕ divisions respectively. The intensity is assumed constant within each solid angle division. The specific PCA approximation is then denoted by $N_\theta \times N_\phi$. Then Eq. (3.4) is replaced by the following equation

$$q_{rad} = \varepsilon \left(\sum_{\mathbf{n}\cdot\mathbf{s}_m<0} |\mathbf{n} \cdot \ \mathbf{s}_m| w_m I(\mathbf{r}, \mathbf{s}_m) - \pi I_b(\mathbf{r}) \right) \tag{3.14}$$

where the w_m is the quadrature weight associated with the directions $\mathbf{s}_m$.

Once the radiative heat fluxes are calculated with the above procedures, the transient temperature development in structures can be obtained by solving Eq. (2.1) together with proper initial and boundary conditions. The finite element method (FEM) is used here to solve this equation and the final global system of equations can be written as [16]

$$\mathbf{C}\dot{\mathbf{T}} + \mathbf{K}\mathbf{T} = \mathbf{Q} \tag{3.15}$$

where $\mathbf{C}$ is the heat capacity matrix, $\mathbf{T}$ represents the nodal temperature vector, $\mathbf{K}$ is the conductivity matrix, $\mathbf{Q}$ is the "load vector". Details of these matrices and vectors and the solution algorithms used to solve the above set of non-linear equations are presented in Section 2.4. A fully implicit backward Euler scheme is used here for the time discretization. Due to temperature dependence of thermal conductivity and specific heat as well as radiation boundary conditions, the above equation can be strongly non-linear and the Newton-Raphson method is used for the solution procedure.

3.4 Validation of the RTE solver

The FEDOM method has been coded in Matlab for the current study based on the numerical strategies discussed in Section 3.3. Two benchmark studies are presented here in order to validate the numerical solutions for enclosures with either radiatively transparent media or strongly participating media.

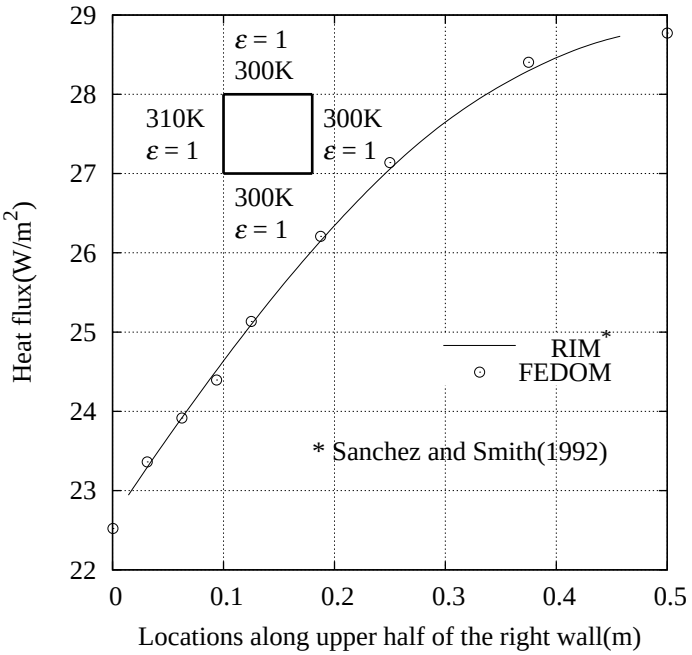

Figure 3.2: Radiative heat flux arriving at the upper half of the right wall in a square enclosure with radiatively transparent medium ($\kappa = 0$ m^{-1})

In the first problem, a rectangular enclosure of size 1m $\times$ 1m with a non-participating medium is examined. All the walls are assumed black surfaces and the left wall is maintained at 310 K while other walls are maintained at 300 K. The problem was first studied by Sanchez and Smith [87] using both the discrete ordinates method and radiation/irradiation method (RIM), where results from the latter were considered "exact". According to the grid independence study, we have divided the enclosure into 30 $\times$ 30 quadratic 8-noded elements and the

total solid angle is discretized using PCA quadrature rules with $N_\theta \times N_\phi = 2 \times 100$. The net radiative heat flux arriving at the upper half of the right wall is presented in Figure 3.2. The RIM results from Sanchez and Smith [87] are used for comparison. It is shown that the solutions from FEDOM agree with the RIM results very well, with negligible local error ($< 1\%$) near the upper-right corner.

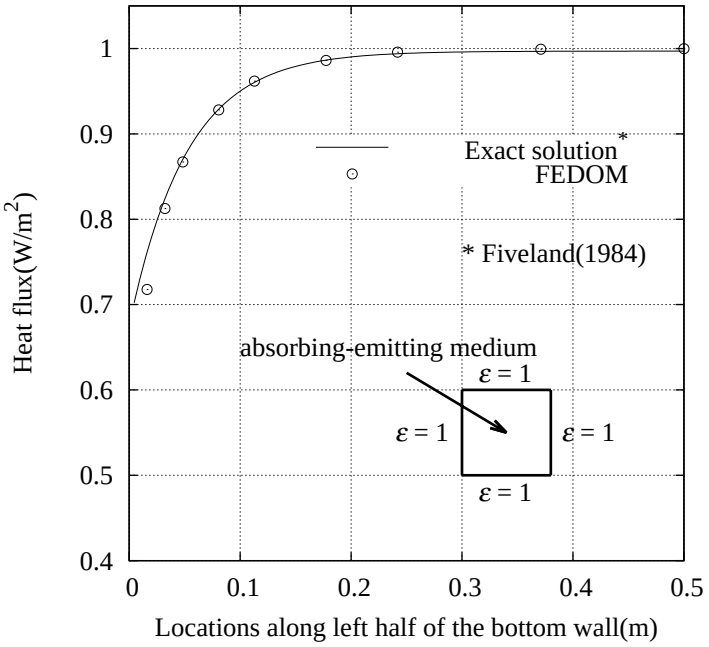

Figure 3.3: Radiative heat flux arriving at left half of the bottom wall in a square enclosure with participating medium ($\kappa = 10$ m^{-1})

The second benchmark problem deals with an enclosure with cold, black walls and filled by an absorbing- emitting gray medium. The medium is maintained at an emissive power of unity with absorption coefficient $\kappa = 10\text{m}^{-1}$. The dimensions of the enclosure are the same as the previous case. This problem is used widely for validation tests since an exact solution is available [86]. Computations are carried out to obtain the net heat flux along the bottom surface of the enclosure. The spatial domain is discretized with 10×10 quadratic 8-noded elements with biased refinement towards the walls. The angular discretization remains the same

as in the first problem. Figure 3.3 shows the comparison between predictions of FEDOM and the exact solutions [86]. It is shown that the flux is accurately predicted along the bottom wall, with local errors lower than 1%.

As shown in Figures 3.2 and 3.3, heat flux distribution is non-uniform along the walls for both cases because of the presence of corners (with c. 30% lower heat flux). This is a typical characteristic for radiation in cavities. In contrast, previous work by Wang [27] has assumed uniform distribution for all the walls in order to find an analytical solution.

3.5 Application to unprotected steel I-sections in post-flashover fires

Steel I-sections represent typical structural members with cavities, where two open cavities are formed by the presence of the upper flange, the lower flange and the web. Figure 3.4 illustrates the schematic of an I-section. Following the approach in [27], an aspect ratio (width to depth), $r = (b - s)/(2(h - 2t))$, is defined in order to quantify the characteristics of radiative exchange in structural cavities. Dimensions of typical steel I-sections with different section factors and aspect ratios are given in Table 3.1 [89].

For structural fire engineering, the most hazardous phase of compartment fires is perhaps the post-flashover fire [38], where the gas temperature may be maintained above 1000 ℃ for a relatively long period (e.g. up to 30 min [39]). In that case, radiation is widely recognized as the dominant mode of heat transfer over

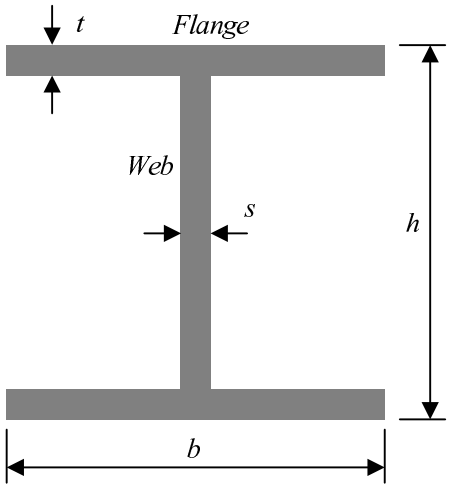

Figure 3.4: Schematic of an steel I-section with two open cavities

Table 3.1: Dimensions and section factors for typical steel I-sections

Section Designation	h (mm)	b (mm)	s (mm)	t (mm)	A/V (m^{-1})	r
UB914 × 305 × 289	926.6	307.7	19.5	32.0	83	0.17
UB762 × 267 × 197	769.8	268.0	15.6	25.4	104	0.18
UB914 × 419 × 388	921.0	420.5	21.4	36.6	71	0.24
UB610 × 305 × 238	635.8	311.4	18.4	31.4	82	0.26
UC305 × 305 × 198	339.9	314.5	19.1	31.4	76	0.53
UC254 × 254 × 73	254.1	254.6	8.6	14.2	166	0.55
UC356 × 406 × 634	474.6	424.0	47.6	77.0	32	0.59
UC356 × 406 × 393	419.0	407.0	30.6	49.2	48	0.59
UC356 × 406 × 235	381.0	394.8	18.4	30.2	78	0.59

convection and conduction [38, 39, 20]. This is normally observed in full scale post-flashover fire tests [39]. Generally speaking, fire should experience a growth phase before reaching flahshover. However, this work assumes post-flashover conditions from the onset of the analysis and the growth phase is not considered. This assumption is made based on two reasons. First, during the growth phase, the

fire only heats up individual members located in the vicinity of the flames, and can reach flashover quickly (e.g., $t < 5$ min [90]), thus heating during this phase is generally negligible. Second, it is during the post-flashover fire that radiation plays a dominant role, which is most relevant to the purpose of the current work.

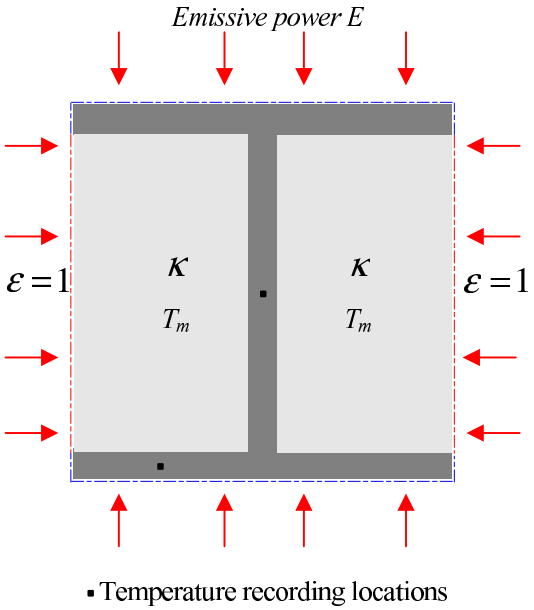

Figure 3.5: Steel I-section exposed to fire and with cavities filled with smoke

Figure 3.5 shows a steel I-section located in a uniformly heating environment, which simulates heating from typical post-flashover fires. The fire environment is represented by the dashed surface, which is assumed black ($\varepsilon = 1$) and emits diffusely at an emissive power E. Thereby two enclosed cavities are presented for the computational model, with each consisting of a red dashed surface and three inner surfaces of the I-section. The boundary condition for radiative heat transfer in cavities is discussed in Section 3.2.1 and is given by Eq. 3.3. Reported material emissivity for steel is in the range of 0.7 to 0.9 [38, 13, 12]. An average value of 0.8 will be used later in this work unless otherwise specified.

Further simplifications are made by assuming that the participating smoke is gray,

emitting-absorbing (but without scattering) at a mean temperature T_m. This is a reasonable approximation as in most large scale fires, smoke is comprised of soot laden combustion products, where soot particulate is the dominant absorber and emitter of thermal radiation [68, 91]. Scattering can be neglected because soot size is generally much smaller than the wavelength within the infrared spectrum [68, 92, 93]. Therefore, the extinction coefficient (β) is equal to the absorption coefficient (κ) for most fire scenarios. Unlike gaseous products such as H_2O and CO_2, soot participates radiatively at all wavelengths and its spectral dependence varies slowly, and as a result, κ for the soot-gas mixture would be a weak function of wavelength [92]. Due to this fact, the spectral absorption coefficient can be replaced by some mean coefficients with sufficient accuracy [92, 94]. The medium temperature (T_m) is approximated by assuming that the smoke is in thermal equilibrium with the fire environment, i.e. identical to the equivalent temperature of the fire environment, $T_m = T_{eq} = (E/\sigma)^{\frac{1}{4}}$.

The mean absorption coefficients discussed above have been widely adopted in fire research [68, 91, 94, 95]. Similarly, for the problems of interest here, the smoke is assumed to be sooty, and the values of mean absorption coefficient κ are parametrically varied from 0 to 30m $^{-1}$. The lower limit $\kappa = 0$ m^{-1} corresponds to a radiatively transparent medium, which could be a reasonable approximation to any fire environment with relatively clean combustion products (e.g. in gas furnace fires [26, 27]). The upper limit ($\kappa = 30$ m^{-1}) corresponds to a soot laden environment, which is more commonly seen in natural fires.

For heat conduction in the steel member, temperature dependent material properties are taken from [12]. All the surfaces of the I-section are subject to

the following boundary condition

$$-k\nabla T = q_c + q_r \tag{3.16}$$

where the convective heat flux is given as $q_c = h_c(T_m - T)$, the radiative heat flux for the outer surfaces (covered by the dashed blue surfaces in Figure 3.5) is $q_r = \varepsilon(E - \sigma T^4)$, while q_r for the inner surfaces is determined by Eq. (3.4). According to parametric analysis in [20], an approximate value, $h_c = 10$ W/m^2·K, is specified for the convective heat transfer coefficient. The initial temperature is 20 ℃.

Having established the computational model, the coupled heat transfer is solved with numerical methods discussed in Section 3.3. Grid independence studies have been performed to ensure that the essential physics are independent of grid size.

3.6 Results and discussions

3.6.1 Model validation

The accuracy of the RTE solver has been validated in Section 3.4. Here the proposed model is further validated with experimental data to simulate the combined mode of heat transfer by radiation, convection and conduction. The case examined is an unprotected steel I-section (UC305 × 305 × 198) subject to standard fire from four sides [96]. The standard fire temperature is given by $T_{fire} = T_0 + 345\log_{10}(8t + 1)$, where T_0 is the initial ambient temperature and t is time. Emissive power of fire is approximated by $E = \sigma T_{fire}^4$. Initial temperature

of the ambient and steel is 10 ℃. Temperatures at the web and flange (locations suggested in Figure 3.5) were measured during the test [96].

The computational model shown in Figure 3.5 is used for this validation problem. In previous work [26, 27], the fire gas in standard fires is treated as radiatively transparent medium ($\kappa = 0$ m^{-1}). This approximation is followed here because the combustion products in standard fire tests are mainly H_2O and CO_2, and their contribution to radiative transfer is not significant along a small path length [38, 84] (less than 0.2 m in this case). As a result, the gaseous mixture has negligible effect on radiative exchange in the cavities while the geometric effect is dominant [27]. The emissivity of steel is taken as 0.7 for the case here.

Figure 3.6 shows the comparison of the predicted temperatures and the measured values. It can be seen that the predictions from the proposed model agree generally very well with the mean values of measured temperatures in the flange and the web. The maximum local deviation between the predicted and measured mean temperatures is less than 3% after 10 min. Predicted temperatures are slightly lower than the measured ones in the first 10 min because the fire temperature is relatively low and radiation heat transfer is less dominant during this stage.

It also noted that the temperatures at the web are higher than those at the flange. This is because that the web is thinner than the flange (Table 3.1) and can be heated up more quickly. Unlike the proposed model, using a lumped heat capacity method can not capture this temperature difference [13].

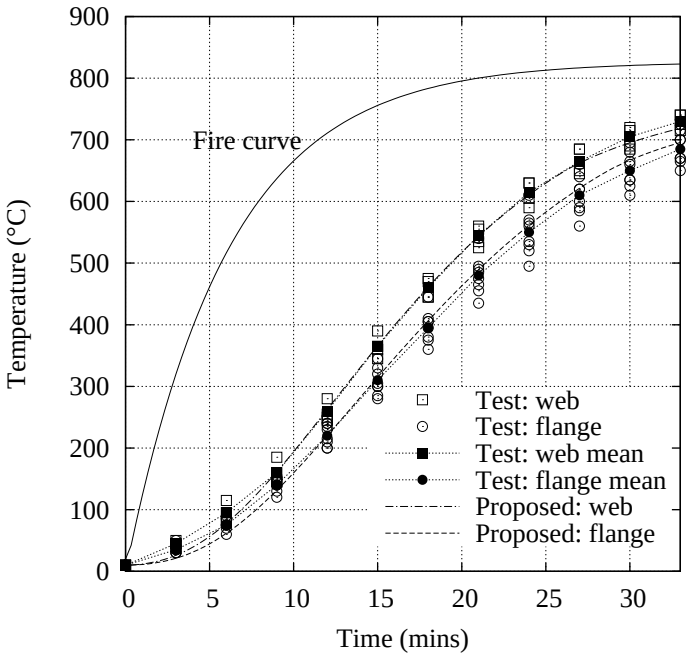

Figure 3.6: Comparison of predicted steel temperatures with experimental data

3.6.2 Effect of section geometry

The model shown in Figure 3.5 is considered here. As pointed out in [27], radiative heat transfer to steel I-sections is influenced by both the cavity geometry and the participating medium. Here we decouple the two mechanisms by assuming that it is radiatively transparent ($\kappa = 0$ m^{-1}) in the cavity and only examine the geometric effect. The steel I-section is maintained at 20 ℃ and exposed to a fire environment at constant emissive power E. Values of E are selected according to typical measured radiative fluxes in full scale post-flashover fire tests [39], i.e. from 100kW/m^2 to 200kW/m^2 for the purpose of parametric study here. Steel I-sections listed in Table 3.1 are examined.

The radiative heat fluxes incident on structural surfaces are spatially non-uniform.

In order to give an overall measure of thermal exposure, two spatially averaged net radiative heat fluxes are defined for the inner and outer surfaces respectively:

$$q_{inner} = \frac{\int_{A_{inner}} q_{rad} dA}{A_{inner}} \tag{3.17}$$

$$q_{outer} = \frac{\varepsilon \int_{A_{outer}} (E - \sigma T_s^4) dA}{A_{outer}} \tag{3.18}$$

where $A_{inner} = 2((b-s) + (h-2t))$, $A_{outer} = 2(b+2t)$.

A dimensionless net heat flux for the inner surfaces is given here for characterizing the geometric effect

$$\tilde{q} = \frac{q_{inner}}{q_{outer}} \tag{3.19}$$

A similar expression is given in [27], where the inner heat flux is normalized by the net blackbody radiative flux, and its physical significance is effective emissivity. However, $\tilde{q}$ here is the result of q_{inner} normalized by q_{outer} and it reflects the effects of geometric attenuation on radaitive heat transfer to I-sections. It is clear that $0 < \tilde{q} < 1$ and lower values would suggest stronger geometric attenuation.

Figure 3.7 shows the variation of the dimensionless heat flux $\tilde{q}$ with section aspect ratio and material emissivity. As can be seen, for a given material emissivity, $\tilde{q}$ increases with decreasing section aspect ratio and is independent of the external emissive power. This is because that the I-section becomes flatter as r reduces, and thus radiation attenuation by the cavity geometry tends to be less important. As a result, the differences between radiative heat fluxes at the inner and outer surfaces would also diminish. It is also interesting to note that, for a given aspect

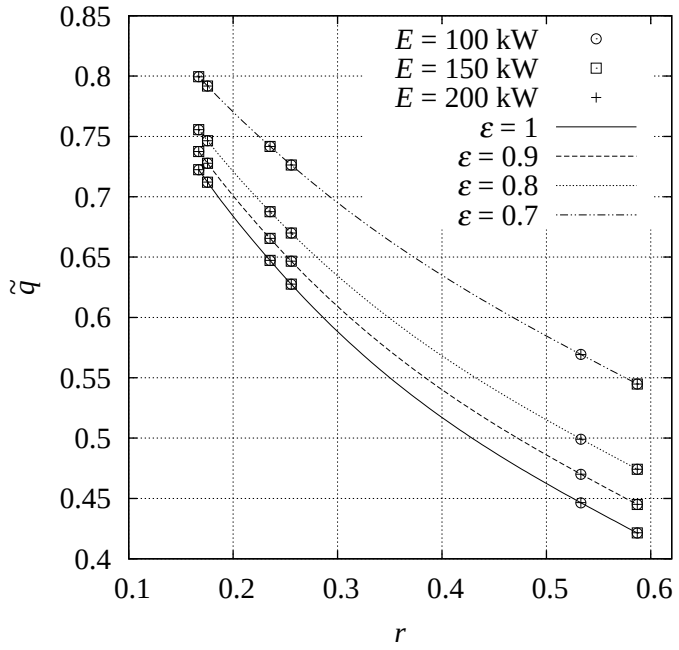

Figure 3.7: Normalized net radiative heat flux along the inner surfaces of the I-section

ratio, $\tilde{q}$ decreases with higher material emissivity. This suggests that the geometric effect is more prominent when the structural surfaces become less reflective (with higher ε). For the range of I-sections studied, $\tilde{q}$ can be as low as 0.48 ($r = 0.59$, $\varepsilon = 0.8$), which means that the net radiative heat flux received by the inner surfaces is only about 48% of the outer one. It is clear that the cavity geometry strongly attenuates the radiative energy.

In addition to aspect ratio, effects of section factor on the net radiative heat fluxes are also examined here. Figure 3.8 shows the evolution of net heat radiative heat fluxes for steel members with different section factors but with the same aspect ratio. At the initial stage, heat fluxes at inner surfaces as well as at outer surfaces are the same for all the sections due to identical aspect ratio and initial temperature. During later stage, heat fluxes are seen to decrease faster for

steel members with higher section factors. As discussed in Section 3.2.2, this is because these members have smaller equivalent thickness and can be heated up faster (steeper temperature increase) towards equilibrium state. Consequently, according to Eq. (3.4), lower net radiative heat fluxes are expected for these thinner I-sections.

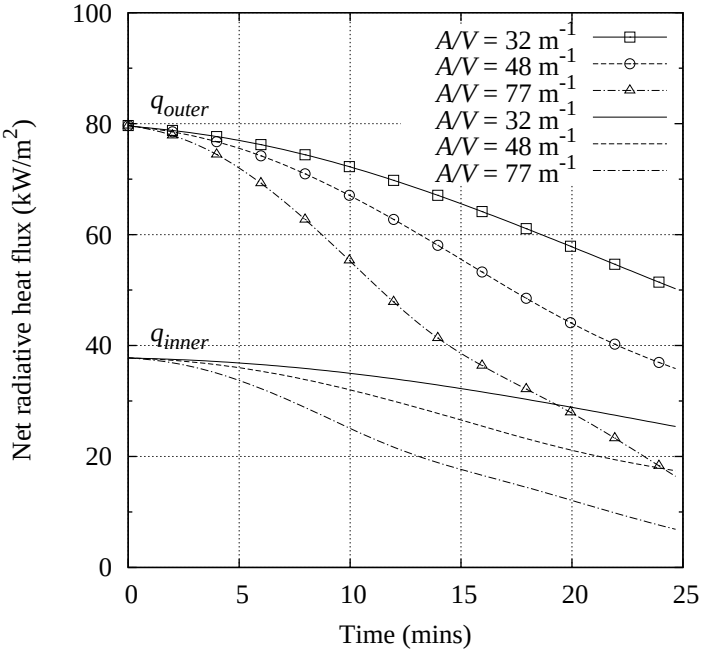

Figure 3.8: Variation of net radiative heat flux with section factors ($E = 100$ kW/m^2, $r = 0.59$, $\varepsilon = 0.8$)

The validation problem studied in Section 3.6.1 is revisited. Figure 3.9 shows the development of net radiative heat fluxes for both the inner and outer surfaces. It is noticed that, due to the geometric effect, q_{inner} is lower than q_{outer} for the entire duration when the steel I-section is exposed to standard fire. The dimensionless heat flux $\tilde{q}$ is relatively stable and is maintained around 0.57, although with slight variations after 15 min. Similar results are also seen in the work in [27].

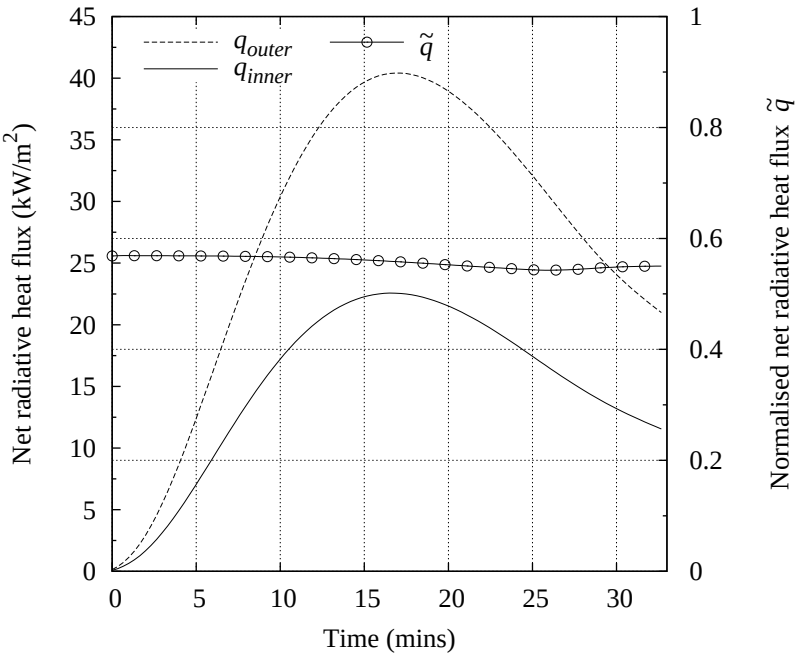

Figure 3.9: Variation of net radiative heat flux for a steel I-section exposed to standard fire ($A/V = 76$ m^{-1}, $r = 0.53$)

3.6.3 Effect of participating medium

In order to examine the combined effects of cavity geometry and participating medium, the steel section UC356 × 406 × 634, which has the largest aspect ratio as listed in Table 3.1, is chosen for the study here.

Specific mean absorption coefficients of the smoke are 0 m^{-1}, 1m^{-1}, 3m^{-1}, 7.5 m^{-1}, 15 m^{-1}, 30 m^{-1}. Using the cavity width as the characteristic length ($L = 188$ mm), the resulting optical thickness ($\tau = \kappa L$) for the first group of absorption coefficients ($0 \sim 3$ m^{-1}) falls in the optically thin region. Accordingly, the second group ($7.5 \sim 30$ m^{-1}) of absorption coefficients is evaluated within the optically thick region. Results in this section are presented for $E = 100$ kW/m^2 only as very similar results were obtained from other levels of emissive power.

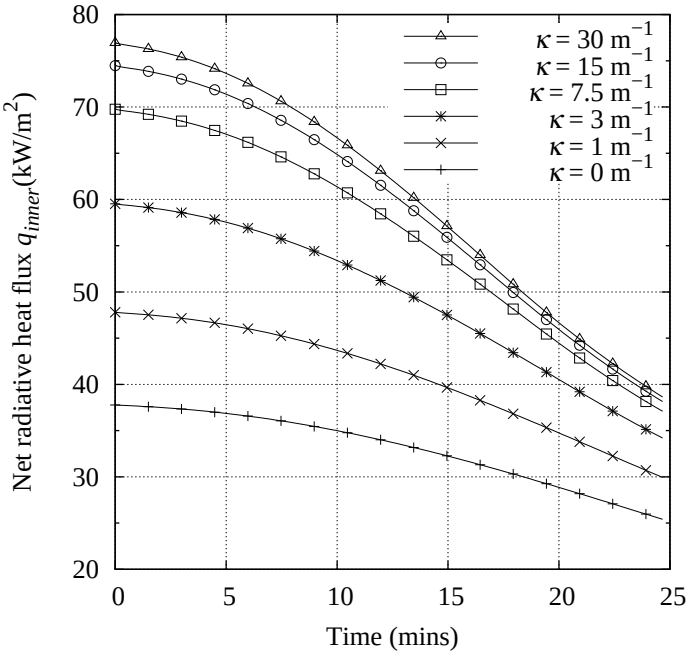

Figure 3.10: Variation of the net radiative heat fluxes for the inner surfaces

Figure 3.10 shows the temporal evolution of the average net radiative heat flux (q_{inner}) for the inner surfaces. It is noted that q_{inner} increases with smoke absorption coefficient. Theoretically, the participating smoke in the cavities attenuates radiative intensities coming from the external fire environment by absorption, while with the opposite effect it also enhances radiative transfer by emission from itself. However, as seen in Figure 3.10, contribution from smoke emission seems to outweigh attenuation since q_{inner} for the radiatively transparent case (with no participating smoke and thus $\kappa = 0$ m^{-1}) is the lowest compared to other cases. q_{inner} is also seen to be more sensitive to absorption coefficient in the optically thin region ($\kappa = 0, 1, 3$ m^{-1}).

Figure 3.11 shows the variation of the normalized net radiative heat flux $\tilde{q}$ as defined in Eq. (3.19). Effects of cavity geometry and participating smoke can be further explored from this figure. With only geometric effect ($\kappa = 0$ m^{-1}),

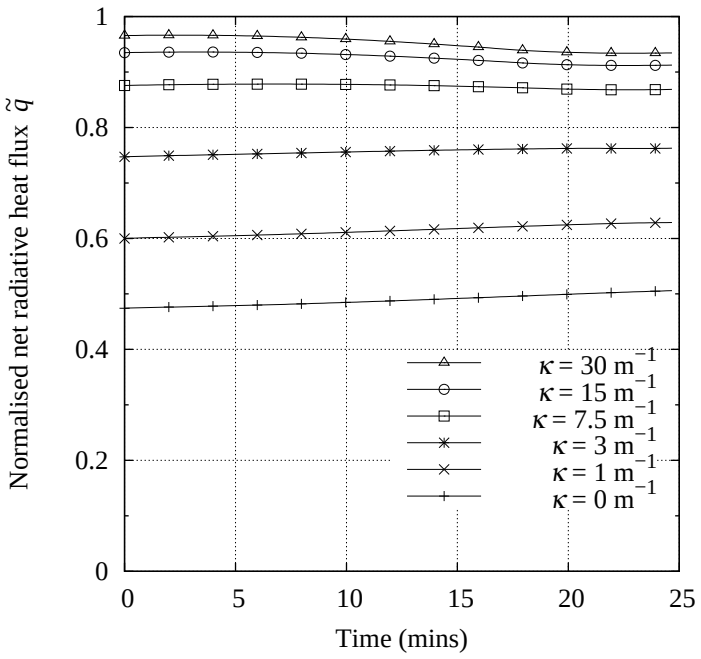

Figure 3.11: Variation of the normalized radiative heat fluxes for the inner surfaces

$\tilde{q}$ is roughly around 0.5, which suggest that the average heat flux at the inner surfaces (q_{inner}) is about 50% of the value at the outer surfaces (q_{outer}). As the smoke becomes more opaque with increasing absorption coefficients, the difference between the two heat fluxes becomes smaller, with $\tilde{q}$ gradually approaching to unity.

Temperatures in the web and flange are plotted in Figure 3.12(a)-3.12(b). The impact of participating smoke on steel temperatures is similar to that on the heat flux as discussed above. Generally, higher temperatures are obtained when the cavities are filled with more opaque smoke (with higher κ), but tend to converge to a relatively close value in the optically thick region. Temperature differences up to 140 ℃ are seen between the most opaque case ($k = 30$ m^{-1}) and the radiatively transparent case ($k = 0$ m^{-1}). Due to smaller thickness, higher temperatures are found again in the web in comparison with those in the flange.

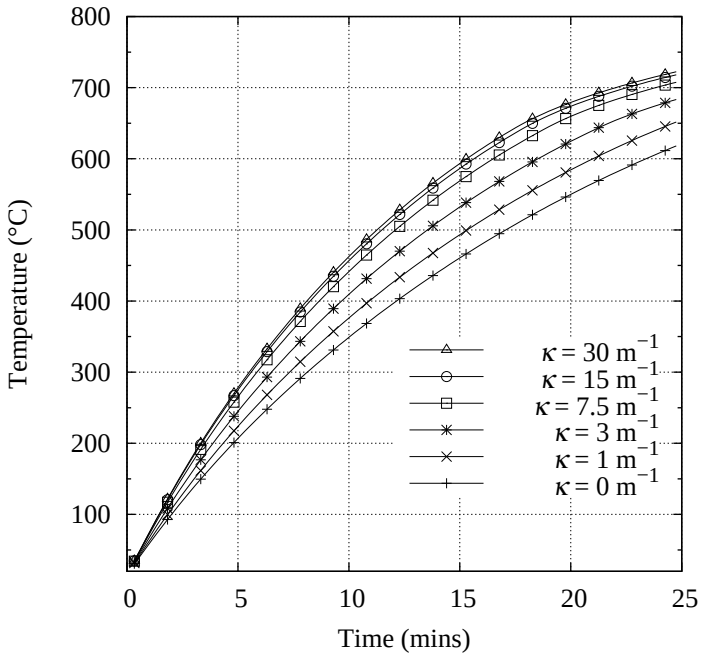

(a) Web

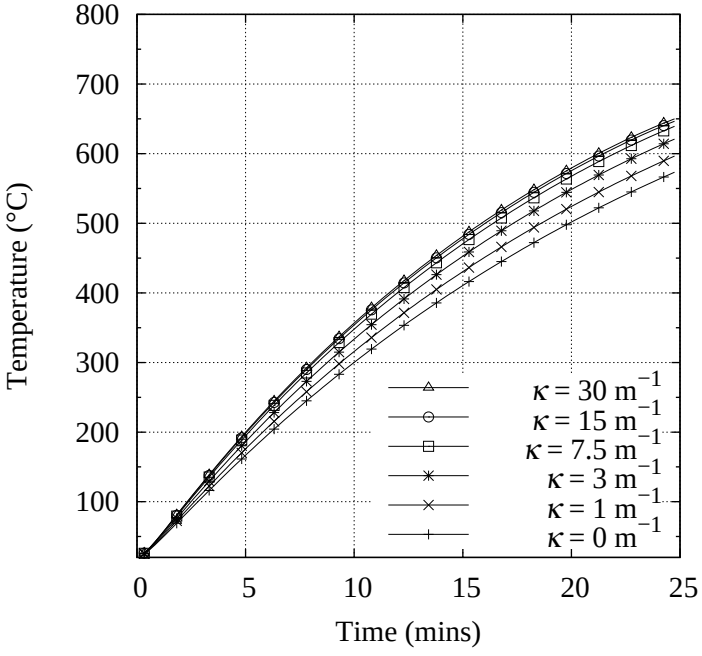

(b) Flange

Figure 3.12: Steel temperatures at different locations ($A/V = 32$ m^{-1}, $r = 0.59$)

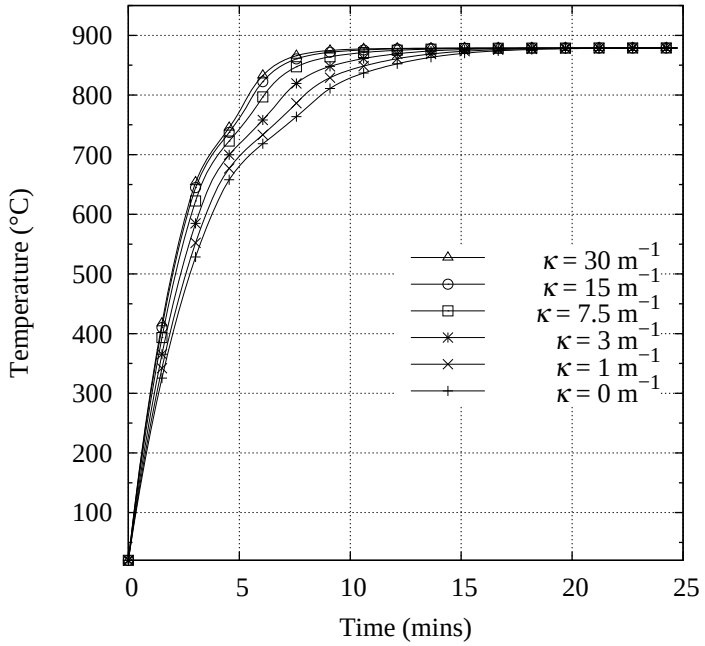

(a) Web

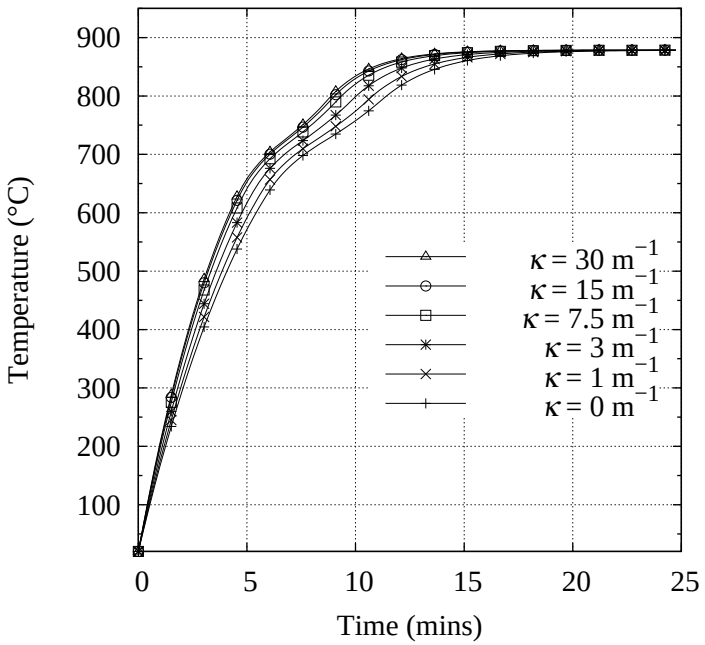

(b) Flange

Figure 3.13: Steel temperatures at different locations ($A/V = 166$ m^{-1}, $r = 0.55$)

Temperature development in steel members with large section factors demonstrates much faster heating rate. As shown in Figure 3.13, temperatures at both the web and flange reach steady state after around 15 min of heating. Due to phase change of steel in the temperature range of 725 $\sim$ 800 ℃ [12], different heating rates are observed during 5 to 12 min. It is interesting to note that, as opposed to the temperature differences in the growth phase, temperatures in the steady state converge to the equivalent temperature (T_{eq} = 879 ℃), irrespective of the variations of smoke absorption coefficient. The convergence of temperatures during this stage can be interpreted as thermal equilibrium between the steel member and its surrounding environment. As a result, the steady state temperature is only related to the fire emissive power.

3.6.4 Comparison with the one-way methodology

The one-way methodology (discussed in Section 3.2.3) akin to those proposed by many other researchers [68, 20, 67] is used here to predict the steel temperatures. Both the one-way calculation and the proposed approach solve the RTE for the open cavities. However, the cavity walls are maintained cold (i.e. T_s = 20 ℃) in the one-way approach, and the incident heat flux obtained from this step is used for the subsequent heat conduction calculation, where re-radiation from the structural surfaces is treated by employing the formula $q = \varepsilon\sigma T_s^4$. Comparisons of steel temperatures are made between the proposed and the one-way methodologies. Our investigation reveals that the temperature difference between the two methodologies are affected by a number of factors. First, although lower predictions are generally seen for the one-way methodology within the period of analysis, much more appreciable under-predictions are found for

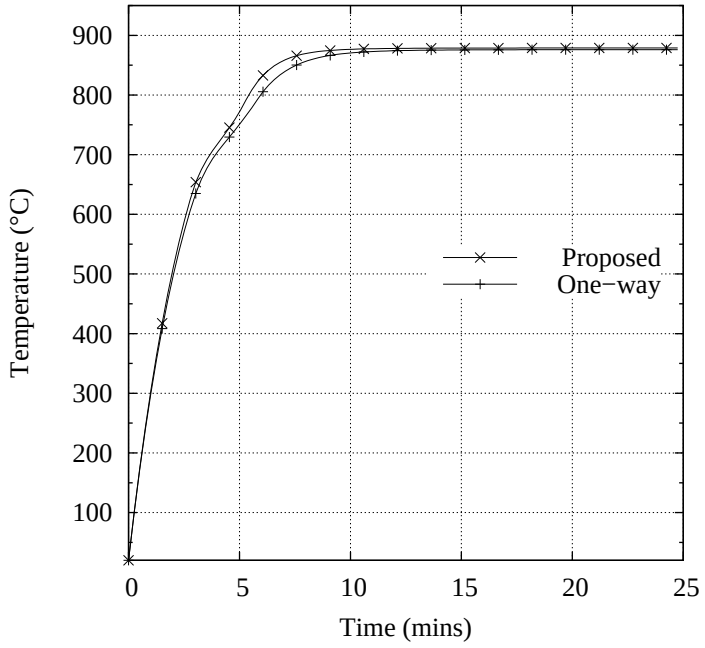

Figure 3.14: Comparison of steel temperatures (at web) calculated by the proposed and one-way methodologies ($A/V = 166$ m^{-1}, $r = 0.55$, $\kappa = 30$ m^{-1})

thinner members (with larger section factors). Second, temperatures predicted by the two methodologies are relatively close in optically thick ($\kappa = 30$ m^{-1}) situations, as shown in Figure 3.14. In contrast, Figure 3.15 shows that larger temperature deviations are observed if the smoke is optically thin ($\kappa = 1$ m^{-1}). The one-way methodology under-predicts temperatures by 80 ℃ for the web and 95 ℃ for the flange. This is expected as in the optically thin situation, the cavity surfaces could "see" each other and radiation between surfaces is important to the net radiative heat flux. On the contrary, the transmittance ($e^{-\kappa L}$) of smoke becomes smaller in the optically thick region, and radiative intensities from one surface to another are significantly attenuated by the smoke absorption. In this case, radiation heat transfer to the structural member is mainly affected by the local smoke temperature.

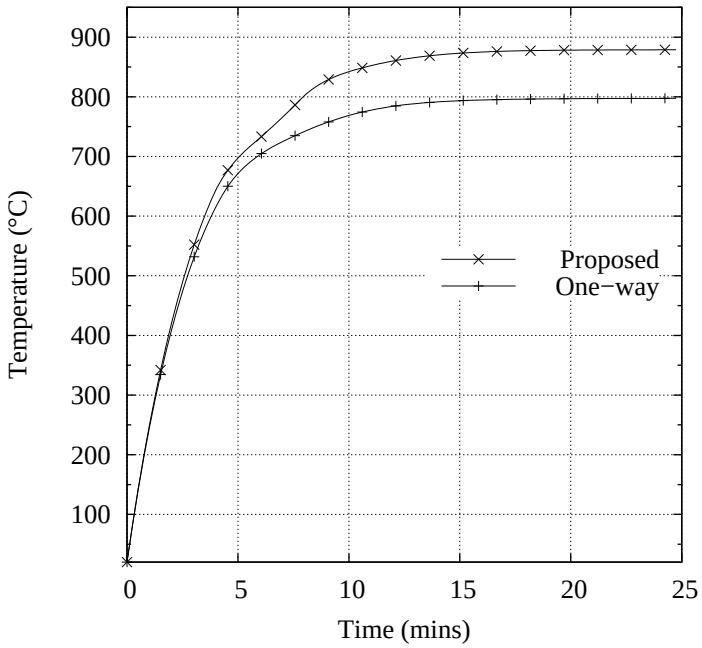

(a) Web

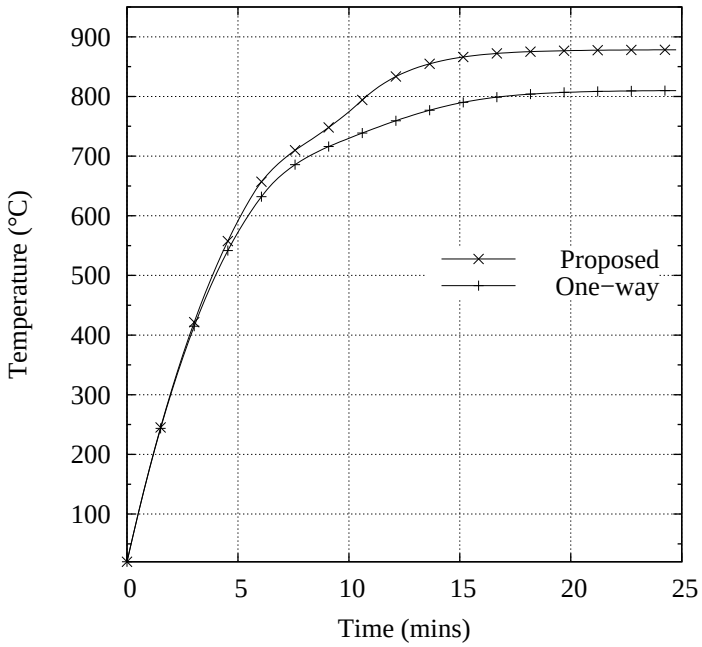

(b) Flange

Figure 3.15: Comparison of steel temperatures calculated by the proposed and the one-way methodologies ($A/V = 166$ m^{-1}, $r = 0.55$, $\kappa = 1$ m^{-1})

Based on the findings discussed above, it can be concluded that the one-way methodology can not accurately predict the net energy gain for I-sections filled with optically thin smoke. This is attributed to the physics of cavity radiation, where the hot cavity surfaces heat each other by radiation and make non-negligible contributions to the total energy gain of the member. However, the one-way calculation simply decouples this process from radiative transfer calculation, and as such, the effects of the self-radiating mechanism is missed. Thus it should be used with care in practice to calculate the radiative heat transfer for structural members with cavities, as the results can be non-conservative.

3.7 Conclusion

A numerical approach is proposed in this chapter to address the coupled heat transfer by radiation and conduction for structural members with cavity geometry. Radiative heat transfer in smoke-filled cavities is solved by FEDOM and heat conduction in the members is solved by the FEM.

This approach is used to model radiative heat transfer to unprotected steel I-sections with symmetrical cavities exposed to post-flashover fires. The coupled heat transfer model is validated with experimental data from standard fire tests. The effects of section geometry (characterized by aspect ratio and section factor) on radiative heat exchange have been confirmed. By defining two spatially averaged radiative heat fluxes, this work quantitatively shows the differences in thermal exposure at inner and outer surfaces of an I-section. Generally speaking, stronger geometric attenuation (i.e. lower net radiative heat fluxes at the inner surfaces) is found in I-sections with larger aspect ratios. In contrast to the

geometric effect, the presence of hot smoke is found to augment radiative transfer by extra emission, and radiative heat fluxes are seen to increase with smoke opacity.

Comparative analysis also shows that the conventional one-way approach could under-predict steel temperatures. Larger under-predictions are found when the cavities are filled with optically thin smoke. More notable under-estimations are seen for steel members with larger section factors. The primary reason for this is that the self-radiating mechanism of I-sections is important in certain circumstances but the one-way approach could not take this into account. These findings are of practical importance for the development of advanced methodologies for calculating fire imposed heat fluxes to structural members.

Chapter 4

Development of a thermal analysis framework in OpenSees

4.1 Introduction

There has been currently a shift from prescriptive design to performance-based design for structural fire safety in many countries [40]. This normally requires greater quantitative understanding of the response of structures subjected to fire, which can be achieved only by considering the fundamental governing principles of fire dynamics, heat transfer and structural mechanics using advanced numerical methods (such as finite element method) [18]. The shift in design paradigm has been undoubtedly propelled by the collapse of the WTC buildings which were designed according to prescriptive code, and by the fact that fire was found accountable for the collapse of this type of tall buildings although there is lack of consensus over the actual collapse mechanisms [97, 2, 98].

Following the collapse of the WTC buildings, a workshop calling upon scientific and engineering experts in relevant fields was held 2002 at National Institute of Standards and Technology (NIST) to identify the research required to underpin meaningful test and predictive methods for analyzing structural performances in real fires. One of the key recommendations from the workshop is to "establish a framework (or more likely a patchwork) of models to couple the fire exposure, the heat transfer, and structural behavior" which incorporates technological advances in structural fire research to support performance-based design alternatives [31]. This area was identified again later as "development of acceptable tools and criteria for undertaking structural fire design", which is among the top ten research and training needs for structures in fire [4, 99]. Generally speaking, there are two categories of software packages used for advanced structural fire analysis, i.e. specialist in-house programs and general purpose finite element (FE) programs [22]. However, it will not be desirable to develop the aforementioned mentioned analysis framework within these two types of programs due to their intrinsic limitations, i.e. the lack of flexibility and long term sustainability of the former owing to small groups of users and developers, and low affordability and thus limited access for the latter because of expensive cost for purchasing and maintenance [7, 66].

As a rational response to the recommendation from the NIST workshop, this work seeks another much more appealing alternative, i.e. developing the above mentioned framework within the OpenSees (Open System for Earthquake Engineering Simulation) platform. OpenSees is an open source object-oriented software framework developed at UC Berekeley and currently supported by PEER (Pacific Earthquake Engineering Research Center). OpenSees has so far focused on providing an advanced computational tool for analysing the non-linear response

of structural frames subjected to seismic excitations. Given that OpenSees is open source (available for free download at `opensees.berkeley.edu`) and has been available for best part of this decade it has spawned a rapidly growing community of users as well as developers who have added to it's capabilities over this period. Furthermore it has an HPC or parallel version for solving large problems on high-performance computing hardware. It therefore represents the largest community of this kind in structural engineering and has the potential to bring together the best structural engineering computational modeling capabilities under one platform accessible to all facilitating new collaborations across geographical boundaries to solve ever more challenging problems. The arguably attractive potential is that of a common community owned research code with a large and growing collection of modelling capability in many areas of structural engineering enabling researchers to collaborate freely and being secure in the knowledge that the fruits of their effort will continue to exist in a living code (until superseded by a better version). Other strengths of the OpenSees framework is the adoption of the object oriented paradigm of software development using C++, which enforces a discipline on the developers and ensures that the framework will develop in a manner that is manageable and easy to maintain and most of the its components are "reusable" by other developers.

The work was initiated in 2009 in Edinburgh towards adding a "structures in fire" modelling capability in OpenSees which will be consistent with the ethos of the other components of OpenSees in terms of being object-oriented and enabling the use of HPC hardware. This chapter presents the work of adding fire and heat transfer modules in OpenSees, as well as relevant verification and validation tests for the developed work.

4.2 Object-oriented programing (OOP) paradigm and OpenSees

From an object-oriented design standpoint, a software system consists of a set of interacting objects rather than a set of interacting functions. An *object* is a collection of data and functions that define the object's attributes and behaviors, and it is the fundamental construct of this design paradigm. The functions that operate on an object's data are referred to as *methods* or *operations*, which are invoked when the object receives a request from another client object. An object encapsulates its data and the implementation details of its methods which are hidden from other objects. This *encapsulation* is one of the key concepts of OOP, which avoids manipulation of crucial data on a global level, and enables the modularity of a large software system.

An object's implementation is defined by its *class*, which specifies the internal data structure of the objects and defines the methods that can operate on its data. An object is an instance of a class, and the instantiation of a class allocates it appropriate data which is bound with the object's methods.

A class may have many subclasses (children) which inherit the data and methods from the base (parent) class. The subclass is also able to extend the functionalities of its base class by redefining the implementations of the base class methods, which realizes code reuse and is referred to as *inheritance* in OOP. The base class may only define a common interface with methods but provides no detailed implementations, and in that case, it is called an *abstract* class. A request to the base class method during run time may be responded differently by the objects of subclasses, which is another key concept of OOP as denoted *polymorphism*.

The Unified Modeling Language (UML) has been widely used for describing object-oriented analysis and design [100]. Two types of essential diagrams, i.e. the class diagram and sequence diagram, are the most important means to illustrate the relationships and interactions between classes.

A class diagram shows the types of objects in the software system and the static relationship among them. Each class is shown in a box with its name (in bold), its methods, and attributes (instance variables). The whole set of methods is also called the *interface* of a class. Abstract classes and methods are written in italicized type while normal type indicates concrete classes and methods. Three types of relationships, i.e. association, generalization (inheritance), aggregation (composition), are shown with different symbols. An association is a solid line between two classes, while generalization is indicated by a line with a triangle pointing to the base class, and aggregation is a solid line with a diamond connecting to the client class. Figure 4.1 shows these graphical notations.

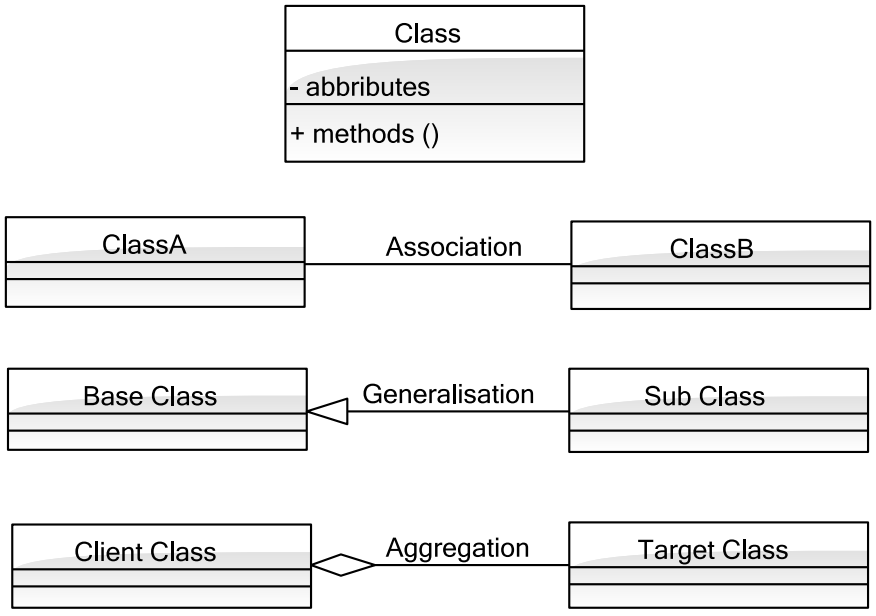

Figure 4.1: Class diagram notations

A sequence diagram captures the dynamic interactions between objects by showing the messages that are passed between them. The interacting objects are placed horizontally on the top of the diagram, each of which is shown with a lifeline that runs from top to bottom. An activation bar is attached to the lifeline when the object is active in the participation. The message passing is shown by an arrow from the calling object to the target object together with the method name. Figure 4.2 shows a simple sequence diagram for clarity.

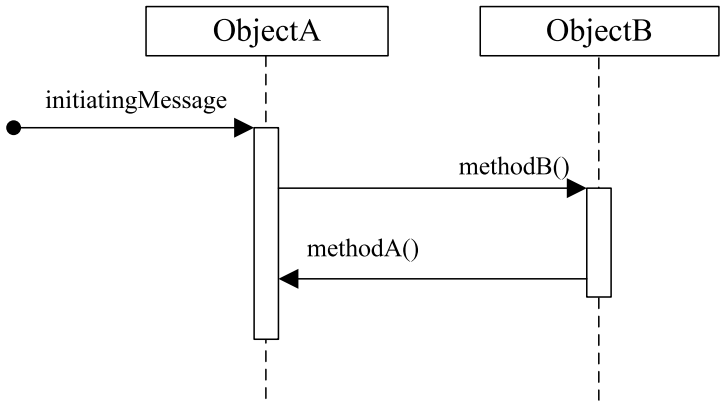

Figure 4.2: Sequence diagram notations

OpenSees is a finite element framework developed using the object-oriented design paradigm as discussed above. It is well designed with computational efficiency, flexibility, extensibility and portability [101, 102]. Figure 4.3 is the class diagram showing some of the high level classes in the framework. Classes such as **Node, Element, SP_Constraint**, **MP_Constraint** and **LoadPattern** are the abstractions of notations relevant to the finite element analysis within the context of structural engineering, which are also referred to as *components* of a FE analysis. A **Domain** object is a repository which holds these components, provides methods to add, query and update the state of these components. An **Analysis** object, which manipulates the FE components held in the **Domain**,

is an aggregation of the mathematical procedures required to solve numerically the equations that govern the structural response. A rich range of matrix storage schemes and algorithms for solving systems of linear equations are also provided in OpenSees. Detailed explanations on these classes and their interactions can be found in [101, 102].

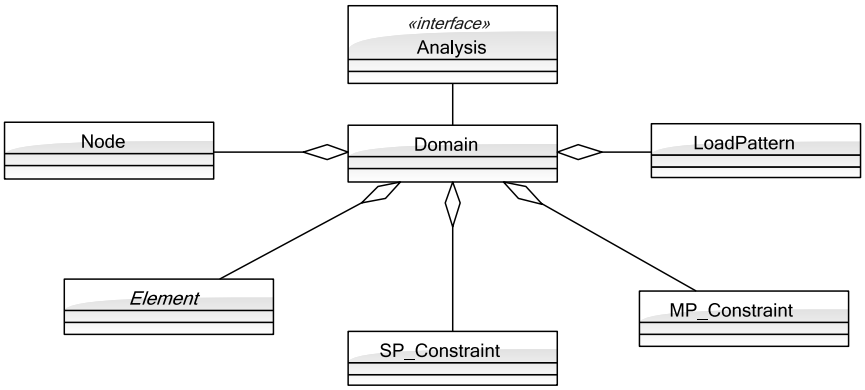

Figure 4.3: Class diagram for the OpenSees framework

4.3 Fire and heat transfer modules developed for OpenSess

4.3.1 Overview of the extended framework

This section presents an overview of the work to extend the OpenSees framework to include a "structures in fire" modelling capability. The development of this capability involves work in the following areas: (1) Fire modelling to provide boundary conditions for the subsequent heat transfer into structural components; (2) Analysis of heat transfer to structural components accounting for thermal property changes at elevated temperatures. (3) Modification of beam and shell

element classes available in OpenSees to develop new classes that account for thermal effects. The third part of work has been addressed by other colleagues in the group [7] and will not be presented here.

Discussions on different fire models relevant to structural fire engineering are presented in Section 2.5, which involve different levels of complexity and accuracy. As an advanced analysis tool for structural fire design, it is important to include a wealth of fire models to aid the design, and offer its users the freedom to select different models in order to meet a consistent level of crudeness in combination with the structural models used. The following models have been implemented in this work to allow a wide range of heterogeneous and homogeneous fire boundary conditions to be applied to the boundaries of the thermal model:

1. Post-flashover compartment fires evolving according to time-temperature curves established in EC 1 [19]. Though simple, this type of fire model is still useful as it represents a comparative method of investigating different fire resistive assemblies and also provides data for verifying computer models [40].

2. Post-flashover natural compartment fires evolving according to parametric time-temperature relationships recommended in EC 1 [19].

3. Localised fires such as isolated burning vehicles in a large car park [103]. The Hasemi empirical model [49, 52] and the Alpert ceiling jet model [55, 56] are the most widely used for this kind of fire scenarios while the former has been formally included in EC 1 [19].

4. Travelling fires for large compartments where flashover is unlikely to occur, and the fire is assumed to burn locally while moving across the whole

compartment. This type of fire was most notably identified in the NIST investigation (based on CFD modelling) of the collapse of the WTC 7 building on September 11, 2001 [71]. A comprehensive review on travelling fires can be found in [6]. It is believed that these type of fires are more likely to occur in modern open plan office buildings with large floor areas. A recent methodology proposed elsewhere [74] has been implemented in this work, and is used to analyse the thermal and structural responses of a composite building in Chapter 5.

The first two types of fire produce spatially homogeneous compartment temperatures where a single temperature is supposed to represent the heating condition for all locations in the compartment at a specific instant of time. The last two types of loading conditions could produce both spatially and temporally non-uniform temperatures/fluxes.

The zone models have not been implemented in the framework, however as will be discussed later, this type of fire models can be readily introduced in the framework in the future due to the well designed interface between the fire and heat transfer modules. The most realistic heterogeneous heating in compartment fires can be produced using a CFD based model. Addition of a full CFD model to OpenSees is not feasible however an interface may be developed in OpenSees to enable a time dependent and non-uniform heat flux boundary condition to be derived from CFD computations.

Once the fire boundary conditions have been determined, the heat transfer to the structural components must be computed to establish the time evolution temperatures within the structure. This is done by adding a 3D conduction

heat transfer modelling capability in OpenSees. In the cases where heat transfer along the longitudinal direction can be neglected, a 2D heat transfer modelling capability for structural sections is also developed, which can save computational resources and offer additional flexibility to users. The finite element method with the solution algorithms discussed in Section 2.4 is used in this work for the development of the heat transfer module.

The modelling of fire and heat transfer as described above enables the most general fire conditions to be modelled in a relatively straightforward manner. The temperature history from the heat transfer module could be stored or recorded for reproduction if only a heat transfer analysis is to be carried out. If a mechanical analysis is to follow, methods are provided to generate a temperature history file for all fibres of beam-column (and slab) fibre elements, which will be discussed in detail in the following section.

In traditional "structures in fire" analysis typically only a one-way coupling is assumed between the heat transfer and the thermo-mechanical analysis, i.e. there is no feedback to the heat transfer calculation from the mechanical analysis, thus the structural deformation is not considered in heat transfer modelling [67]. This assumption is reasonable for the global structural behaviour modelling that is the aim of this work. Local detailed investigation of, for instance, concrete spalling behaviour typically requires a fully coupled thermo-mechanical analysis also including mass transport of multi-phase fluids in the concrete pores, for example [104]. Though important, there is no plan so far to include this kind of analysis in this work.

All the new developments have been validated (presented in Section 4.4) and are to be included in the future general release of OpenSees (by PEER and UC Berkeley)

so that any interested engineer or researcher can use the software framework freely for research purposes. The source code for the new modules is currently accessible in public domain at the University of Edinburgh OpenSees wiki site [105] which hosts all the newly developed code as well as example problems and detailed documentation so anyone can reproduce the results presented in this work.

4.3.2 Implementation in OpenSees

This section introduces the software architecture and the interaction mechanisms of the thermal analysis framework developed in OpenSees, which consists of a heat transfer module and a fire module.

4.3.2.1 Heat transfer module

Figure 4.4 shows the high-level classes for the fire and heat transfer modules. A **HeatTransferDomain** creates the analysis environment for a **HeatTransferAnalysis** object by aggregating components of a finite element model, e.g. **HeatTransferNode**, ***HeatTransferElement***, ***HeatTransferMaterial***, **TemperatureBC**, ***HeatFluxBC*** and ***BoundaryPattern***. Methods to add, remove, query and update the status of those components are provided. A ***HeatTransferAnalysis*** object has to be associated with a specific **HeatTransferDomain** object to perform the heat transfer analysis.

With heat transfer (HT) module developed, OpenSees is capable of solving both two-dimensional and three-dimensional heat conduction problems subjected to transient boundary conditions. This is achieved by using the developed

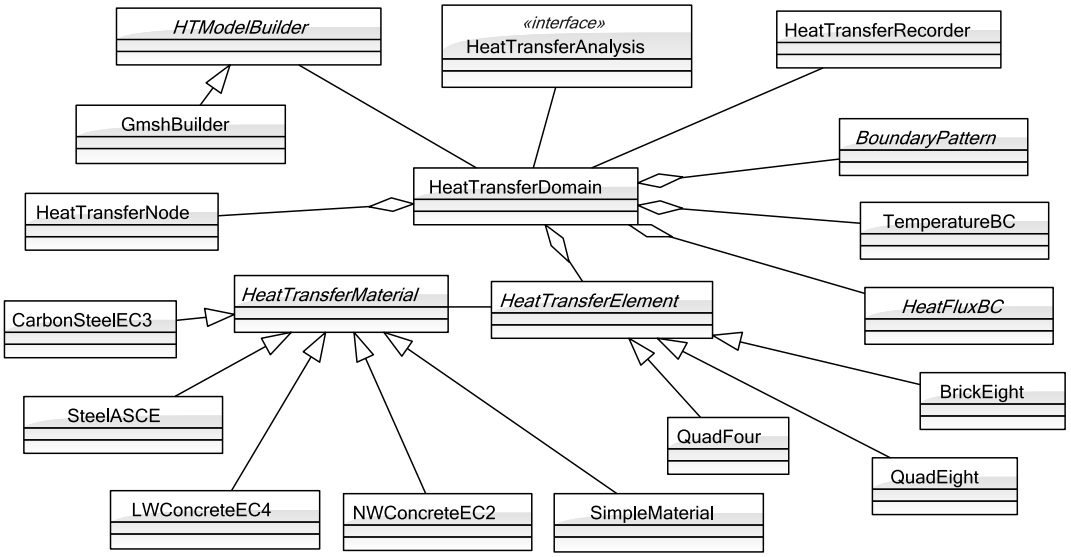

Figure 4.4: Class diagram representing heat transfer FE components

module in conjunction with existing classes in the OpenSees framework, e.g. the solver classes. The HT module works relatively independently but its software architecture resembles the existing one of OpenSees since both of them use the finite element method to solve their own governing equations. This makes it possible to take full advantage of the rapid and continuing development of the OpenSees framework to optimize the heat transfer module in the future.

A ***HTModelBuilder*** object is responsible for creating the objects for the finite element analysis model, and applying the global boundary conditions for a heat transfer analysis. The subclass ***GmshBuilder*** provides implementations based on the mesh generated by the external software application Gmsh, which is an open source and cross-platform finite element mesh generator being downloadable at `http://geuz.org/gmsh/`. It supports both command line driven and GUI-based meshing options, and is designed to provide a fast, light and user-friendly meshing tool with parametric input and advanced visualization capabilities [106, 107]. The interface of ***GmshBuilder*** is shown in Appendix A. It is

also possible to use any mesh formats generated by other packages, provided that appropriate subclasses of ***HTModelBuilder*** are created in the future. A **HTRecorder** object can be used to record the temperature history at a single node or a set of nodes.

```
class HeatTransferNode : public HeatTransferDomainComponent{
 public:
   HeatTransferNode(int tag, int ndof, double Crd1, double Crd2);
   HeatTransferNode(int tag, int ndof, double Crd1, double Crd2,
      double Crd3);
   ~HeatTransferNode();

   // public methods for obtaining the nodal coordinates
   const Vector& getCrds(void) const;
   // public methods for obtaining trial and converged nodal
      responses
   const Vector& getTrialTemperature(void);  // T
   const Vector& getTrialTdot(void);  // Ṫ
   const Vector& getTemperature(void);  // T
   const Vector& getTdot(void);  // Ṫ
   // public methods for updating the trial and converged nodal
      responses
   int setTrialTemperature(const Vector& );
   int setTrialTdot(const Vector& );
   int setResponse(double value, int dof_number);
};
```

Figure 4.5: Interface for **HeatTransferNode** class

The **HeatTransferNode** class is created by modifying the **Node** class in the existing OpenSees framework that was designed for structural analysis. A **HeatTransferNode** corresponds to a specific node in a FE discretization of a heat transfer problem. It encapsulates its coordinates, temperatures and temperature derivatives (in respect to time), with methods to modify and query those quantities also provided. The interface of **HeatTransferNode** is shown in Figure 4.5.

A ***HeatTransferElement*** object represents a specific element in the FE discretization of a heat transfer problem and it is the basic computational unit returning the tangent matrix and residual vector at elemental level. As given in Eqs. (2.16) and (2.17), both the tangent and residual vector can be decomposed into four parts considering contributions from the transient term, conduction, convection and radiation respectively. Methods are designed to support this decomposition for a more flexible architecture which facilitates using different solution algorithms and time integration rules as discussed in Section 2.4.2. ***HeatTransferElement*** is an abstract class and its instantiation relies on its subclasses. Currently the four-noded and the eight-noded quadrilateral elements and the 8-noded brick element are implemented for both 2D and 3D heat conduction problems. The interface of ***HeatTransferElement*** is shown in Figure 4.6. The interpolation functions **N** for the isoparametric elements and the quadrature rules are also encapsulated within each element object. The interpolation functions and Gauss-Legendre quadrature rules given in [16, 37] are used for the current elements.

Each ***HeatTransferElement*** is also associated a ***HeatTransferMaterial*** object, which holds the information on temperature dependent material properties, e.g. thermal conductivity, density, specific heat, and enthalpy. Methods are given to set the trial temperature of the material object and obtain the correct information at a given temperature, as shown in Figure 4.7. ***HeatTransferMaterial*** is an abstract class and its current subclasses include **NWConcreteEC2** (normal-weight concrete), **LWConcreteEC4** (light-weight concrete), **CarbonSteelEC3**, **SteelASCE**, which are implemented according to the material properties given by the Eurocode and ASCE manual as discussed in Section 2.2. **SimpleMaterial** is implemented for the purpose of accepting user given material properties.

```
class HeatTransferElement : public HeatTransferDomainComponent{
  public:
    HeatTransferElement(int tag);
    virtual ~HeatTransferElement();

    // methods dealing with nodes associated with element and face
    virtual const ID& getExternalNodes(void)  = 0;
    virtual const ID& getNodesOnFace(int faceTag) = 0;

    // methods dealing with converged and trial status
    virtual int commitState(void);
    virtual int update(void);

    // methods to return the linearized tangent matrices and
       residual vectors
    virtual const Matrix& getCapacityTangent(void) = 0; // M^{c_p}
    virtual const Matrix& getConductionTangent(void) = 0; // M^{k}
    virtual const Matrix& getRadiationTangent(void) = 0; // M^{r}
    virtual const Matrix& getConvectionTangent(void) = 0; // M^{h_c}
    virtual const Vector& get_Q_Transient() = 0;  // R^{c_p}
    virtual const Vector& get_Q_Conduction() = 0; // R^{k}
    virtual const Vector& get_Q_Radiation() = 0;  // R^{r}
    virtual const Vector& get_Q_Convection() = 0;  // R^{h_c}

    // methods to apply heat flux boundary conditions
    virtual void zeroFlux(void);
    virtual int addPrecribedSurfFlux(PrescribedSurfFlux* theFlux,
       double factor) = 0;
    virtual void applyConvection(Convection* theConvection, double
       factor);
    virtual void applyRadiation(Radiation* theRadiation, double
       factor);
  };
```

Figure 4.6: Interface for **HeatTransferElement** class

Other material models can also be readily introduced by providing subclasses of ***HeatTransferMaterial***.

A **TemperatureBC** object specifies the existence of Dirichlet boundary condition at structural boundaries, while a ***HeatFluxBC*** object specifies Neumman boundary conditions. A ***HeatTransferElement*** object keeps a number of ***HeatFluxBC*** objects acting on its faces and enables imposition of multiple

```
class HeatTransferMaterial: public TaggedObject{
    public:
    HeatTransferMaterial(int tag);
    virtual ~HeatTransferMaterial();

    // methods to update status and obtain material properties
    virtual int setTrialTemperature(double) = 0;
    virtual const Matrix& getConductivity() = 0;
    virtual double getRho() = 0;
    virtual double getSpecificHeat() = 0;
    virtual double getEnthalpy() = 0;
    virtual HeatTransferMaterial* getCopy() = 0;
};
```

Figure 4.7: Interface for **HeatTransferMaterial** class

flux boundary conditions on any of its faces. However, a ***HeatFluxBC*** object can have only one single ***HeatTransferElement*** as its attribute, and can be associated with only one face of this element. Figure 4.8 shows the interface of ***HeatFluxBC*** class, which has three subclasses, i.e. **Convection**, **Radiation** and **PrescribedSurfFlux**. The method ***getTypeTag()*** is provide to differentiate the types of heat flux objects by returning different constant values, i.e. 1 for **Convection**, 2 for **Radiation** and 3 for **PrescribedSurfFlux**.

```
class HeatFluxBC : public HeatTransferDomainComponent{
    public:
    HeatFluxBC(int tag, int eTag, int fTag);
    virtual ~HeatFluxBC();

    virtual void setDomain(HeatTransferDomain* theDomain);
    virtual void applyFluxBC(double factor) = 0;
    int getElementTag(void) const;
    int getFaceTag() const;

    virtual int getTypeTag() = 0;
};
```

Figure 4.8: Interface for **HeatFluxBC** class

Objects of **TemperatureBC** and ***HeatFluxBC*** themselves do not have transient behaviors. Instead, a **BoundaryPattern** class is introduced to bind the **TemperatureBC** and ***HeatFluxBC*** objects with ***TimeSeries*** objects, which are defined in the existing OpenSees framework to specify arbitrary time-varying histories. Figure 4.10 shows the interface of this class. A **BoundaryPattern** can be associated with any number of ***HeatFluxBC*** and **TemperatureBC** objects by invoking ***addTemperatureBC()*** and ***addHeatFluxBC()*** methods. When a request is sent to **applyBCs()**, the **BoundaryPattern** object will invoke the methods **applyTemperatureBC()** and **applyFluxBC()** respectively on the **TemperatureBC** and ***HeatFluxBC*** objects it holds. The relationships between classes for normal transient as well as fire imposed boundary conditions are shown in Figure 4.9.

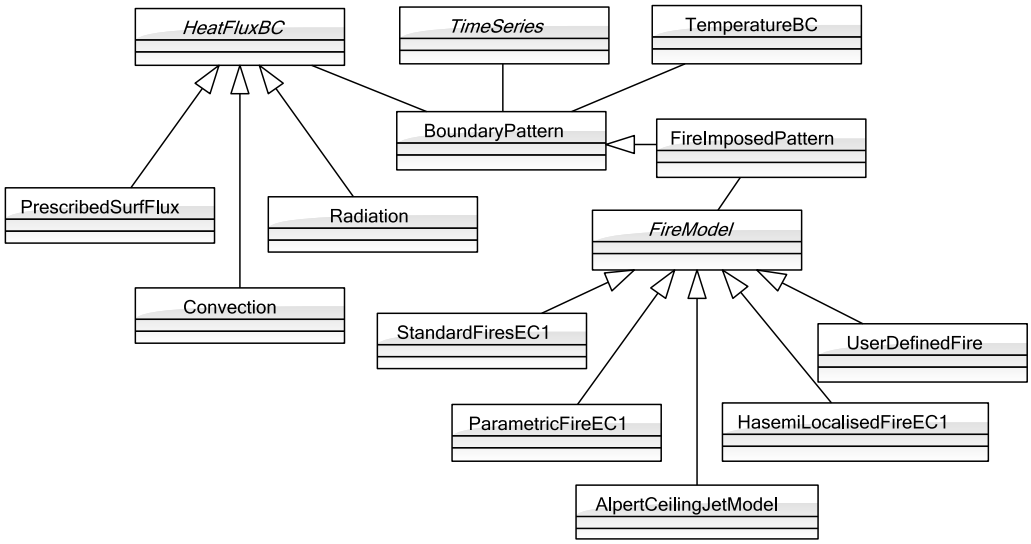

Figure 4.9: Class diagram representing time-dependent boundary conditions and the fire models

The ***HeatTransferAnalysis*** is an interface class (with all methods being abstract), whose subclasses implement the mathematical procedures required to solve numerically the governing equations using the finite element method. A

```
class BoundaryPattern : public HeatTransferDomainComponent{
  public:
    BoundaryPattern(int tag);
    virtual ~BoundaryPattern();

    // method to set the associated TimeSeries and
       HeatTransferDomain
    virtual void setTimeSeries(TimeSeries *theSeries);
    virtual void setDomain(HeatTransferDomain *theDomain);

    // methods to add BCs
    virtual bool addTemperatureBC(TemperatureBC* );
    virtual bool addHeatFluxBC(HeatFluxBC* );

    // methods to apply BCs
    virtual void applyBCs(double time = 0.0);
};
```

Figure 4.10: Interface for **BoundaryPattern** class

HeatTransferAnalysis object is actually an aggregation of objects of other classes defined for the analysis system. The architecture of the analysis system is very similar to the existing one of OpenSees [101, 102], which consists of a range of classes that are slightly modified based on the existing classes in OpenSees for the purpose of heat transfer analysis. The class diagram and the relationships between these classes are further discussed in Appendix B.

4.3.2.2 Fire module

As shown in Figure 4.9 and 4.11, subclass **FireImposedPattern** is implemented to specify the temporal heat flux boundary conditions determined by different types of fire models as discussed in Section 2.5. A **FireImposedPattern** object has a ***FireModel*** object as its attribute which encapsulates the algorithms to calculate the heat fluxes. This approach is also referred to as *Strategy Pattern*

in object-oriented software design [108], which has been widely used in object-oriented finite element implementations [102]. By encapsulating the algorithms in the subclasses of ***FireModel***, this pattern avoids the code duplication and flat class hierarchy that would result from implementing the algorithms by subclassing the **FireImposedPattern** class. In this case, a strategy is a ***FireModel*** and its client is a **FireImposedPattern** object. The encapsulated algorithms are interchangeable at run time and the client object (**FireImposedPattern**) has no need to know the implementation details. This loose coupling makes the **FireModel** class greatly extensible and addition of new models does not require changes in the client classes. In fact, the **FireImposedPattern** class may be considered as an interface between the fire and thermal modules, through which the two modules are able to interact with each other.

```
class FireImposedPattern : public BoundaryPattern{
  public:
    FireImposedPattern(int tag);
    virtual ~FireImposedPattern();
    // method to associate FireImposedPattern with FireModel
    virtual void setFireModel(FireModel* theFireModel);
    // method to apply fire imposed heat fluxes
    virtual void applyBCs(double time = 0.0);
};
```

Figure 4.11: Interface for **FireImposedPattern** class

The interface of ***FireModel*** class is shown in Figure 4.12. Each ***FireModel*** object is also associated with a **HeatTransferDomain** object. The method **applyFluxBC()** is provided to calculate the fire imposed heat fluxes, which is an abstract method and must be redefined by subclasses with detailed implementations. When the method **applyFluxBC()** is invoked, the ***FireModel*** object will calculate the boundary heat fluxes at relevant time intervals and locations, and

then pass the fluxes to ***HeatFluxBC*** objects by invoking corresponding methods on these objects. Some fire models (e.g. localized fires) need geometric information of the target location to determine the fluxes. This can be obtained from the associated ***HeatFluxBC*** object which carries an element tag and a face tag, with which the locations of target element faces are determined.

```
class FireModel{
    public:
    FireModel();
    virtual ~FireModel();

    virtual void setDomain(HeatTransferDomain* theDomain);
    virtual void applyFluxBC(HeatFluxBC* theFlux, double time) = 0;
};
```

Figure 4.12: Interface for **FireModel** class

The discussions so far have mainly centered around the two class diagrams in Figures 4.4 and 4.9, which show the static relationships between the classes. It is also interesting to see the run-time interactions between the objects using the sequence diagrams as introduced in Section 4.2. Figure 4.13 shows the sequence diagram between the fire and heat transfer modules. As can be seen in the figure, when the message **applyBCs()** is invoked, the **HeatTransferDomain** object will initiate the homonymic method on the **FireImposedPattern** object, which iterates over all the ***HeatFluxBC*** objects held by the **FireImposedPattern**. Once the **FireModel** object receives the **applyBCs()** message, it passes the surrounding temperature T_a and the irradiation (incident radiation flux) q_{ir} to the **Convection** and the **Radiation** objects respectively, which then bind themselves onto the lists held by the elements. The lists of ***HeatFluxBC***s will be needed when forming the elemental tangent matrices and residual vectors in the subsequent operations. It is clear from this figure that the execution of an initial

method call is followed by a number of distributed messages passing between the collaborating objects, which is a typical style of OOP benefiting the extensibility, flexibility and maintenance of large software systems [101, 102, 109, 100]. For example, due to the loose coupling between classes achieved with this approach, the addition of a new subclass for **FireModel** (such as an interface for processing CFD results or a RTE solver handling complicated radiative transfer in structural cavities as used in Chapter 3) would require only minor or even no changes of the interfaces of other classes. This is particularly important to leave a well-designed interface open as there is a rapid change of design fires for structural safety in the recent years.

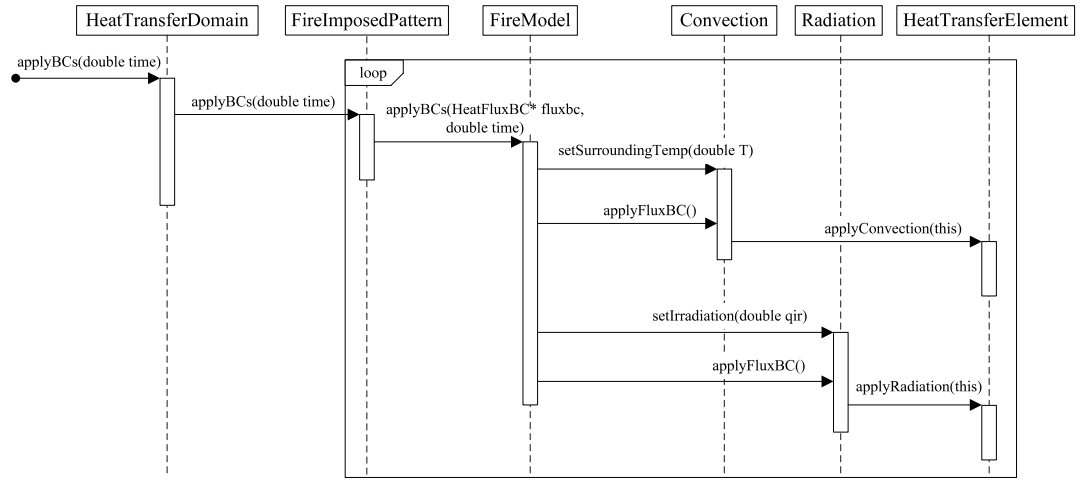

Figure 4.13: Sequence showing the interaction between the fire and heat transfer modules

4.3.2.3 Interface between heat transfer module and structural module

Perhaps the beam/column elements are the most widely used for structural modelling due to their high accuracy and efficiency. Each element has a section definition which may be further divided into several fibers in order to account for

the effect of temperature gradient across the structural section [110, 111], where each fiber can take a specified temperature value.

```
class HTSTRCInterface{
public:
  HTSTRCInterface(int numNodes, int numDim, HeatTransferDomain*
     theDomain);
  virtual ~ HTSTRCInterface();

  // return the node number for a given point
  int getClosestNode2D(double x, double y);
  int getClosestNode3D(double x, double y, double z);

  // return the node numbers in a boxed region
  const ID& getNodesInRegion2D(double x1, double x2, double y1,
     double y2);
  const ID& getNodesInRegion3D(double x1, double x2, double y1,
     double y2, double z1, double z2);
};
```

Figure 4.14: Interface for **HTSTRCInterface** class

The most straightforward way to pass the heat transfer results to structural analysis is to record a number of temperatures over the section. Then the structural model generates the desired temperatures for each fiber by interpolating these temperatures obtained from the heat transfer analysis [112, 78]. This capability has also been included in the current version of extended OpenSees, which is able to receive up to 9 temperature points across the depth of a section [7]. It is an efficient way to follow if a 2D heat transfer analysis is performed for the structural section. In the case of a 3D heat transfer analysis, the data transmission is not so straightforward due to the increased level of complexity caused by the different meshes used in the structural and heat transfer modelling. It is desirable to efficiently locate relevant nodes in a heat transfer analysis to produce the temperatures needed by the fiber sections in a structural analysis. This problem may be addressed by using efficient searching algorithms based on

the K-D tree data structure [113]. For this purpose, the class **HTSTRCInterface** is developed while its implementation is based on the work presented by Michael at MIT [114], and its interface is shown in Figure 4.14. A **HTSTRCInterface** object is associated with a **HeatTransferDomain** object, and it creates a K-D tree at its instantiation for all the nodes held in the domain. Methods for the searching in both 2D and 3D spaces are provided. The **getClosestNode3D()** returns the nodal number which suggests the closest node to the specified point and is subsequently used to record the temperature for for that point. The **getNodesInRegion3D()** returns all the nodes which are located within the 3D region bounded by a fiber and are used to produce an average temperature for that fiber. All these operations are performed only once before the heat transfer calculation.

It is also highly desirable that the temperature profile from a heat transfer mesh using continuum elements can be automatically mapped to a structural mesh using beam-column elements [7]. Although the interface currently developed does not provide such an advanced functionality, the methods implemented still provide some convenience when seeking collaboration between heat transfer and structural analyses, and it has laid down essential foundations for further development towards automatic data mapping and exchange.

The thermal analysis framework developed hereto consists of a large number of classes being newly developed or modified from the existing OpenSees framework. A complete list of these classes is shown in Appendix C.

4.4 Verification and validation of the framework

The work of verification and validation is required in the process of seeking numerical solutions to complicated physical problems. The verification is viewed as a low level activity which checks if a model implementation accurately represents the developer's conceptual description of the model and the solution to the problem, while the validation is a high level activity which determines the degree to which a model is an accurate representation of real world problems [21]. In this section, the thermal module discussed in the foregoing context is first verified through three benchmark tests where analytical solutions are available. These problems may not be realistic from fire engineering point of view, but their relative simplicity makes it possible to assess the correctness of the numerical algorithms by comparing with the analytical solutions. The modules are then validated against experimental data from large scale fire tests [115, 116].

4.4.1 Verification with analytical solutions

The first problem examined is a bar of 0.1m in length with a fixed temperature at its left end (T_L) and with sinusoidal temperature changes at its right-end (T_R), where $T_L = 0$ ℃ and $T_R = 500sin(\pi t/40)$ ℃. This example was also also used in [16] to examine the general performance of the solution procedures of a finite element program and its transient modelling capability in particular due to the rapid temperature changes at the right end of the bar. The initial temperature of the bar is at 0 ℃. For the sake of clarity, constant material properties of steel is assumed here, i.e. $\rho = 7850$ kg/m^3, $c_p = 600$ J/kg·K, $k = 54$ W/m·K. The problem is modelled using four-noded and eight-noded quadrilateral elements as

well as 8-noded brick element together with a backward difference time-integration scheme. A depth of 0.02 m is assumed for the bar when using 2D elements while a cross section of 0.02 m×0.02 m is assumed when using the 3D brick element. The bar is uniformly discretised into 10 elements along its length, and the time step used is 2 seconds for all the cases. The analytical solution of the transient

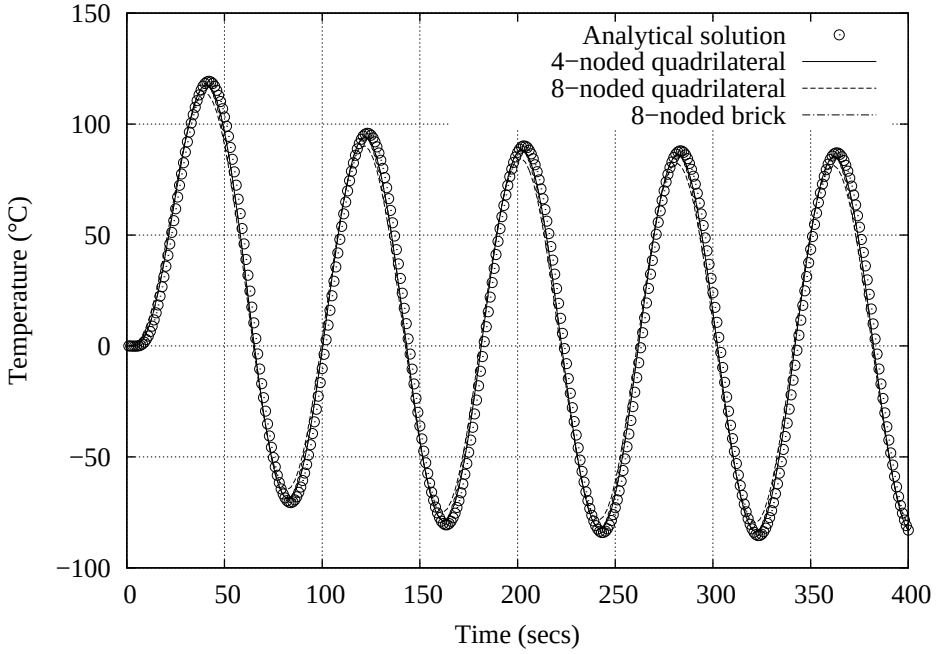

Figure 4.15: Analytical solution and FEM solution of the temperature development at a target location

temperature development at any location in the bar was presented in [16, 117]. Figure 4.15 shows the the temperature history at a target location at a distance of 0.03 m from the right end. It can be seen that, although the 8-noded element which uses quadratic interpolation functions produces slightly larger deviation at the peaks, the FEM results using all three types of elements generally agree well with the analytical solution. This example demonstrates that the thermal module developed is able to accurately deal with transient heat conduction problems with rapid changes of boundary conditions.

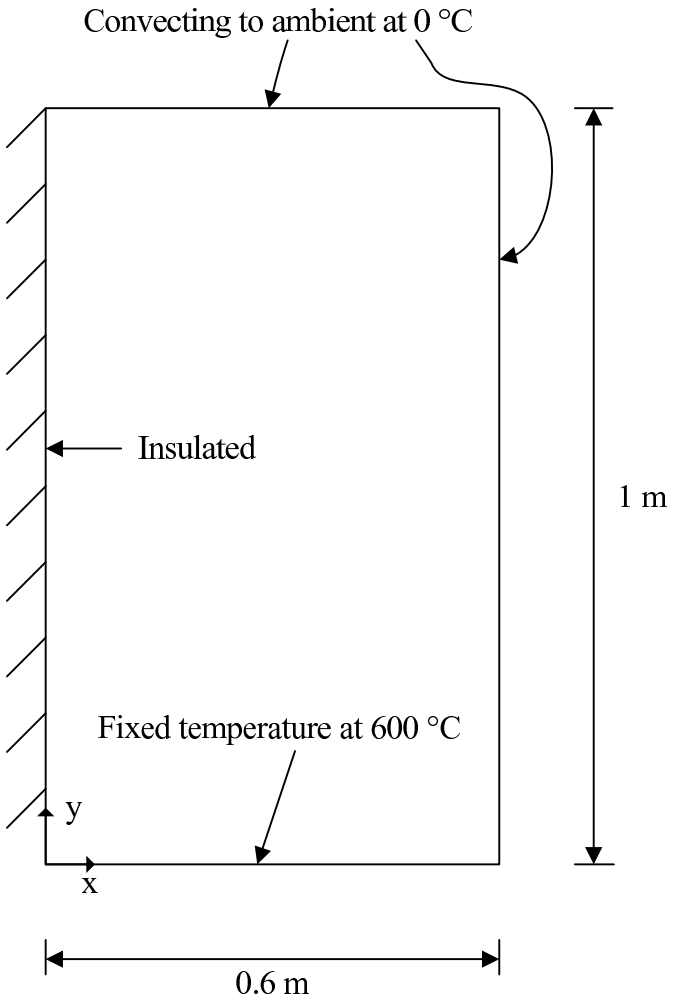

Figure 4.16: Heat transfer in a two-dimensional steel plate with discontinuous boundary conditions

The second problem examined involves heat transfer in a two-dimensional domain with strongly discontinuous boundary conditions, which was also used in [16] for the verification purpose. The problem definition was shown in Figure 4.16, where a fixed temperature is specified for the bottom surface and the insulation boundary condition ($q = 0$ W/m^2) is specified for the left surface. The other two surfaces are subjected to a convective boundary condition with ambient temperature at 0 ℃. A convective heat transfer coefficient of 35 W/m^2·K is used here, which is recommend in [19] for heat transfer calculation in natural fires. Material properties for steel are used as specified in the first benchmark problem above.

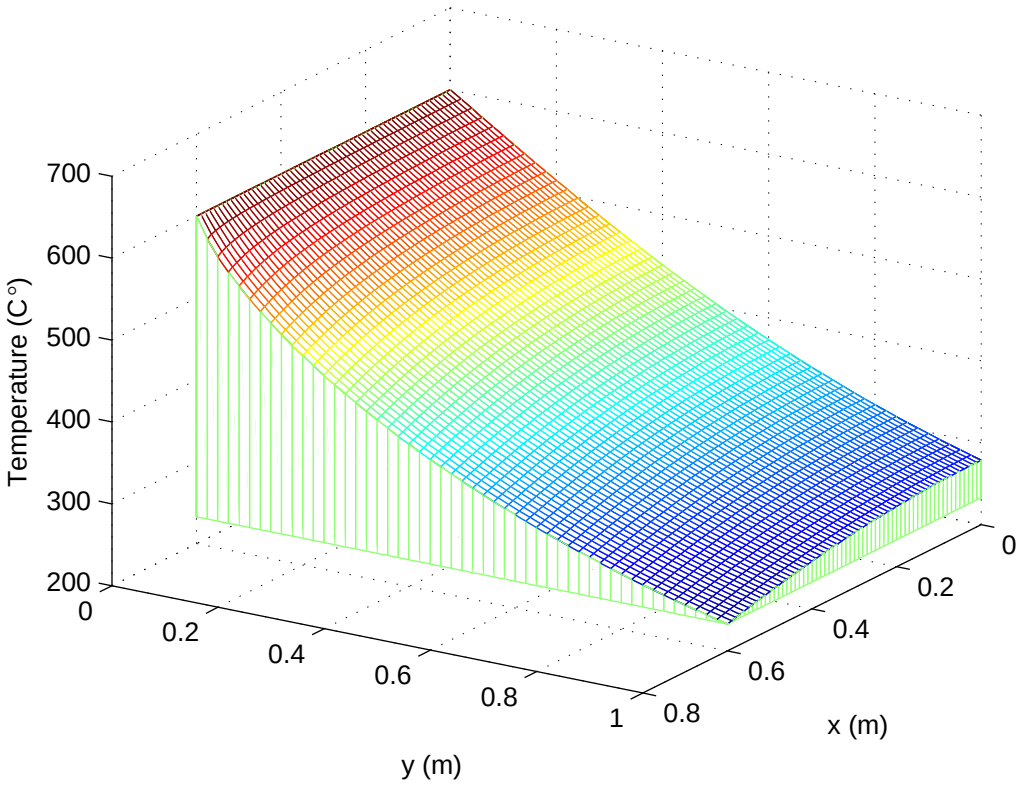

Figure 4.17: Steady state temperature obtained from the analytical solution

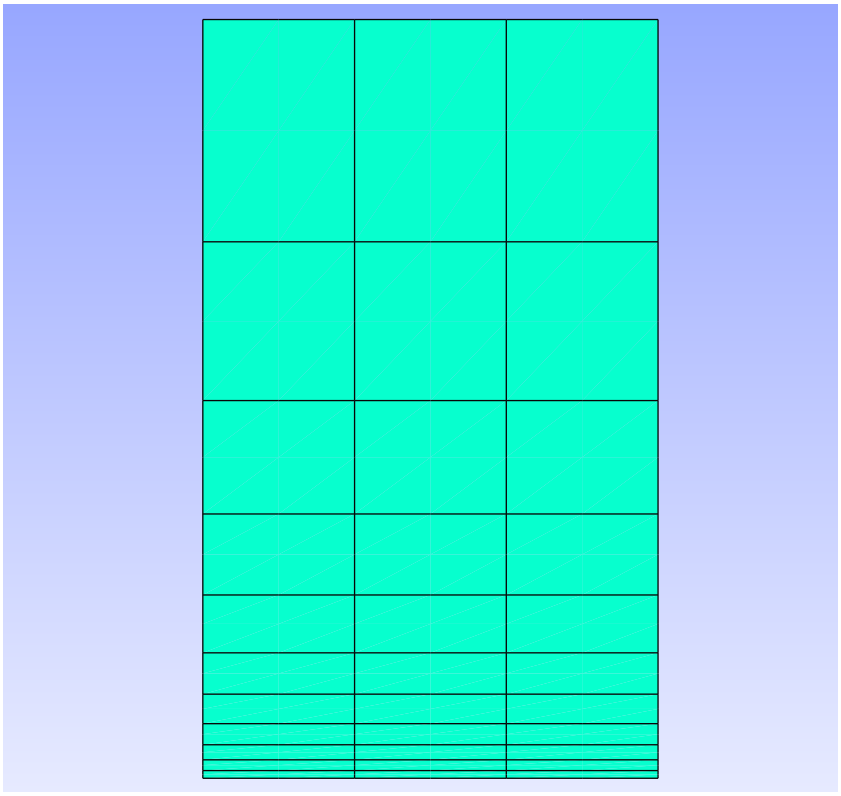

(a) 2D 4-noded/8-noded elements

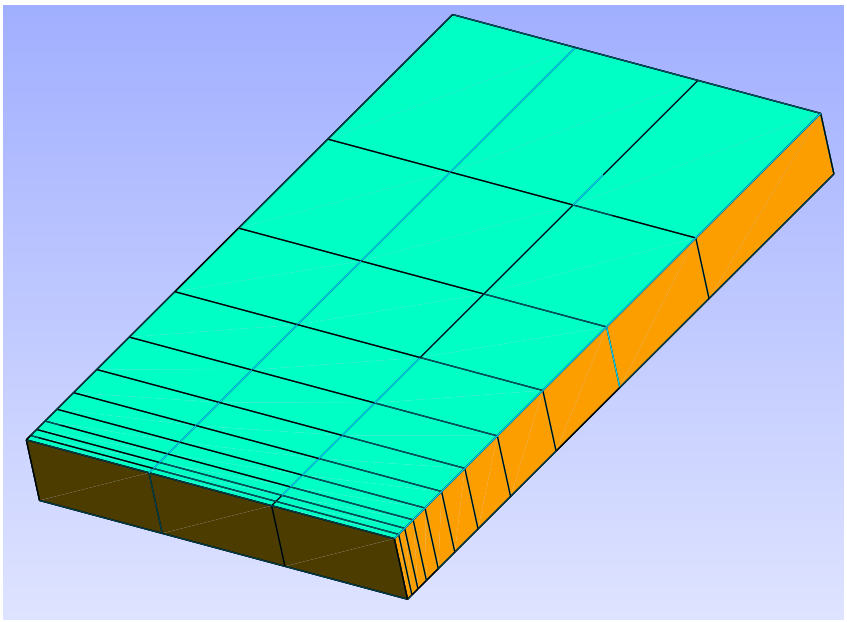

(b) 3D 8-noded elements

Figure 4.18: Finite element mesh used in the modelling

The analytical solution to this problem was given in [16, 117]. Figure 4.17 shows the steady state temperature for the whole domain using the analytical solution, which suggests a sharp temperature gradient around the bottom right region where a discontinuity of boundary conditions exists between the two boundary surfaces. Therefore, biased (towards the bottom surface) finite element meshes are used in the modelling as shown in Figure 4.18. A depth of 0.1 m is assumed for the plate when using the 3D 8-noded elements. The steady state FE solution is obtained using the transient algorithms with a time step of 30 seconds. Figure 4.19 shows the predictions and analytical solutions for the steady state temperatures at the right side of the plate. It can be seen that the FE results agree with the analytical solutions very well, and the large temperature gradient along the right-side boundary is accurately captured although relatively coarse meshes are used in the finite element modelling.

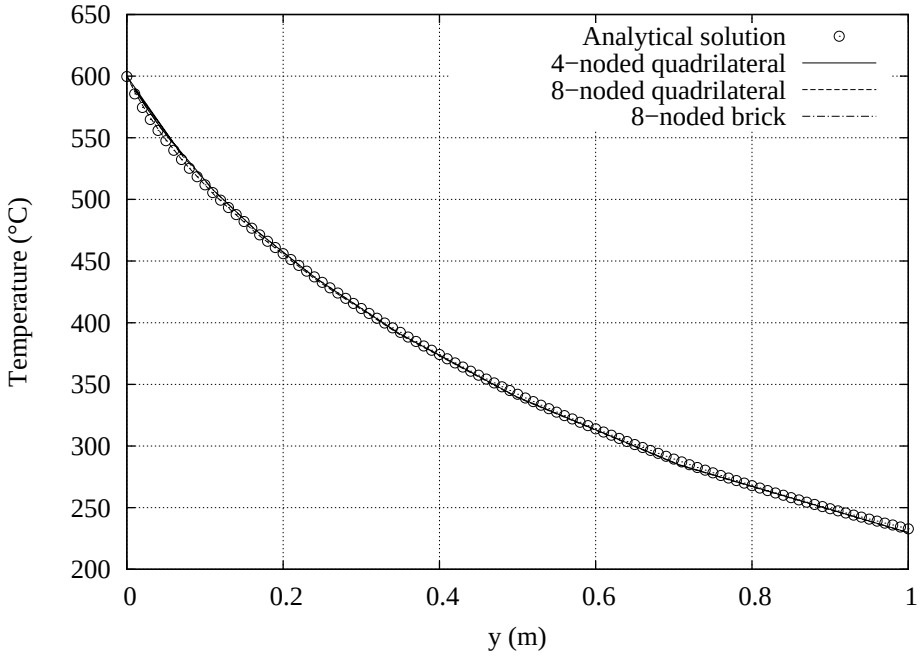

Figure 4.19: Analytical solution and FEM solution of the steady state temperature distribution along the right-side boundary

The last benchmark problem is used to assess the algorithms implemented to model the the phase change phenomenon. As discussed in Section 2.2, phase change is commonly seen in construction materials at high temperature (such as concrete with moisture content, carbon steel), where a drastic change of specific heat occurs within a narrow temperature band. Modelling heat transfer with direct evaluation of heat capacity would encounter numerical difficulties due to the large value of latent heat within the temperature band. The *apparent heat capacity method* (or *enthalpy method*) (see Section 2.2) is normally used to address this problem, which approximates the heat capacity with several averaging methods as given by Eq. (2.5).

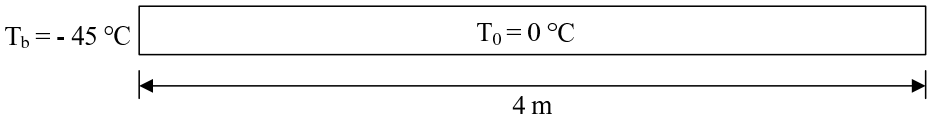

Figure 4.20: Configuration of a bar undergoing isothermal phase change (solidification)

The problem considered here is for isothermal phase change (solidification) of a bar as shown in Figure 4.20. This problem is widely used in existing publications as a standard test example for isothermal phase change [16, 118, 119], and its analytical solution is available in [16, 117]. Numerical parameters required for this problem include $\rho = 1.0$ kg/m^3, $c_p = 1.0$ J/kg·K, $k = 1.08$ W/m·K, $T_f = -0.1$ ℃, $L = 70.26$ J/kg, where T_f and L are the freezing temperature and latent heat of the liquid respectively.

As suggested in [16], a temperature range for the evolution of the latent heat is normally needed when using the *enthalpy method*. A 5 ℃ temperature range is used here to approximate the isothermal phase change. Figure 4.21 shows the actual variation of the enthalpy and the approximated changes within the

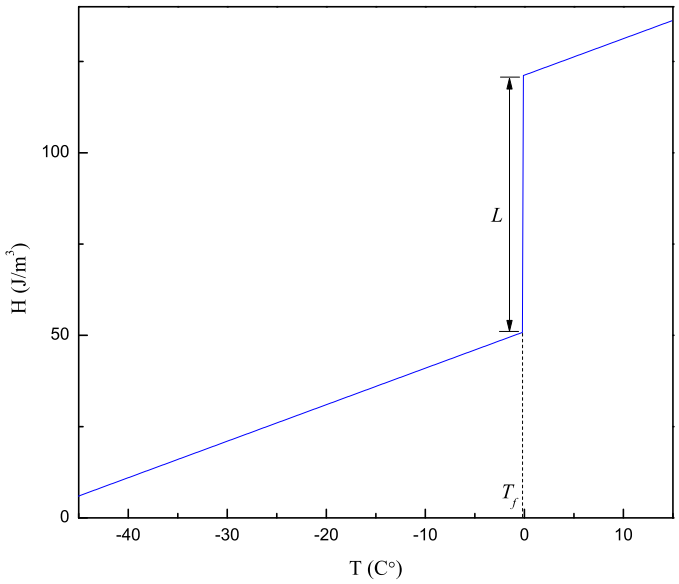

(a) Actual enthalpy

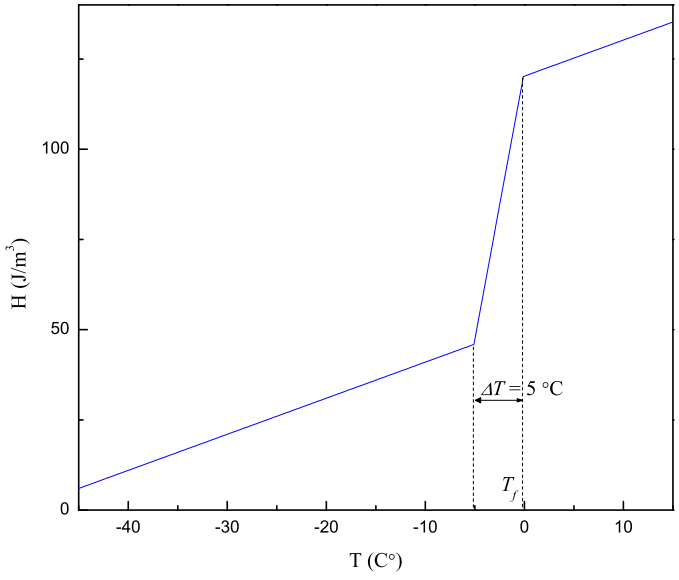

(b) Approximate enthalpy

Figure 4.21: Variation of enthalpy with temperature

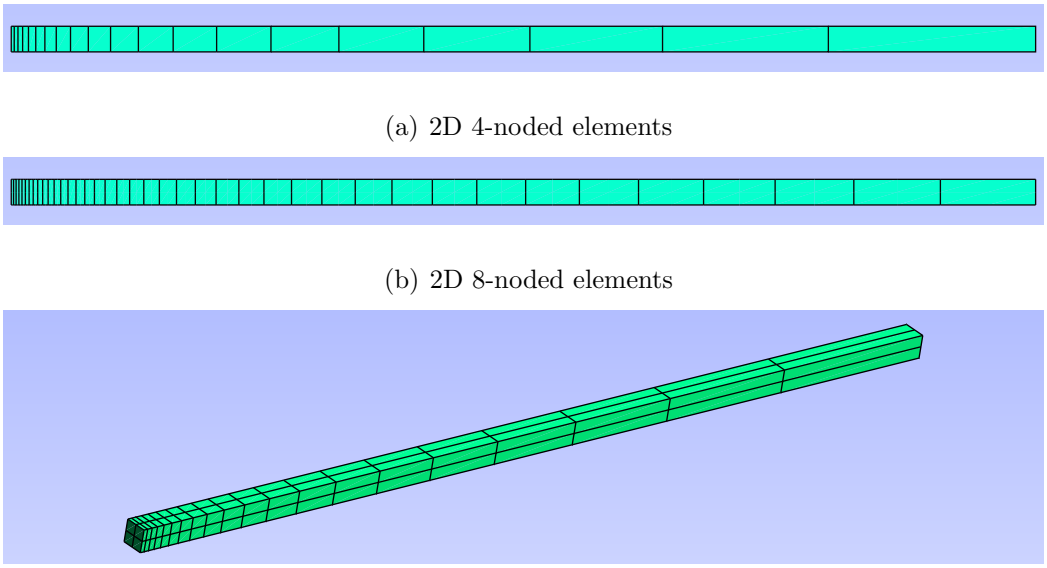

(a) 2D 4-noded elements

(b) 2D 8-noded elements

(c) 3D 8-noded elements

Figure 4.22: Finite element mesh used for the phase change modelling

temperate range. Smaller temperature interval would represent more accurately the isothermal changes, but also requires much finer time steps and spatial discretization according to the numerical tests carried out in this work. The finite element mesh for different elements is shown in Figure 4.22, where the mesh is refined towards the left end due to large temperature gradient in that region. A depth of 0.1 m is assumed for the bar when using 2D elements while a cross section of 0.1 m×0.1 m is assumed when using the 3D brick element. The transient temperature development at 1 m from the left end is examined, and the FE results are compared with the analytical solutions as shown in Figure 4.23. The modelled results are seen to agree with the analytical solutions with satisfactory accuracy except those during $0.5 \sim 1$ seconds. This is because that the material starts the isothermal solidification process at the freezing temperature (T_f) during this time interval, but the isothermal change is approximated with a 5 ℃ temperature interval in the modelling as shown in Figure 4.21. The results

can be improved if a smaller temperature interval is used but at the cost of much more computational resources due to correspondingly smaller time steps and finer FE meshes. In fact, this example represents a severe test as phase change with a relatively wide temperature interval, rather than isothermal change, is more commonly seen in structural members subjected to fire. It is also noted that the 8-noded quadratic element is not as efficient as other linear elements to address the phase change problem here, since it requires much finer meshes and an order of magnitude smaller time step to achieve similar level of accuracy as other elements.

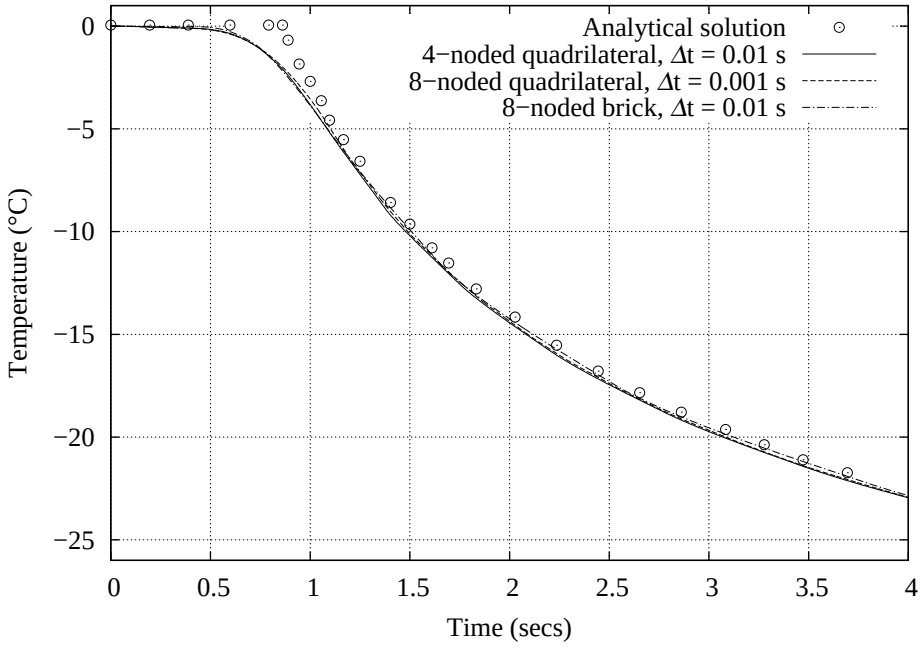

Figure 4.23: Analytical solution and FEM solution of the temperature development at the target location

4.4.2 Validation with experimental data

This section presents the validation work by comparing the predictions from the extended OpenSees framework (for both the fire and the heat transfer modules) with data obtained from full-scale fire tests which were carried out at the Building Research Establishment's (BRE) Cardington laboratory in the UK [115, 116]. These fire tests have provided a wealth of information about the thermal responses of full scale structures in fires, some of which have been investigated using other finite element packages [120, 121]. In the interest of validation, measured temperatures from Test 1 (restrained beam test) and Test 2 (2D plane frame test) are used here.

In Test 1, a composite beam (UB305×165×40) was heated up along its length by a gas fired furnace built to its underside. The complete set of temperature measurements recorded in the beam and surrounding structure was extensive. The temperatures in the steel beam were recorded at many points along its length and through the depth but the temperatures in the slab were only recorded at limited locations. Figure 4.24 shows the thermocouple locations on two beam sections (GD 3 and GD 4), where the numbering of thermocouples follows the convention used in [115]. As in [120, 121], the surrounding fire temperatures as near as possible to the section of the member where the selected thermocouples were located was used as the boundary conditions for the subsequent heat transfer modelling, i.e. the temperatures of thermocouples 150-153 for the section at GD 3 and thermocouples 154-157 for section at GD 4. Although the location of the adjacent surrounding thermocouples was some distance from the surface of the member, it is found that the local temperature variations at those thermocouples were small and the surrounding temperatures were sufficiently representative of

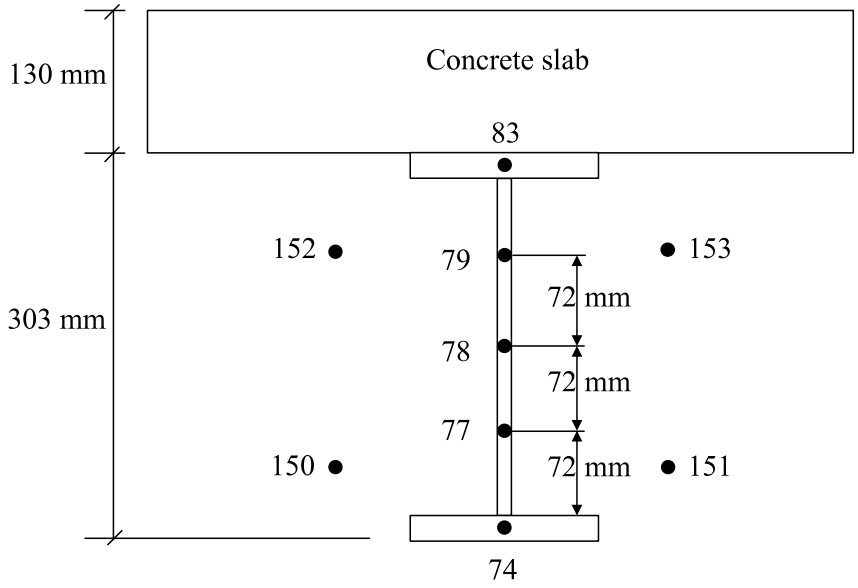

(a) GD 3

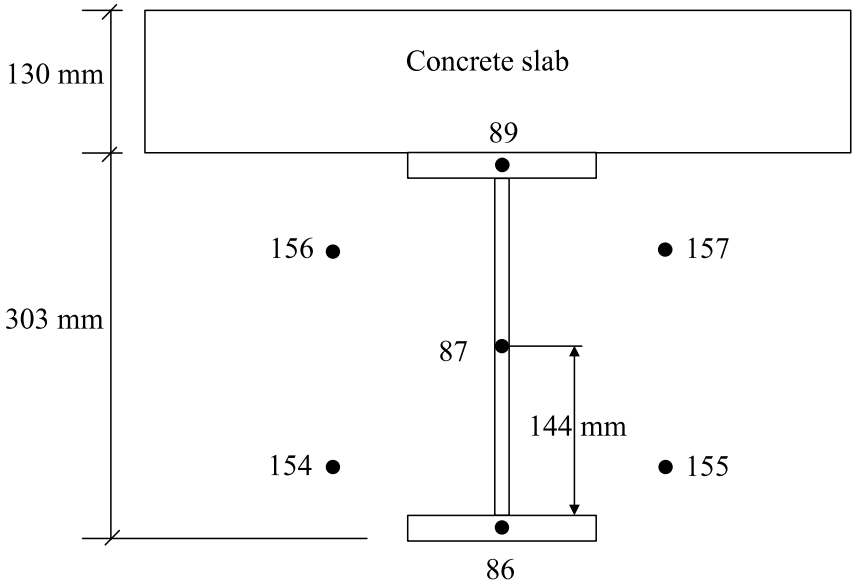

(b) GD 4

Figure 4.24: Thermocouple locations in the beam sections and surrounding fire environment

the member's thermal exposure as shown in Figure 4.25. The finite element model of the beam section is shown in Figure 4.26, where the concrete slab on top of the beam is included in order to account for the heat sink effect. It is assumed that the 0.9 mm thick metal deck between the beam and the slab would not significantly affect the heat transfer and thus it is not included in the finite element model.

The temperature-dependent material properties of steel are taken from [13] and the phase change happening around 735 ℃ is included. The thermal properties for the concrete slab are taken as those for light weight concrete, i.e. $\rho = 1900$ kg/m^3, $c_p = 840$ J/kg·K and temperature dependent thermal conductivity according to [122]. The top surface of the concrete slab is assumed to be exposed to ambient environment of 7 ℃. The bottom surface of the slab and three sides of the beam are exposed to the fire with temperatures at appropriate surrounding locations as suggested in Figure 4.24. The convection coefficients for fire-exposed surfaces and unexposed surfaces are taken as 25 W/m^2·K and 4 W/m^2·K respectively [13]. An emissivity of 0.7 is specified for the concrete slab and 0.9 for the steel beam. As discussed in Chapter 3, the calculation of radiative heat transfer from fire to steel I-sections can be complicated due to the presence of two open cavities. However, this effect is not considered here as the aspect ratio of the cavity is relatively low ($r = 0.28$), which means that the geometric attenuation of radiative heat fluxes at the inner surfaces is not prominent (see [30] or Chapter 3). The transient analysis starts at the initial temperature of 7 ℃ and with the backward difference time integration scheme at a time step of 30 seconds.

Figure 4.27 shows the comparison of predicted steel temperatures with the measured values. It is first noted from the measured data that the temperatures at the top of the flange are generally lower (up to 100 ℃) than the temperatures

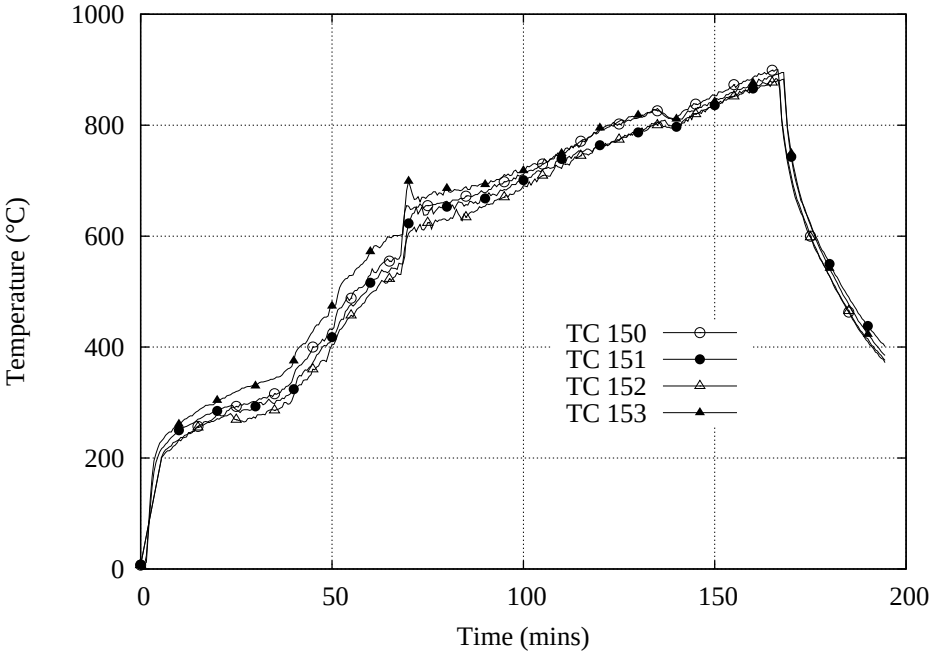

(a) GD 3

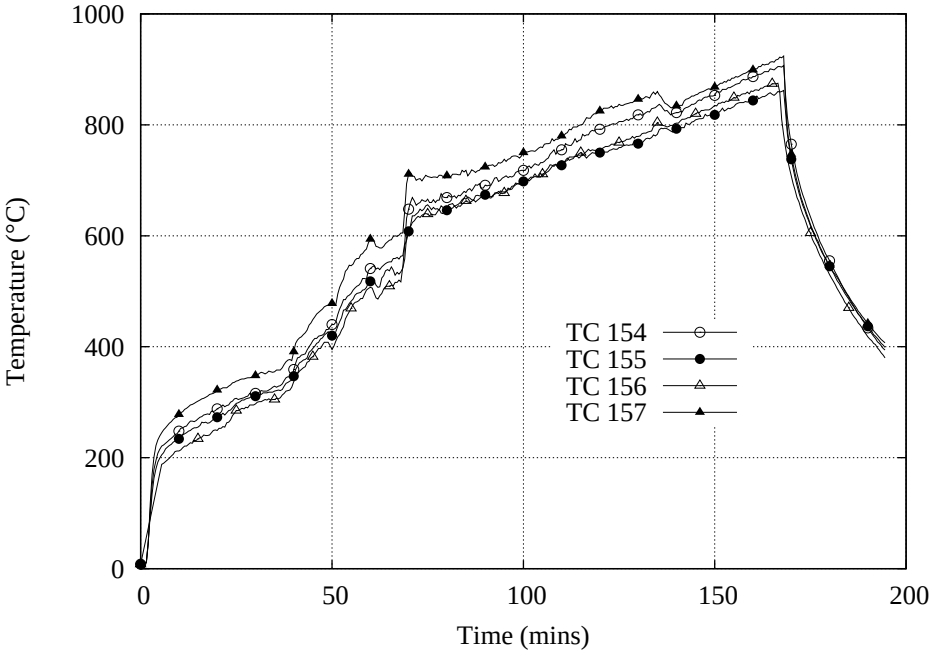

(b) GD 4

Figure 4.25: Fire temperatures in the proximity of beam sections

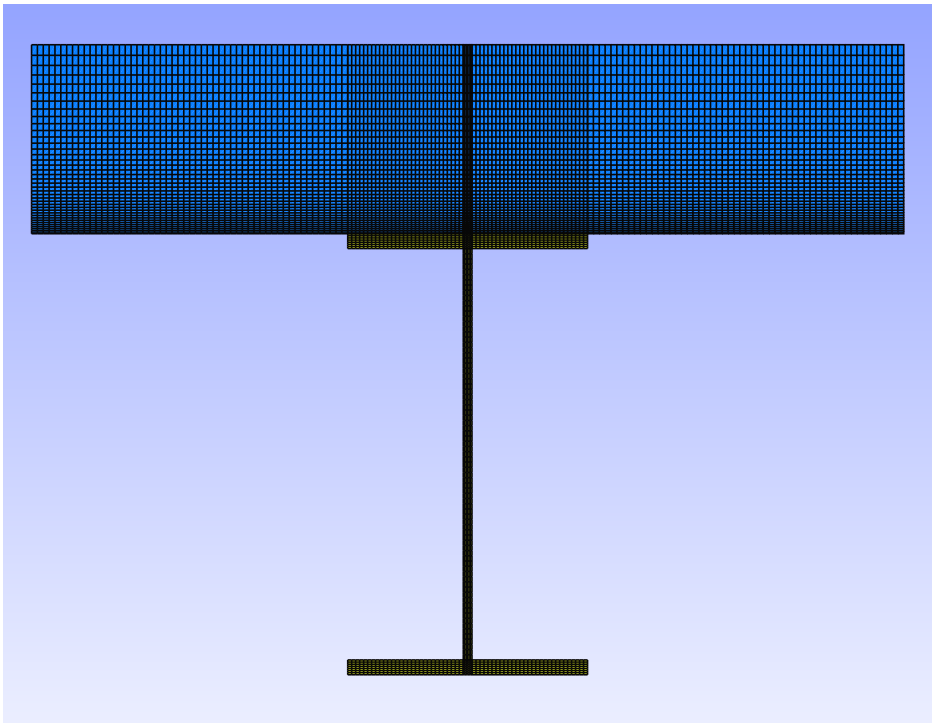

Figure 4.26: Finite element mesh for the composite beam section

at other locations in the beam as a result of the heat sink effect of the neighboring concrete slab. The predicted temperatures are generally very close to the test data except TC 83 and TC 89 which are located in the top flanges. This temperature discrepancy could be associated with the uncertainties in the thermal properties of the concrete slab, particularly its thermal conductivity and specific heat which were identified as the key factors affecting the predicted temperatures in concrete slab [120]. However, given that adequate accuracy has been obtained for most of the temperatures in the beam, performing a comprehensive sensitivity analysis like in [120] is not of the interest here.

The validation work is further extended to the measured data for the concrete slab in Test 2 which involved heating a series of beams and columns across the full 21 m width of the building on the fourth floor using a gas furnace [115]. The

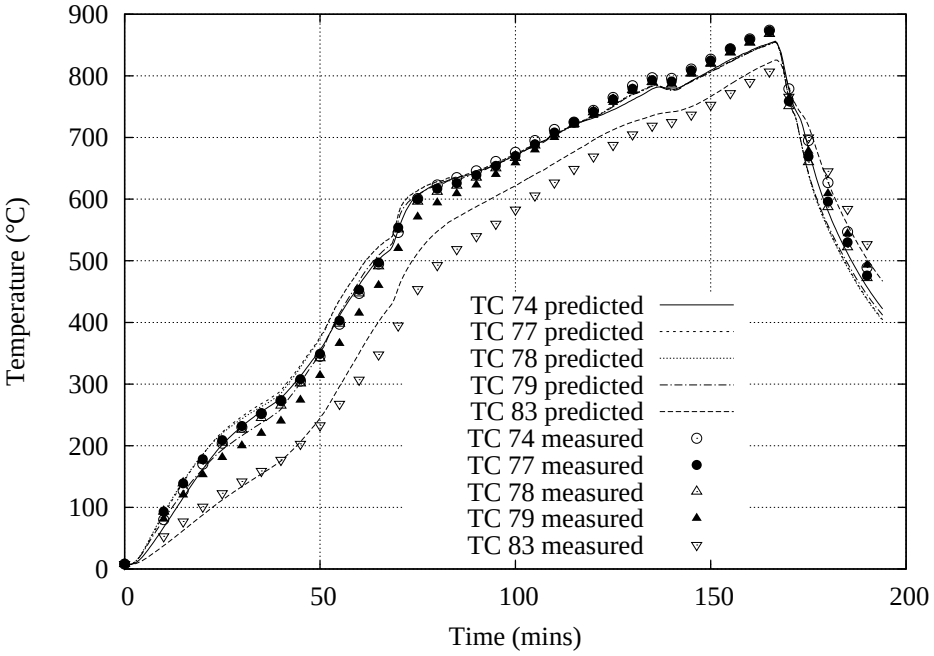

(a) GD 3

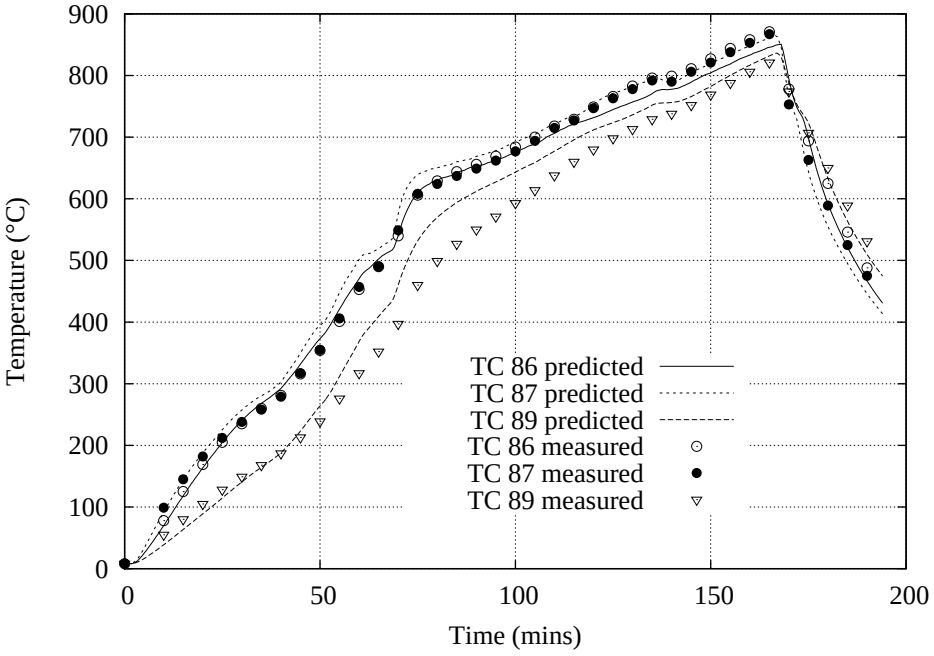

(b) GD 4

Figure 4.27: Predicted and measured temperatures in the beam section

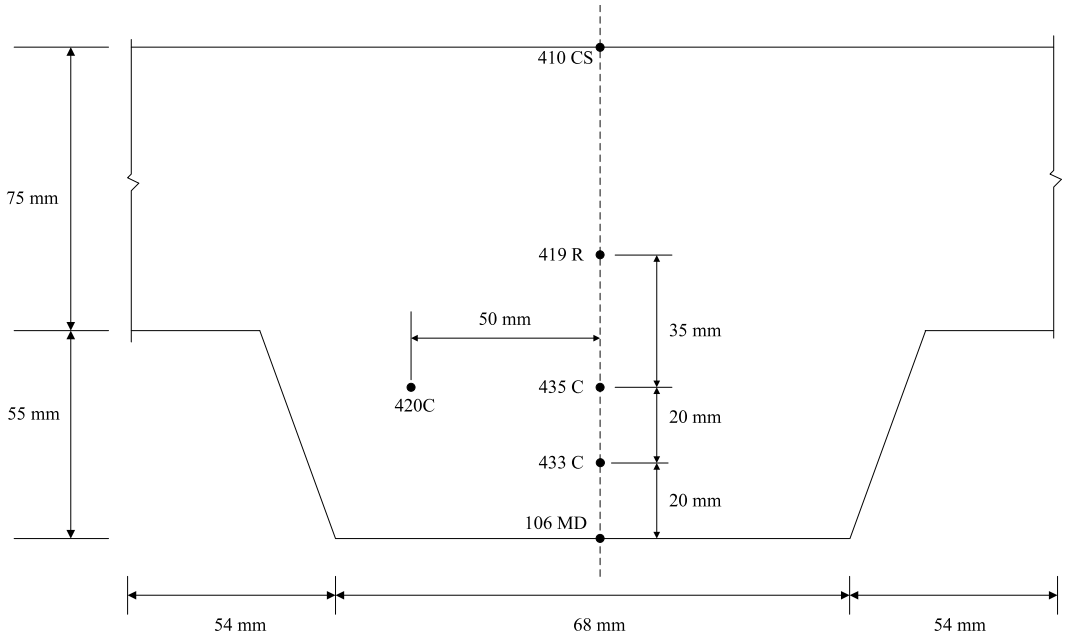

Figure 4.28: Thermocouple locations in the concrete slab (CS2)

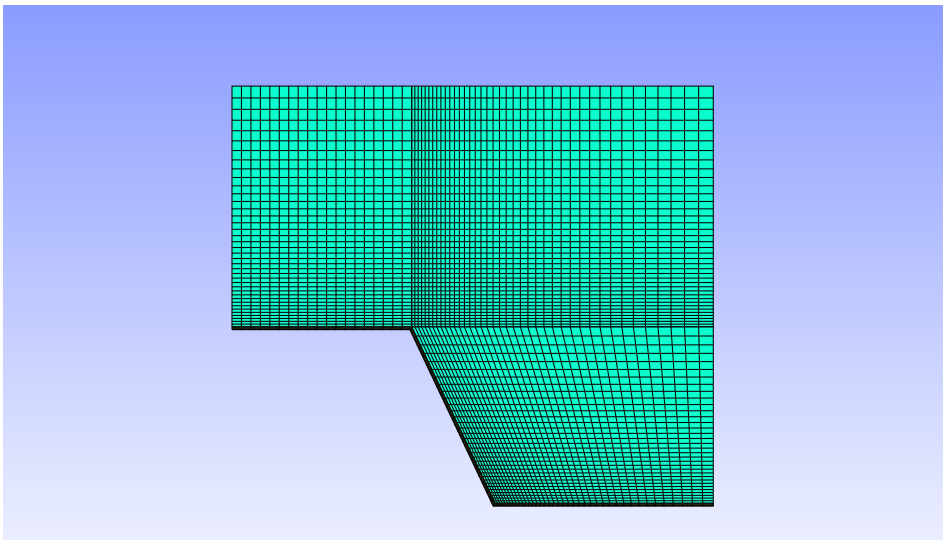

Figure 4.29: Finite element mesh for the concrete slab

dimensions of the concrete slab and the thermocouple locations in its cross section is shown in Figure 4.28. In this case, no steel beam is attached to the bottom of the slab but the geometry of the trough and rib is considered in the finite element model as shown in Figure 4.29. The metal deck is also included in order to represent the concrete slab more accurately. It is assumed that the metal deck and the concrete slab are in perfect contact, i.e. no air gap is formed between them. The emmisivity of the steel deck is taken as 0.6 in that its surface was not heavily oxidized as the steel beam in the test and should be more radiatively reflective [116]. Other parameters for the boundary conditions are the same as those used in the foregoing validation problem. The initial temperature in this case is 11 ℃.

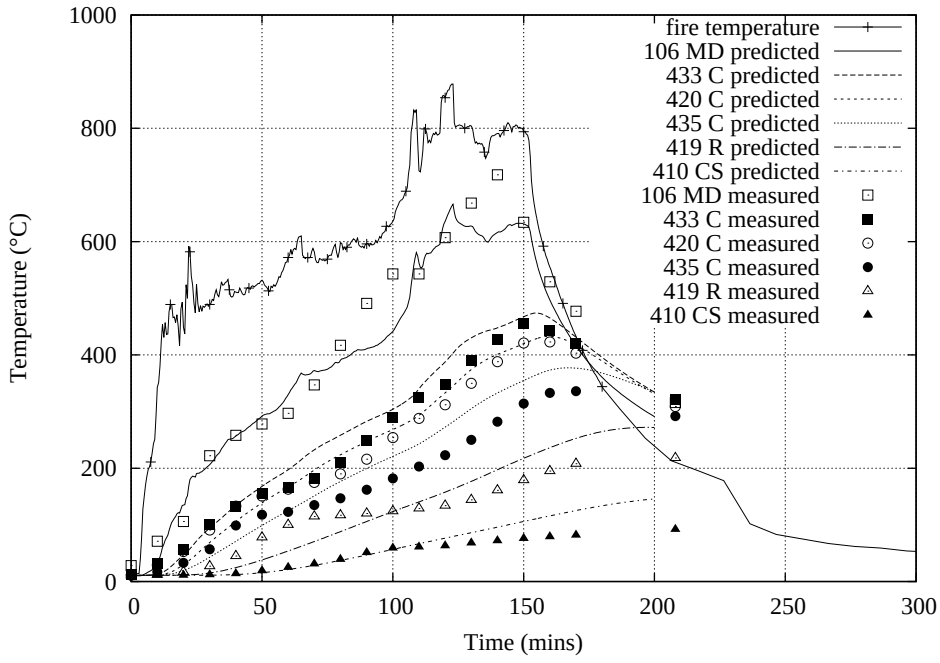

Figure 4.30: Predicted and measured temperatures in the slab

Figure 4.30 shows the predicted and measured temperatures in the slab. As seen in [120], the largest discrepancy between the predicted and measured

temperatures is seen in the metal deck (TC 106 MD). This may be associated with the actual variations of fire temperatures during the test, while the uniform exposure temperature is used in the modelling as there was only one surrounding thermocouple available in the proximity of the slab section. Comparisons at other locations through the depth of the slab are more satisfactory, although the finite element model slightly over-predicts temperatures by around 50 ℃. As in the discussion on the first validation example, this over-prediction may be firstly attributed to the constant heat capacity used in the modelling for the light weight concrete, whereas in reality the heat capacity should be temperature dependent and higher than the value used here due to the latent heat needed for the moisture content transforming from liquid phase to water vapor [120]. However, due to the lack of information on the actual amount of moisture in the concrete slab at the Cardington test, the temperature dependency of heat capacity is not considered in this validation test. In addition, as concrete is type of porous material there exists a coupled heat and moisture transfer mechanism at elevated temperatures [123]. Exclusion of these phenomena would give more conservative predictions (higher temperatures) but the overall predictions from OpenSeesHT indicate an adequate match with the test data considering that many uncertainties existed in the tests.

4.5 Conclusions

A thermal analysis framework dedicated to structures-in-fire modelling has been added into OpenSees by including the new fire and heat transfer modules. Following the object-oriented design paradigm, this framework is developed to be consistent with the ethos of OpenSees such as flexibility and extensibility. The

software architecture and the interactions between classes are discussed in this chapter. The design of the interface between the fire and heat transfer modules enables them to interact with each other either in a one-way or two-way fashion and the addition of a new fire model does not need any or only minor changes to the interfaces of the heat transfer module which is a great merit of the present thermal analysis framework. Methods have been provided to either record the nodal temperature history or spatially averaged temperature history for each fibre in structural elements.

The heat transfer module uses the finite element method (FEM) as a general numerical approach to address heat conduction in structural members which allows for accurate prediction of heat transfer in complex geometries (such as steel joints [124]). A number of severe benchmark tests covering different aspects of the problem are carried out by comparing the predicted results with analytical solutions. It can be concluded that the heat transfer module demonstrate accurate predictions and robust performance for transient analyses. Then the extended OpeenSees framework with both the fire and the heat transfer modules is validated using experimental data from the Cardington large scale tests. The general agreement between the FE results and the measured data is good, although with slight discrepancy which are thought to be attributed to the uncertainties in the surrounding temperatures and the thermal properties of the light-weight concrete and moisture propagation effects. The application of the thermal analysis framework and its collaboration with the structural module is the topic of the next chapter.

Chapter 5

Using OpenSees for thermal and structural analysis of a composite tall building in horizontally travelling fires

5.1 Introduction

Most of the studies in the past have used codified design fires (such as the standard fires and parametric fires) for modeling the response of structures in fire. Almost all these design fires attempt to simulate the effects of post-flashover fires and inherently assume spatially uniform fire temperatures within the compartment [38, 19]. However, recent work has shown that even in post-flashover fires, the distribution of fire temperatures in relatively small compartments is not uniform

[125]. Furthermore, fire accidents have shown that in larger spaces, fires tend to travel rather than burn uniformly and simultaneously [74]. These observations have drawn the attention of researchers who have questioned the application of conventional design fires on modern structures with large spaces [72, 3]. However, perhaps due to lack of proper understanding of traveling fires, conventional temperature-time curves are still used, and an artificial time-delay has been introduced in order to study the effects on structural performances. For example, Ellobody *et al.* [126] used the parametric temperature curves to represent the traveling fires in a large compartment which was divided into a number of zones and each zone was subjected to a parametric fire curve at different time intervals.

To address this problem and meet the need of structural fire design for modern structures, Rein and Stern-Gottfried [72, 74, 6] have developed a novel methodology which represents traveling fires more realistically by including key aspects of fire dynamics in large enclosures. This methodology has undergone a number of iterations over its development. The major merit of this methodology over conventional post-flashover fire models is to horizontally divide the whole fire environment into two regions, i.e. "near field" and "far field", which generates spatially non-uniform and transient temperature curves for the whole floor. Different approaches can be adopted to calculate the fire generated thermal environment in these two regions including CFD calculations. However, using CFD approach for large building can be computationally restrictive and expensive [72]. Therefore, Stern-Gottfried *et al* [74, 73] adopted an empirical correlation to calculate the far-field temperatures which has the advantage of rapid resolution of the thermal environment with sufficient accuracy for engineering applications. This methodology has been applied to study the structural responses of a concrete

structure. Results showed that conventional design fires may not be considered conservative when compared to some traveling fire scenarios [74, 77].

The traveling fire methodology developed by Rein and Stern-Gottfried [6] has been proposed for the performance-based structural fire design of modern buildings which are beyond the validity of conventional design codes. However, this would normally require detailed thermal and structural modeling in order to quantify the actual response of structures to fire, which naturally requires robust and easy to use structural simulation software. There are many commercial finite element packages (such as ABAQUS, ANSYS, DIANA etc.) that offer excellent capabilities for most routine modeling activity in research and in the commercial and consulting organizations. These codes can however be restrictive for a field that is growing at a rapid pace (as the field of structures and fire is, with increasing interest and development in both research and industry). Furthermore, the licensing costs can be prohibitive for researchers who have limited resources despite academic discounts.

For the above reasons, this work has chosen OpenSees software framework to develop "structures in fire" analysis capability that could be used by researchers all around the world at no cost [7]. The OpenSees framework was initially developed at UC Berkeley as an open source community code for simulating the response of framed structures to earthquakes [101]. It has been recently extended at the University of Edinburgh by adding new software modules and modifying existing codes. New capabilities include heat transfer modeling in structural members with fire imposed boundary conditions, and thermal-mechanical modeling using both beam and shell elements with temperatures calculated by the heat transfer module [7].

The recently developed travelling fire methodology [6] has been implemented in the OpenSees framework, which has then been used to investigate both the thermal and structural responses of a generic composite structure subjected to a range of horizontally travelling fires. Composite structures made of concrete slabs and steel beams are a popular form of tall building construction preferred by architects and engineers because they optimize the use of materials and enable rapid construction. However, the effects of travelling fires on the performance of this type of construction have not been examined in detail before. A study examining the effects of horizontally traveling fires on the response of a concrete structure in fire has been performed in [77]. The results demonstrated that traveling fires of medium fire sizes were producing a more conservative estimate of the structural response compared to parametric fires. However, the results of this study are limited to concrete structures of the particular layout examined in [77]. Further investigation will be carried out in this work to examine whether these conclusions are applicable to a composite structure too. Lamont *et al.* [112] studied the response of a small composite frame under "short hot" and "long cool" parametric fires. The authors concluded that the most detrimental fire was the "short hot" fire as large deflections were developed in very short time although the "long cool" fire resulted in higher displacements for some elements but much later in terms of time. These findings were challenged by the results in [127] where the authors examined the behaviour under "short hot" and "long cool" fires of an eleven-story building. The results showed that there was no failure when they considered a "short hot" fire but a "runaway" failure was seen for a part of the structure involving 10 m beams under a "long cool" fire. Until further research is carried out, these studies suggest that the worst case scenario for each structure

can not be a priori defined and that it depends on the structural materials and layouts used.

5.2 The travelling fire methodology

In the traveling fire methodology, the fuel is normally assumed to be uniformly distributed across the whole floor plate with a fire load density q_f (MJ/m^2). Assuming the fire burns with an area of A_f (m^2) and with a constant heat release rate per unit area $\dot{Q}''$ (kW/m^2), this corresponds to a power, $\dot{Q} = A_f\dot{Q}''$ (kW), for this particular size of fire. Each fire area would have a constant burning time , which is given by [6, 74]

$$t_b = \frac{q_f}{\dot{Q}''} \tag{5.1}$$

The floor area where the fire has traveled across is deemed to be burnt out. Note that t_b is a characteristic burning time of the near field, and is determined by fuel load density and the properties of the fuel but independent of fire sizes.

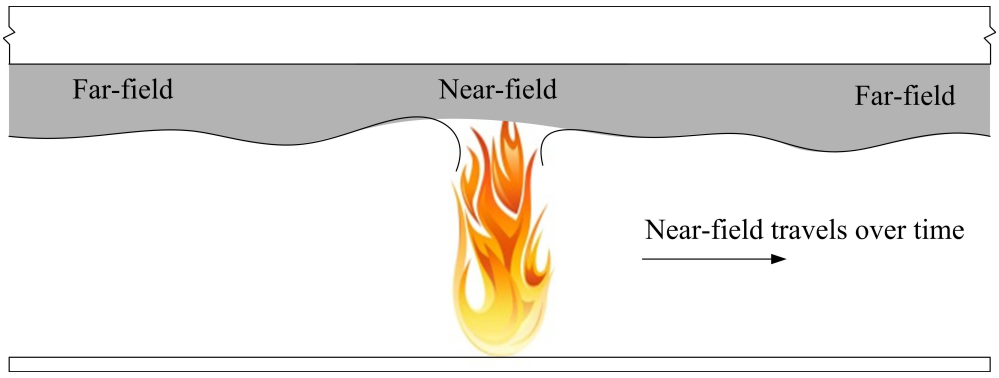

Figure 5.1: Illustration of a travelling fire with near field and far fields

As the fire travels across the floor, the thermal environment can be divided into

two horizontal regions, namely, "near field" and "far field", with reference to the fire source at any time interval (as illustrated in Figure 5.1) [74]. The near field is the burning region of the fire, and a constant representative temperature may be assumed [74, 72, 77]. The far-field is the region remote from the burning area where the structure is mainly heated by hot smoke moving away from the fire source. The fire temperature of the far field may be determined by the empirical Alpert correlation [74, 77, 55, 56]

$$T_{max} - T_{\infty} = \frac{5.38(\dot{Q}/r)^{2/3}}{H} \tag{5.2}$$

where T_{max} is the maximum temperature in the ceiling jet, T_{∞} is the ambient temperature, $\dot{Q}$ is the heat release rate of the fire, r is the distance from the fire center, H is the floor height.

The use of Alpert's correlation has been shown to be conservative and adequate by comparing the calculated ceiling jet temperatures with CFD modeling results [6]. Good agreement between the results was found which justifies using this simple empirical correlation to predict the far-field temperatures. Eq. (5.2) produces a monotonically decaying temperature distribution along the distance away from the fire. One constraint should be noted that this correlation is only applicable to unconfined ceiling jet and no accumulated smoke layer should be present [56]. Therefore, possible structural members such as beams under the ceiling should not have a depth which could violate the validity of this correlation.

As a result of the traveling nature of fire, any location above the fire floor would experience sequentially the initial far-field heating, the near-field heating, the posterior far-field heating, and the cooling to the ambient (20 ℃), where gas temperatures during the first and third phase are determined by Eq. 5.2. The

arrival time of the near-field is dependent on both the traveling speed and the distance from the fire origin. Therefore, the traveling fire methodology produces spatially and temporally varying heating conditions across the floor, which can not be naturally addressed by conventional design fires such as the parametric fire curves as given in EC 1 [19]. Figure 5.2 shows a typical temperature curve at any arbitrary location above the floor [74].

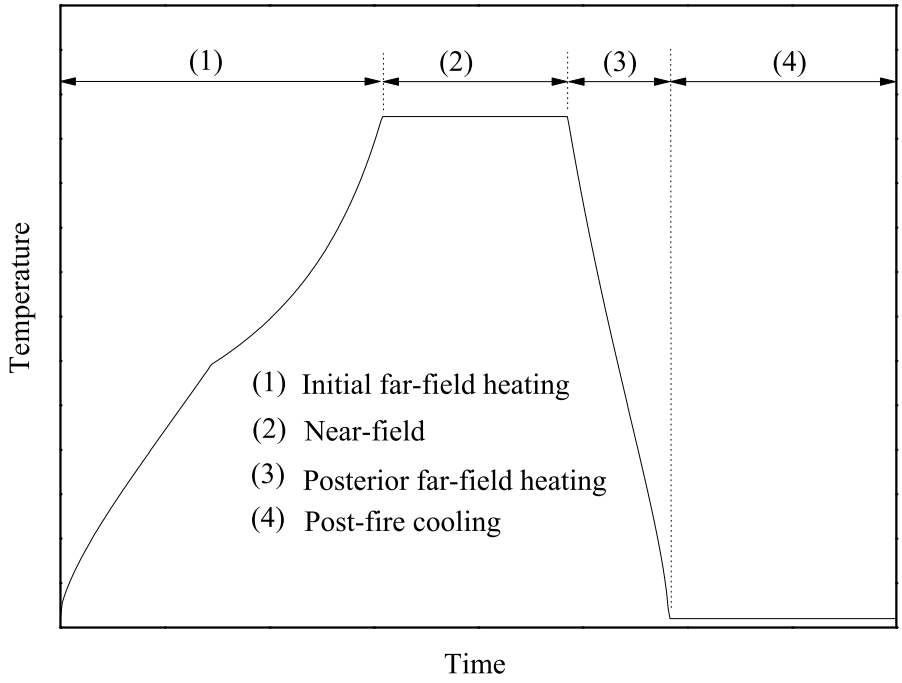

Figure 5.2: Near-field and far-field exposure at an arbitrary location above the floor

5.3 Case study of a composite structure

5.3.1 The structure

The structural layout examined in this work is a generic modern tall building with a floor height of 4 m. The typical floor plan is shown in Figure 5.3, which

could possibly produce fire propagation similar in form to that of the WTC towers [71]. The dimensions of the beams are selected according to preliminary design criteria. These are UB 533×210×122 for the girders, UB406×140×39 for the primary beams and UB356×171×51 for the secondary beams. The floor area A_{total} is 1152 m^2, with a core of 192 m^2. The presence of the core is important to structural behavior and should be taken into account when performing structural analysis. However, it is a reasonable approximation to neglect the core when calculating the fire temperatures [74].

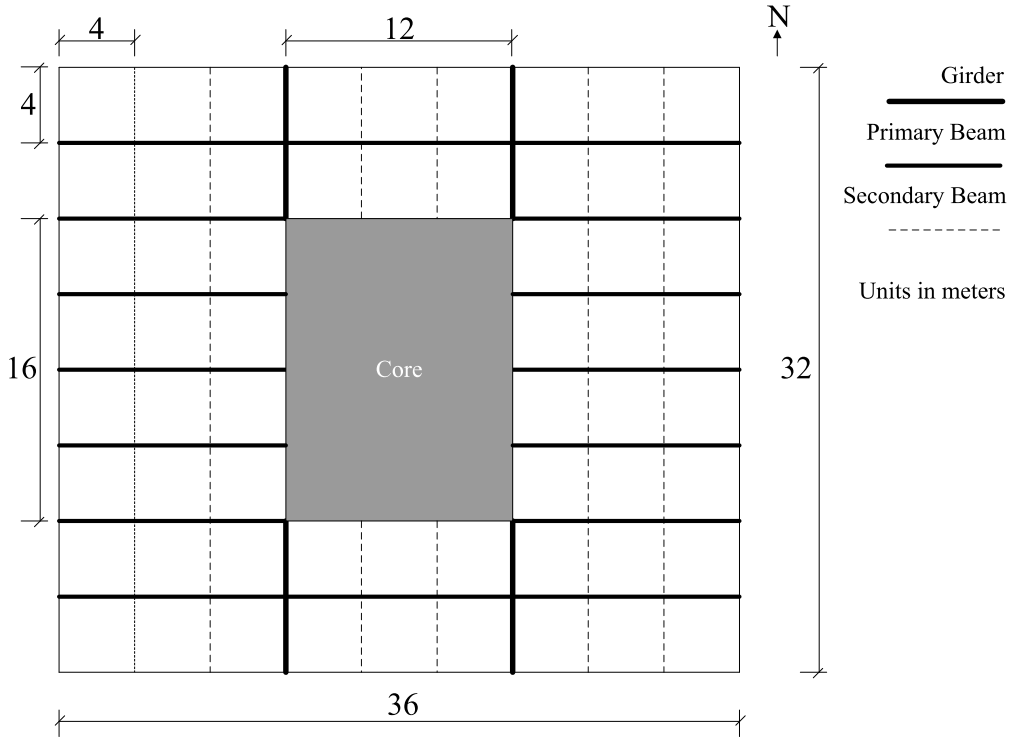

Figure 5.3: Schematic plan view of the structure

5.3.2 The travelling fire scenarios

The building is assumed to be used for office purpose and the fuel is uniformly distributed on the floor plate with a characteristic fire load density of 420 MJ/m^2 as given in [19]. Mass burning rate of typical office fuels are reported in the range of 20∼40 g/m^{2}s [128], which suggests that the heat release rate per unit area would range from 320 to 640 kW/m^2 if we assume a typical heat of combustion of 16 kJ/g for cellulose fuels [38]. An average value of 480 kW/m^2 is taken in this work. It is assumed that the fire travels in a linear path from the west to the east of the floor and extends over the whole width of the building, which is similar to the treatment used in [74, 77]. The initial length of the fire is $L_0 = 0.1$ m, and then it maintains a constant length L_f (near-field) once the fire has grown to the specified size A_f,

$$L_f = \frac{A_f}{W} \tag{5.3}$$

Larger fires would travel faster, and the travelling speed s (m/s) is characterized by [6]

$$s = \frac{L_f}{t_b} \tag{5.4}$$

For this linearly traveling fire, the total burning time may be calculated by the following equation [74]

$$t_{total} = t_b(\frac{L - L_0}{L_f} + 1) \tag{5.5}$$

The size of fire is a major variable in the traveling fire methodology, which balances the far field temperature and the total burning time [74, 72, 77]. In this work, the

fires are varied from 4% to 50% of the floor area. Other parameters associated with the fire size are summarized in Table 5.1.

Table 5.1: Summary of the travelling fire scenarios

A_f(m^2)	Fire size	L_f(m)(Eq. (5.3))	$\dot{Q}$(MW)	t_{total}(min)(Eq. (5.5))	s(m/min)(Eq.(5.4))
48	4%	1.5	23	364.0	0.1
96	8%	3	46	189.3	0.2
192	17%	6	92	102.0	0.4
288	25%	9	138	72.8	0.6
384	33%	12	184	58.3	0.8
480	42%	15	230	49.5	1.0
576	50%	18	276	43.7	1.2

The temperature distribution in the composite floor (on top of the ceiling of the fire compartment) along the longest direction will be examined, as the structure along this direction is more susceptible to stability issues in case of a fire. Figure 5.4 shows a linear traveling fire and four locations (A, B, C, D) for the temperature analysis across the floor. The schematic of the composite section and corresponding temperature locations on the section are indicated in Figure 5.5.

5.3.3 Fire and heat transfer modelling in OpenSees

The recently developed fire and heat transfer modules in OpenSees [7, 33] are used in this work to calculate the transient temperature rise in the composite structure. As a result of the traveling fires, the heat transfer in the composite floor could have a fully three dimensional character; however, we have chosen to ignore

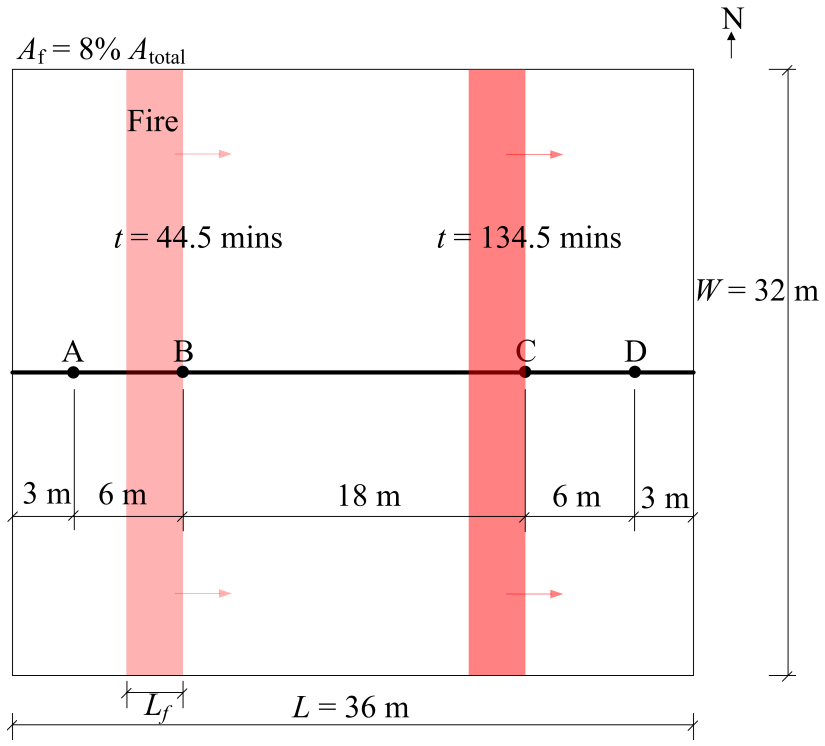

Figure 5.4: Schematic of the linearly traveling fire across the floor plate

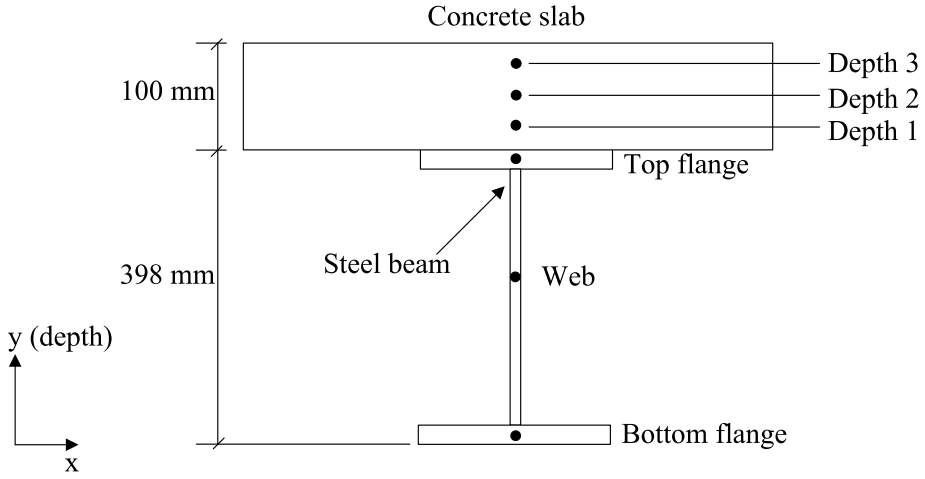

Figure 5.5: Dimensions of the the composite section and temperature locations

heat conduction along the direction of fire propagation to simplify the problem and reduce the computational expense. Furthermore, the rate of heat conduction along that direction would be much slower than the fire traveling speed [6]. Hence

two dimensional heat transfer analyses are carried out for separate sections at the locations (A, B, C, D) specified in Figure 5.4. This approach is justified by Franssen *et al.* [103], who showed that even if a steel member is subject to highly localized heating conditions, a series of separate two dimensional heat transfer analyses represent fully three dimensional heat transfer analyses with adequate accuracy.

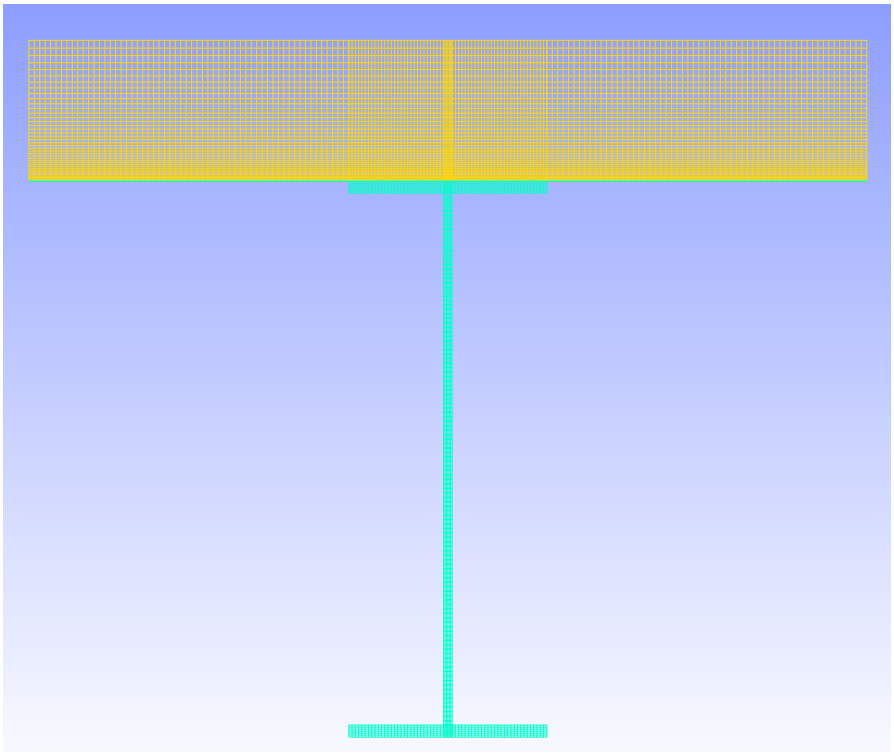

Figure 5.6: Finite element model of the the composite section

A 0.9 mm thick metal deck between the steel beam and the concrete slab is included in the finite element model. The temperature-dependent material properties of concrete (with a moisture level of 1.5%) and steel are taken from [122] and [12] respectively. The top surface of the concrete slab is assumed to be exposed to ambient environment of 20 ℃. The bottom surface of the slab and three sides of the beam are exposed to the thermal environment generated

by the traveling fires. The convection coefficients for fire-exposed surfaces and unexposed surfaces are taken as 25 W/m^2·K and 4 W/m^2·K respectively [19]. An emissivity of 0.7 is specified for both the concrete and steel according to [122]. The finite element model of the composite section is shown in Figure 5.6. Radiative attenuation in the I-section cavities is not considered here as the aspect ratio of the cavity is relatively low (0.18) for the steel member examined, which suggests that the geometric attenuation of radiative heat fluxes at the inner surfaces is not prominent [30] and the uniform thermal exposure for all the section surfaces may be considered as a reasonable approximation. Using the extended OpenSees framework as presented in Chapter 4, the sample code implemented to perform the thermal analysis with travelling fires is shown in Figure 5.7.

5.3.4 Structural fire modelling in OpenSees

A two dimensional substructure is modeled that represents a 12 storey slice of the building along the longest span (12m) floor area. The core of the building is assumed to be rigid. By including appropriate number of floor below and above the fire floor ensures that the stiffness of the surrounding structure is accurately modeled. It is recognised by the authors that although a two-dimensional representation does not take into account the load redistribution effects however previous research that compared two and three dimensional models in [129, 130] has demonstrated that a two dimensional model can accurately predict the performance of a perimeter column-floor interaction system in fire. Particularly in the context of traveling fire methodology, a much more inexpensive two dimensional model can efficiently provide a first overview of structural behaviour of a building under different traveling fires that maybe otherwise be much more

```
int main()
{
HeatTransferDomain* theDomain = new HeatTransferDomain();
GmshBuilder* theModelBuilder = new GmshBuilder(*theDomain,"
    primaryBeam.msh");
theModelBuilder->BuildModel(); // create the finite element model

// set boundary conditions for the top surface of the slab
int tag1 = 1;
theModelBuilder->setConvectionBC(h0, Ta, tag1);
theModelBuilder->setRadiationBC(epsilon, sigma, alpha, qir, tag1);

// create analysis objects
......
// set the boundary conditions for the fire-exposed surfaces
int DirFlag = 0; // indicating structural member perpendicular to
    travelling direction
int tag2 = 2;
double Qdot = 480*1e3; // HRR per square meters, 480kW/m2
double Tf = 1423.15; // set near-field temperature 1150C

double delta_t = 10; // set time step
int numSteps = 1200;

for(int i=0;i<numSteps;i++){
    t = t + delta_t;
    int numSteps = 1;
    //determine the locations of leading edge (X2) and trailing edge
        (X1) of the fire
        ......
    //determine the area of near-field
    Af = (X2-X1)*L;
    Qf = Af * Qdot;  //determine HRR
    //create Alpert Fire Model according to the new locations
    AlpertCeilingJetModel* themodel = new AlpertCeilingJetModel(crd1
       , crd2, crd3, Qf, H, Ta, Tf, 2);
    theModelBuilder->setLinearTravellingFireBC(themodel, X1, X2, L1-
       LA, hc, Ta, Tf, epsilon, sigma, alpha, DirFlag, tag2);
    theAnalysis.analyze(numSteps, delta_t);
    }
}
```

Figure 5.7: Sample code for the thermal analysis in OpenSees using the travelling fire methodology

expensive to conduct using three dimensional models. All the structural members of the building (column, slabs and beams) were modeled using the two-node displacement based and distributed plasticity **dispBeamColumn2DThermal** elements. Plasticity for these elements was chosen to be monitored in five locations along the length of each element and using a fiber section approach along the depth of each element. An appropriate number of elements have been used to take into account the p-delta effects while a co-rotational transformation is used to incorporate the large displacements developed. The composite action of the floor between the steel beam and the concrete slab is achieved by modelling them with separate series of elements that are connected with multipoint rigid link constraints that tie the corresponding degrees of freedom (translations and rotation). At the rigid core end the steel beam and the slab (forming the composite floor) are both pinned to a rigid lateral restraint. This connection also simulates a fixed-end connection for the composite floor. A fixed connection is also assumed for the floor-column connection. This assumption implies that translations and rotations of the beam and column at the node joining the two members are constrained to be identical. It should be noted that connection or reinforcement failure is not taken into account in the current paper.

For the steel columns and beams a yield strength of 300 N/mm^2 and modulus of elasticity of 210 GPa were used. The concrete slab was assumed to have a compressive strength of 30 N/mm^2 and a tensile strength of 5% of its compressive strength adopting a modified Kent and Park model [131] as its material constitutive model. The steel reinforcement was assumed to have yield strength of 475 N/mm^2. The temperautre dependence of material properties for steel and concrete in OpenSees are based on Eurocodes [11, 13]. During the cooling stage of a fire, steel is assumed to regain its stiffness and strength, while the compressive

strength, strain corresponding to compressive strength and ultimate (crushing) strain of concrete do not recover during cooling and were varied according to [122]. Thermal strains are generally assumed to be reversible. An implicit dynamic procedure is used in this work to overcome numerical instabilities caused due to the high restraint to thermally induced displacements. For the case of traveling fires, big numerical instabilities are present due to highly localised temperatures and steep heating curves compared to parametric fires or exponential fire curves [129]. The numerical scheme selected for the dynamic analysis is an implicit solution with a Hilber-Hughes-Taylor integrator with $\alpha = 0.7$ to add numerical damping to the model [132].

5.4 Results and discussions

When examining composite members in fire, it should be noted that the thermal response affects significantly the structural response. Significant information on the structural behaviour under thermal effects was gained based on the Cardington tests over the previous years [110]. Composite floors are designed for flexure but also carry loads through compressive and tensile membrane action. During the heating phase, the composite section experiences a mean temperature rise which leads to overall compression in a laterally restrained member. It also experiences a thermal gradient over the depth of the section which leads to a uniform hogging moment along the length of a rotationally restrained member (which is usually the case, at least at low temperatures). The hogging moment also causes compression forces in the bottom flange of the steel beam. Further research by Lamont *et al.* [112] has investigated the behaviour of composite members under a "short-hot" and a "long-cool" fire scenarios. Their research has

shown that in a "short-hot" fire the composite section experiences higher thermal gradients and in the case of a "long-cool" fire the composite section has a higher mean temperature. When exposed to high temperatures concrete experiences creep and loses its load bearing capacity, and steel reinforcement at 550 ℃ loses almost 50% of its strength and 70% of its stiffness [13]. That is why concrete slabs are required to have an appropriate cover to the steel reinforcement. Law *et al.* [77] suggested that the peak temperature at the rebar location could be used as a criterion to measure the structural performance. The thermal and structural responses of the composite structure subjected to different traveling fire scenarios will be further discussed in detail in the following sections.

5.4.1 Thermal response

5.4.1.1 Temperature rise

Typical fire temperatures and the temperature histories through the depth of the beam and concrete slabs are shown in Figure 5.8 for four locations across the floor, which is shown for a fire with small size (8% of the total floor area). It is clear that the heating condition is strongly non-uniform across the floor in traveling fires. It is interesting to note that the fire curves are symmetric for the geometrically symmetric locations (A and D, B and C). This is because that the far field temperature is a function of relative distance to the fire center as given in Eq. (5.2). Note, according to the "equal area hypothesis" [38], the fire severity at location A (96 mins) and location D (186 mins) would be the same due to identical areas under the two fire curves (above a reference temperature of 300 ℃). However, temperatures in the beam at location D (186 mins) are up to 77%

higher than the corresponding values at location A (96 mins), while temperatures in the slab (depth 3) at location A (96 mins) are up to 102% higher than those at location D (186 mins). Similar results are also found for other traveling fire scenarios in this work. This clearly goes against the traditional measure of fire severity in terms of the "equal area" concept which links fire severity to the area under the temperature-time curve [38].

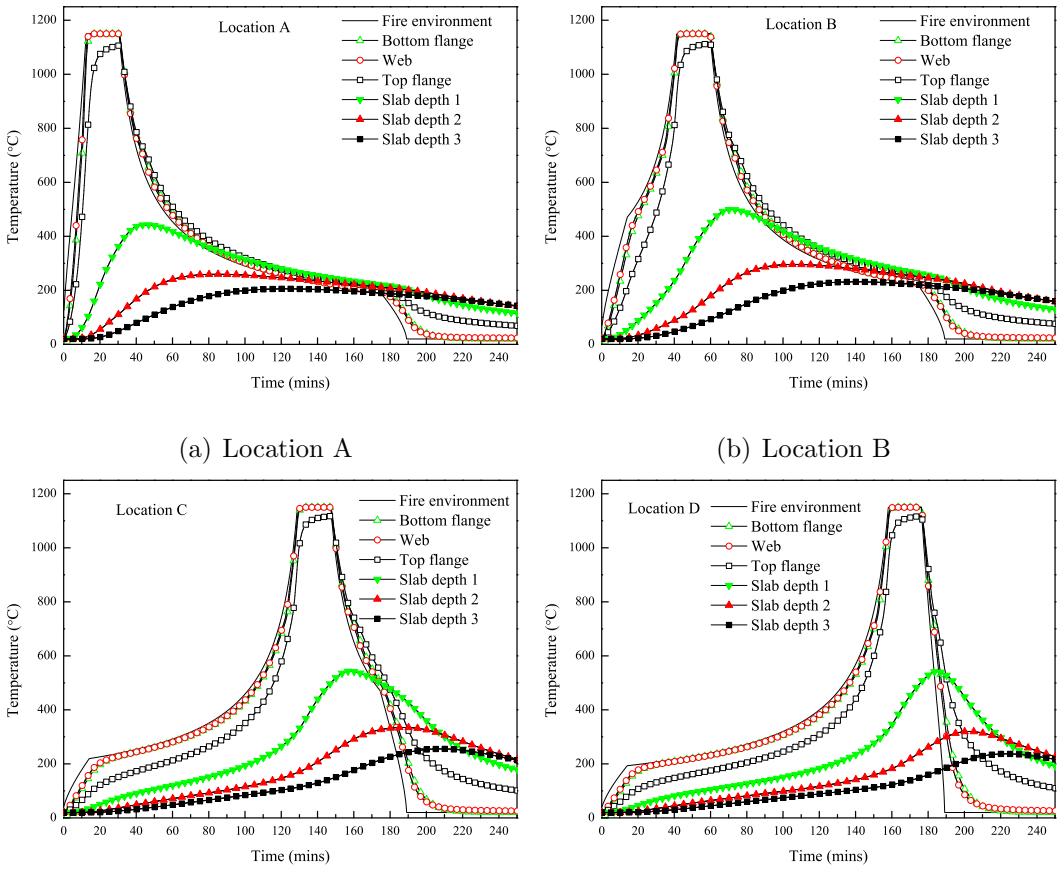

(a) Location A

(b) Location B

(c) Location C

(d) Location D

Figure 5.8: Temperature rise in the composite section subjected to traveling fire (8% of the floor area) at different locations

The peak temperatures at the bottom flange and centre of the web reach the near field temperature (1150 ℃) in all the cases, although peak values for the top flange

are slightly lower. Therefore, the time taken to reach a critical temperature seems to be a more meaningful parameter for the investigation here, as unprotected steel members may fail rapidly in fires [38]. The critical temperature is taken as 550 ℃ as this value is often used as a simple failure criterion for steel members [38]. As shown in Figure 5.9, it takes shorter time for the beam to reach the critical temperature when exposed to larger fires. This is expected as larger fires travel faster and lead to earlier arrival of the near-field heating. It takes slightly longer for the top flange to reach 550 ℃ due to the heat sink effect of the concrete slab. As pointed out in [6], the time to reach a specified temperature depends not only on fire siezes but also the distance relative to the fire origin. Location A has the shortest distance to the initial fire location and it is the earliest to experience the near field heating. Therefore, the steel beam there suffers the most detrimental heating conditions compared to other locations, which reaches 550 ℃ within 2.5 mins for the 42% fire size, corresponding to a heating rate of 220 ℃/min. However, it should be noted that global structural fire performance is not simply determined by local critical temperatures, and mechanical interactions between structural members need to be considered as well.

Figure 5.10 shows the variations of peak temperatures in the concrete slab. As shown in the figure, smaller fires such as 4% and 8% fire sizes produce the highest temperatures at every location. This is due to the fact that smaller fires produce lower far-field temperature but burns for much longer time. As given in Table 5.1, the total burning time for the 4% fire is about 7 times as that for the 42% fire. Plus concrete has very low thermal conductivity, which means more heat would penetrate through the concrete slab subjected to smaller traveling fires. Similar results are also found by Law *et al.* [77], who suggested that smaller fires (10%∼20%) represent an optimum heating balance between far-field temperature

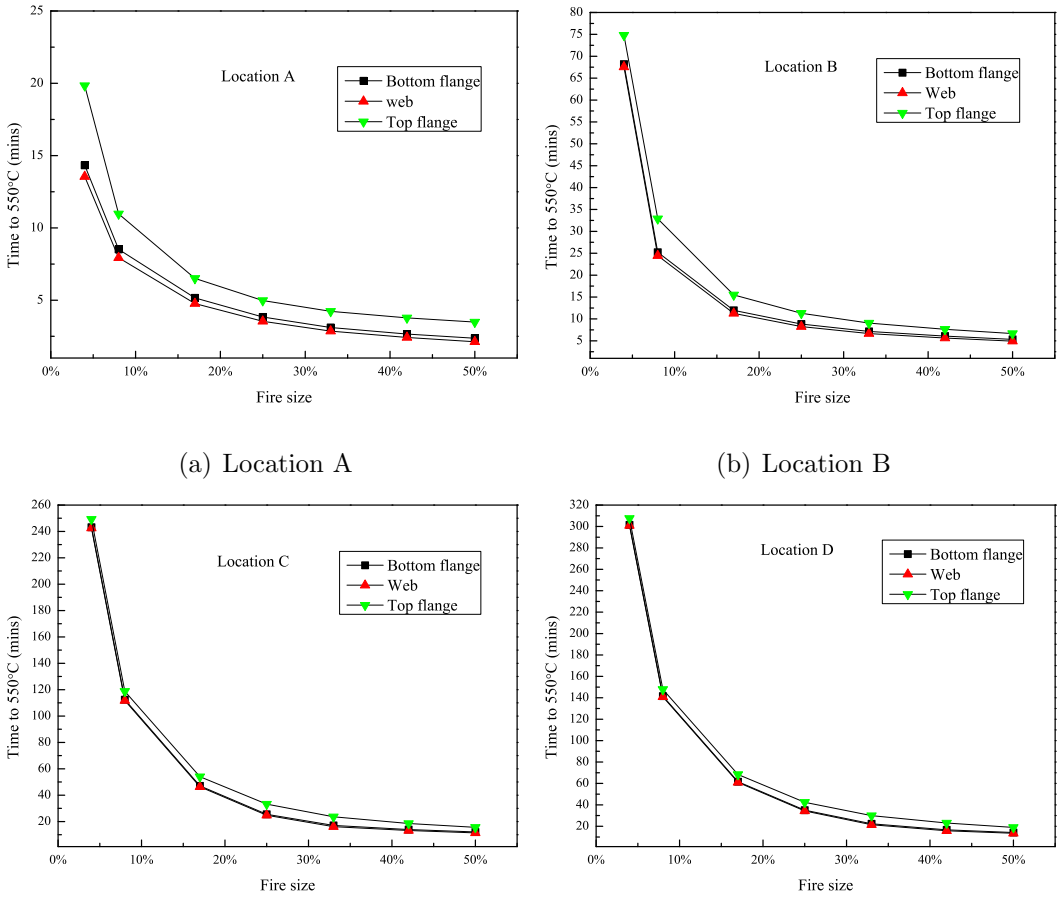

(a) Location A (b) Location B

(c) Location C (d) Location D

Figure 5.9: Time taken to reach reference temperature (550 ℃) different locations

and far-field heating duration. Therefore, in light of peak temperature reached in the concrete slab, the 4% fire would be the most onerous in the current case study. It is also noted that peak values increase with the distance away from fire origin, as temperatures in Figure 5.10(c) and 5.10(d) are generally higher than the corresponding values in Figure 5.10(a) and 5.10(b), which was also seen in previous studies for concrete structures [74, 77]. Similar to what we discussed above, this is because that further locations experience a relatively long period of far-field heating prior to the arrival of near-field as shown in Figure 5.8.

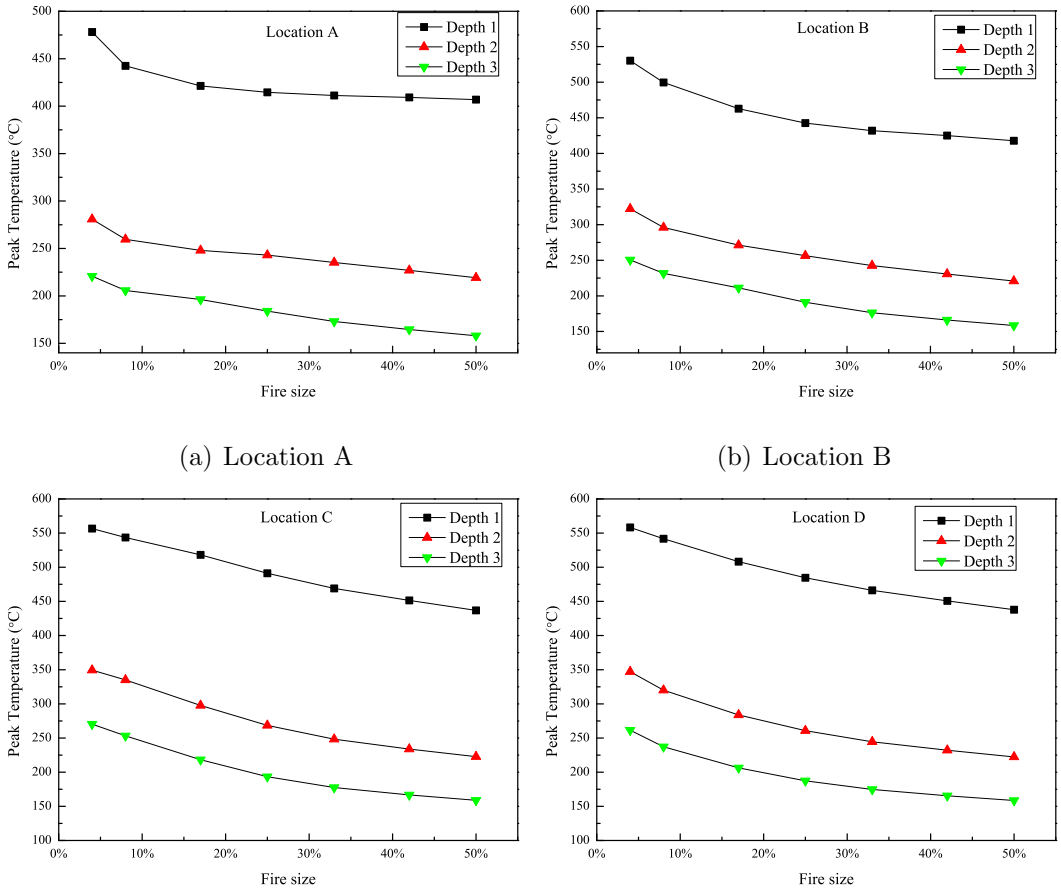

(a) Location A

(b) Location B

(c) Location C

(d) Location D

Figure 5.10: Peak temperature in the concrete slab at different locations

5.4.1.2 Through-depth thermal gradient

As mentioned at the beginning of this section, thermal gradient through the depth of the composite floor plays an important role in determining the structural behavior of composite structures. This section examines the effect of traveling fires on the thermal gradients in composite sections at different locations across the floor plate.

Figure 5.11 shows the through-depth temperature profiles in the steel section at

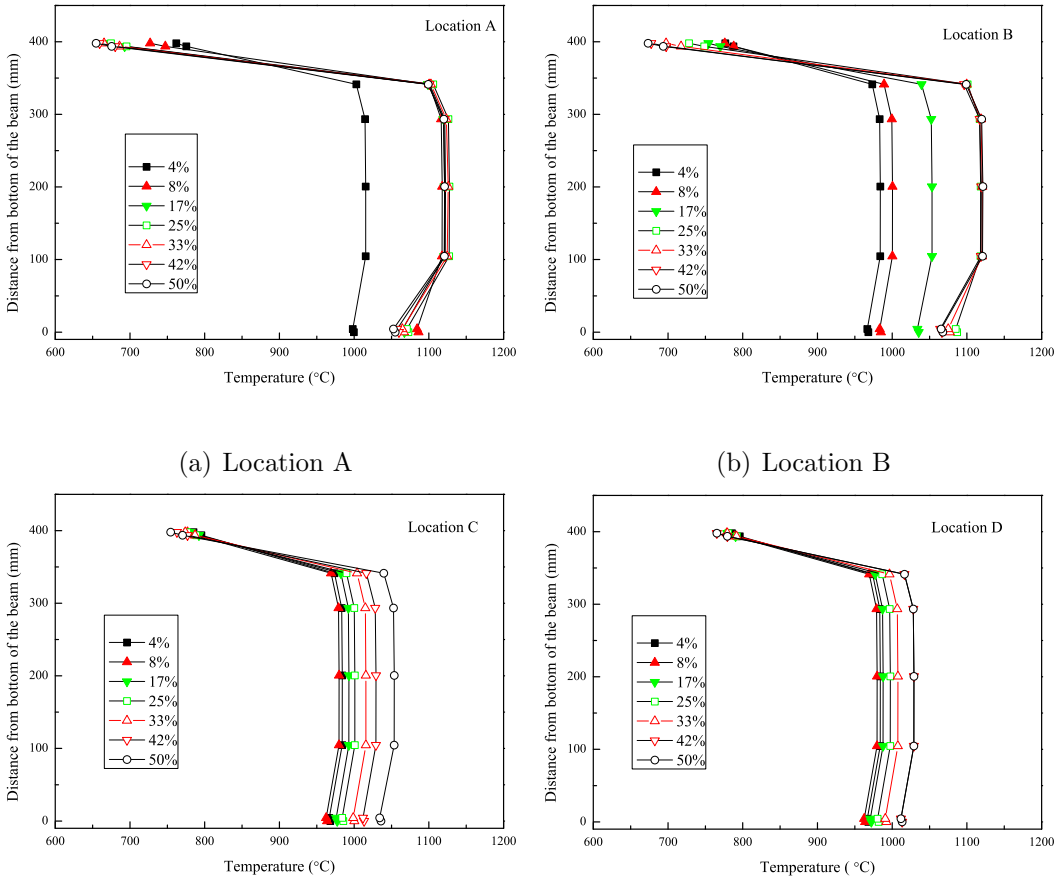

(a) Location A (b) Location B

(c) Location C (d) Location D

Figure 5.11: Through-depth temperature profile for the beam at different locations

the four locations, where the gradients can be readily identified. Temperature profile in the section should be transient, and each single profile curve in these figures represents the maximum through-depth thermal gradient in the course of temperature development in the beam section under a specific fire scenario. It is noted that the temperature does not strictly follow a linear distribution across the whole section depth. Temperatures in the bottom flange and most part of web are relatively close, although with values in the web slightly higher. This is because that the web being modelled is slightly thinner than the flanges. Large gradients are observed between upper region of the web and the top flange. This is due to

the heat sink effect of the concrete slab which has an appreciable effect on the thermal gradient in the beam section, with temperatures in the top flange up to 400 ℃ lower than those in the web. These through-depth temperature profiles indicate that using a uniform temperature distribution or a uniform thermal gradient for the whole beam section may not be realistic. Incorporating this thermal gradient can have significant influence in modeling steel beams in fire [133]. Figure 5.11 also shows that larger fires (25∼50%) produce greater thermal gradient than smaller fires at all of the four locations (more obvious at location A and B). This is because larger fires generate higher far-field temperatures and travel faster across the floor plate. Besides, they have shorter burning durations and thereby structural members are subjected to more intense heating within shorter time. The results are similar to those found in the study of effects of "long-cool" and "short-hot" parametric fires [112], where "short-hot" fires burn out quicker and produces larger thermal gradient through the section depth. It is also noted that the gradients generally decrease with the distance from the fire origin, which makes sense as beams at further locations experience longer and less rapid initial far-field heating.

Figure 5.12 shows the temperature profiles (selected according to the maximum overall through-depth gradients) in the concrete slab at different locations across the floor. Unlike those for the steel beam, much steeper gradients are found within shallower regions of the slab, while smaller gradients are found in deeper regions. The through-depth temperature profiles are smoother and demonstrate much stronger non-linear behaviour compared to those for the steel beam. Temperature gradients seem to be insensitive to the fire sizes at location (A) close to the initial fire origin. At locations further away from the fire origin (B,C,D), fire size has some effects on the thermal gradients indeed, i.e. smaller fire sizes tends

to produce smaller gradients but higher temperatures particularly in shallower regions which should be again attributed to the longer initial far-field heating from smaller fires. These spatial variations in temperature profiles seem to be more realistic but can not be obtained by conventional post-flashover fire models which assume uniformly heating throughout the whole compartment.

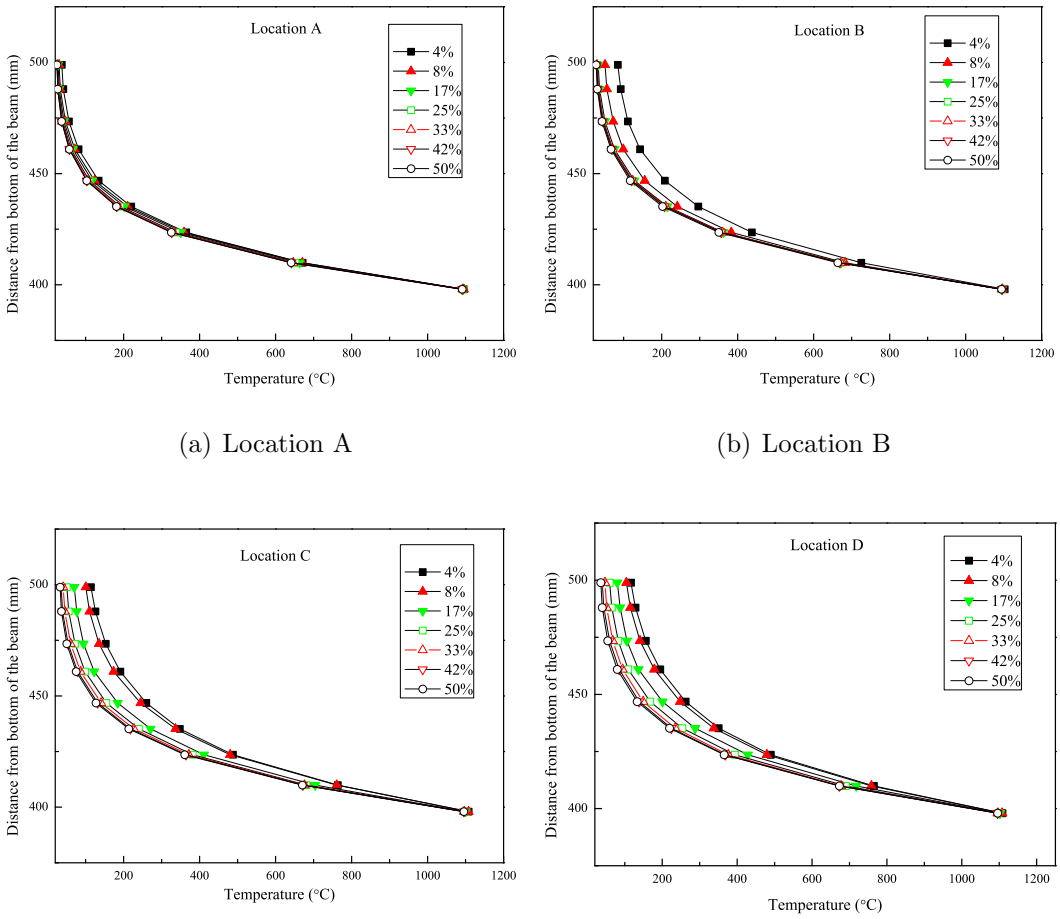

(a) Location A (b) Location B

(c) Location C (d) Location D

Figure 5.12: Through-depth temperature profile for the slab at different locations

It should be noted that, due to the difference in mean temperatures between in the steel beam and concrete slab, the largest contribution to the overall effective thermal gradient in a composite section would come from this temperature

difference. In terms of its structural effect it can be an order of magnitude larger than the gradients within the beam or the slab on their own.

5.4.2 Structural response

It will be interesting to examine the structural response of the structure under different traveling fire sizes as well as to compare them with the parametric fires. Two parametric fires are also considered with the same fire load density as given in Section 5.3.2, but with different ventilation conditions (opening factors 0.0264 $m^{0.5}$ for the "long-cool" and 0.186 $m^{0.5}$ for the"short-hot" fires respectively). In all the metrics examined for the building in this thesis, the structure did not show any sudden collapse bahaviour. So the most onerous scenario that could lead to failure can not be identified for this case study.

5.4.2.1 Global behaviour

The global structural behaviour under different fire sizes can be seen in Figure 5.13(a) and 5.13(b) for sizes 4% and 50% respectively. Due to significant difference in legth scales between the global structure and floor deformation, the deformed shape under different fire scenarios cannot be readily differentiated in Figure 5.13. The different characteristics of different sizes of traveling fires as well as parametric fires will be examined in detail by comparing several metrics at a number of typical locations along the floor. The deflections of the floor at the midspan as well as locations at 3 m (1/4 of the span) and 9 m (3/4 of the span) are shown in Figures 5.14 - 5.16 respectively. The figures show that the traveling fires examined in this work produced higher deflections at all locations for all the sizes compared to the

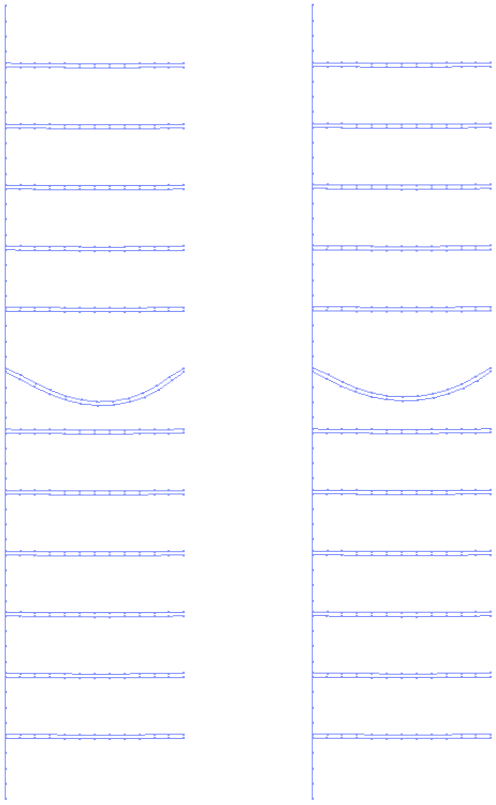

(a) fire size 4% (b) fire size 50%

Figure 5.13: Deformed shape under travelling fires of different sizes

parametric fires. Concerning the different sizes of traveling fires, it is seen that the smaller fire sizes result in higher maximum deflection (around 2500mm) but at a later time especially as the distance from the fire origin becomes larger (e.g. 3/4 of the span). It is interesting to note also that as the fire sizes become larger (over 25%) the results begin to converge for all the locations. In addition for all locations the "short hot" parametric fire results in higher maximum deflections and faster than the long cool parametric fire. It should be highlighted that deflections are reported here as a structural dimension and does not imply that higher deflections as those seen in case of the traveling fires (around L/5) will lead to failure of the structure. It is common practice to assume a L/20 deflection limit criterion

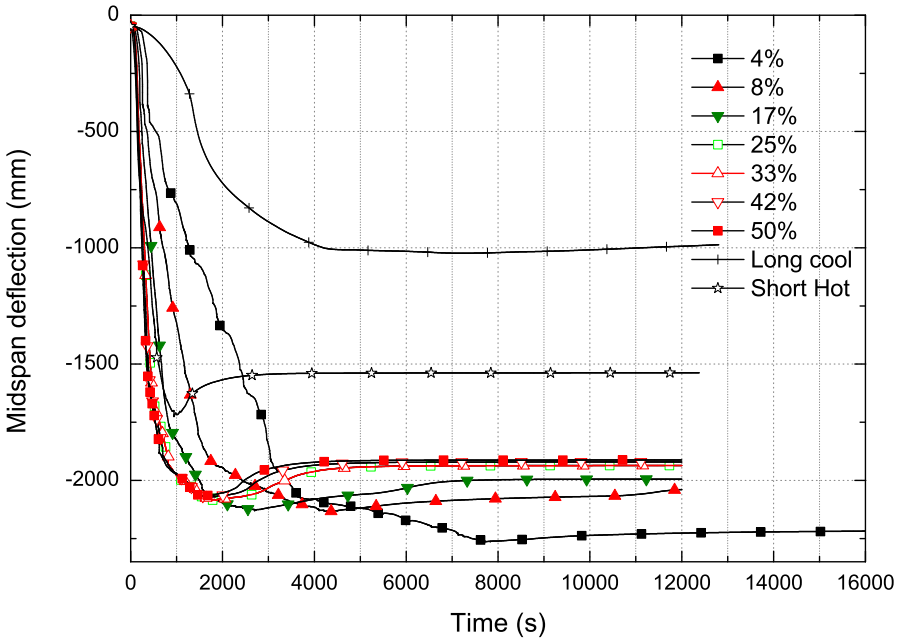

Figure 5.14: Deflection at midspan of the composite floor

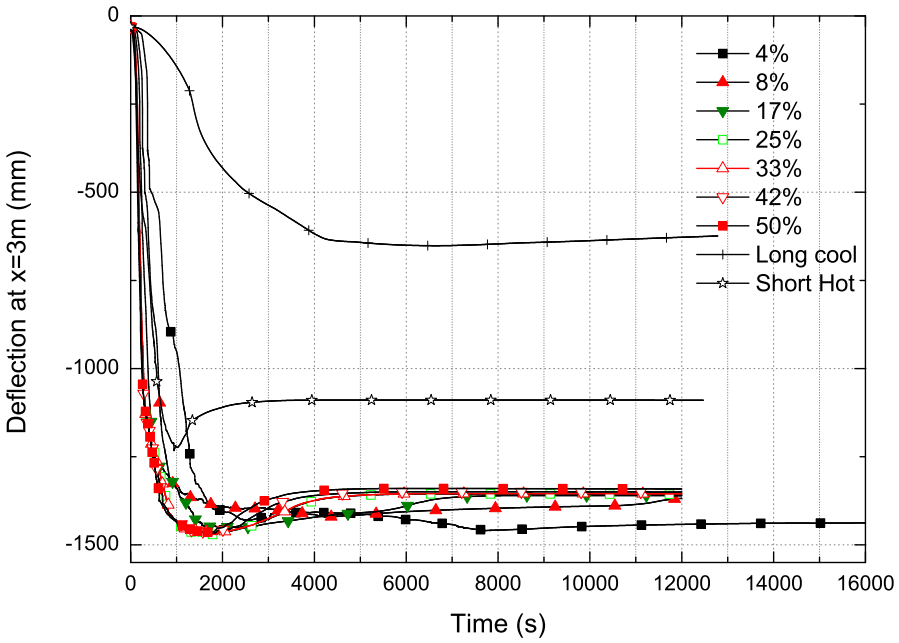

Figure 5.15: Deflection at 1/4 of the span of the composite floor

which is based on furnace tests however this criterion does not imply collapse [127]. Previous research in Cardington demonstrated that composite structures

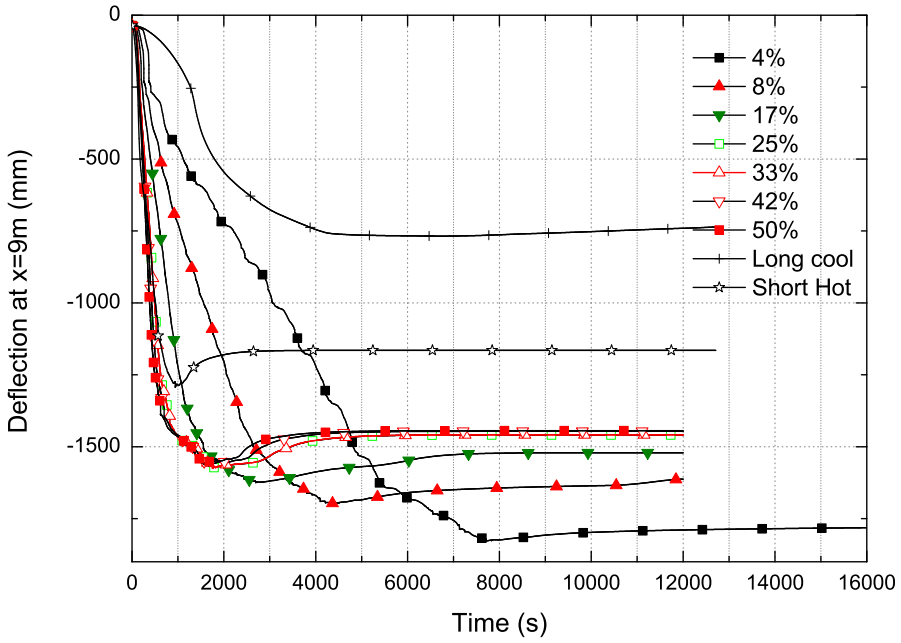

Figure 5.16: Deflection at 3/4 of the span of the composite floor

were able to sustain large deflections by using tensile membrane action to carry the loads, although a breach of horizontal compartmentation can occur [127], and that deflections are associated with thermal strains and not with mechanical strains thus do not necessarily imply damage [1, 134].

Figure 5.17 plots the horizontal displacement at the floor column connection at the fire floor. It can be seen that for all traveling fire sizes as well as parametric fires that the floors initially expand pushing the column outwards (negative direction) and then with the large deflections developing in the floor, the column pulls back inside (positive direction). The parametric fires cause the floor to expand to the same order of magnitude, about 25 mm, compared to the traveling fires at about 15 mm. The parametric fires also cause larger pull back compared to the traveling fires with the "long cool" fire achieving the highest value, although much later than other fire scenarios. It should also be noted that the traveling fires reach a similar maximum inward displacement as the "short hot" fire, with the larger

fire sizes achieving it earlier than the "short hot" fire. Stability of the column is ensured for all the cases as there is no sudden change.

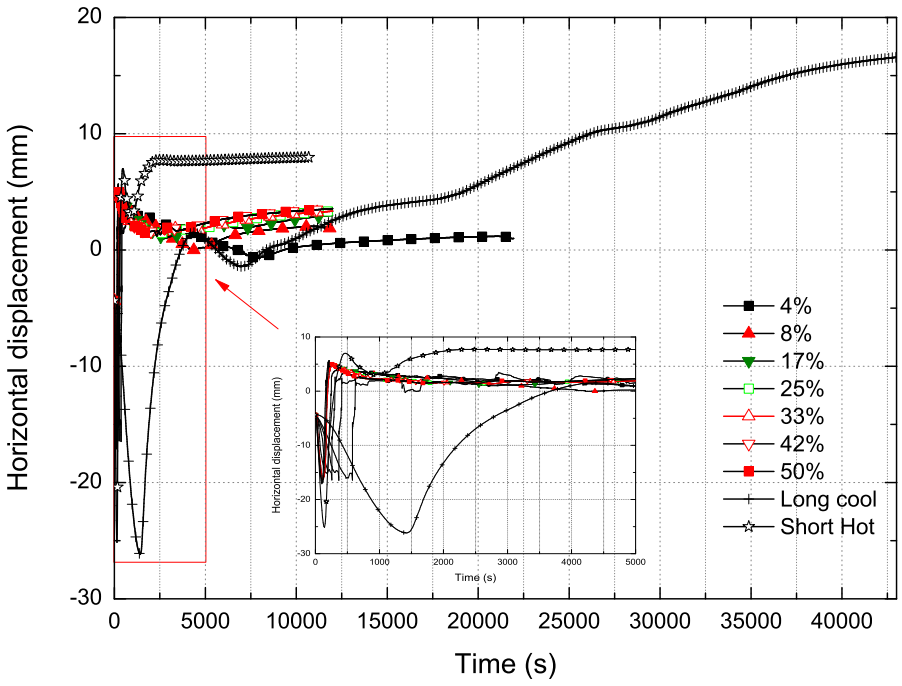

Figure 5.17: Horizontal displacement of the composite floor (negative and positive displacements indicating outward and inward movement respectively)

5.4.2.2 Local response

It would be interesting also to examine the horizontal reactions at the floor connection to the stiff core which represent the variation of the membrane forces in the fire. Figures 5.18-5.20 show the membrane forces of the floor as well as the forces of steel and concrete alone respectively. It can be seen that for both the traveling and parametric fires, the floor is initially in compression and then snaps into tension. The maximum compressive force reached is similar for both the parametric fires and traveling fire scenarios with those of the parametric fires

being higher. This is expected as in the case of a uniform fire, yielding will take place simultaneously along the length of the steel beam as well as development of plastic strains during simultaneous cooling that cause large tensile forces as the steel beam is regaining its strength [1, 135]. Larger fire sizes lead to quicker transition to tension as well as higher maximum tensile force reached. The "long cool" parametric fire also achieves higher tensile force after 22000 seconds. The axial forces in steel as shown in Figure 5.19 play a major role in the composite response in relation to concrete (Figure 5.20). This is expected as the composite floor is predominantly in tension and since concrete is weak in tension the forces are carried by the reinforcement and the steel beam. It should be mentioned here that reinforcement failure which would be critical in such a scenario is not accounted in the current model as it is outside the scope of the current paper however designers should take this possibility into account.

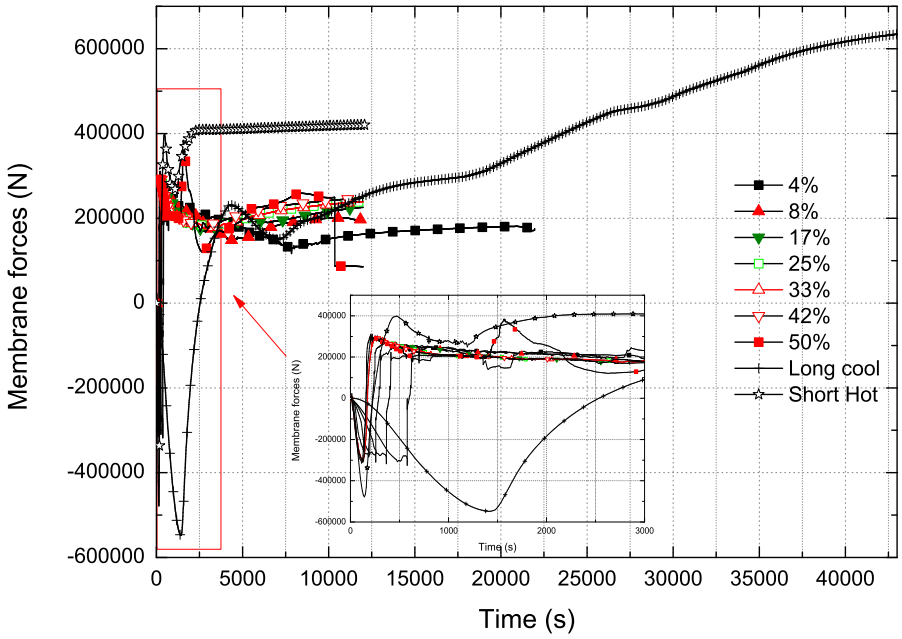

Figure 5.18: Membrane forces of the composite floor (negative and positive forces indicating compression and tension respectively)

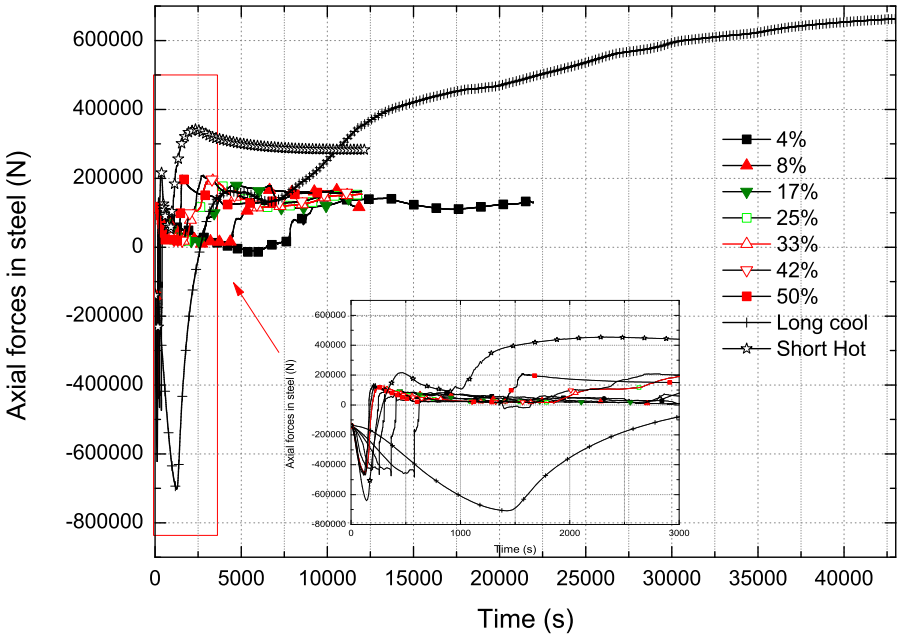

Figure 5.19: Axial forces in the steel beam (negative and positive forces indicating compression and tension respectively)

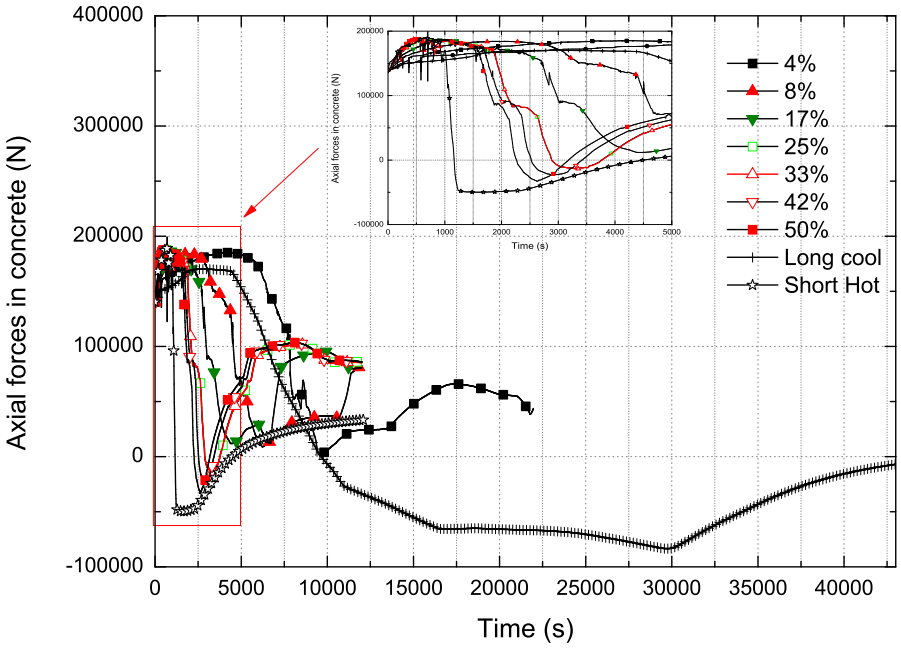

Figure 5.20: Axial forces in the concrete slab (negative and positive forces indicating compression and tension respectively)

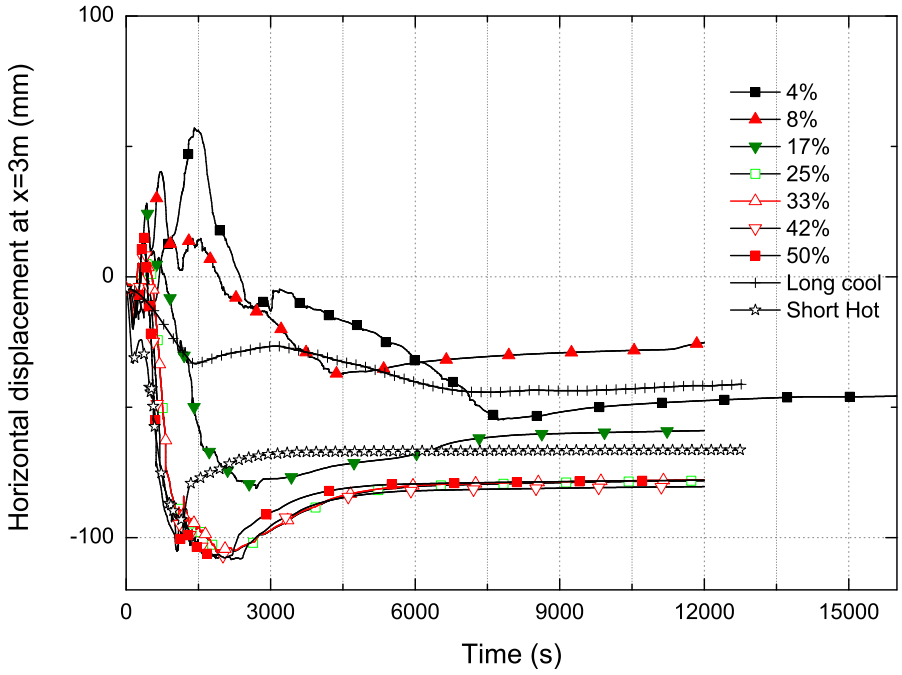

Figure 5.21: Horizontal displacement at 1/4 of the span (negative and positive displacements indicating outward and inward movement respectively)

Figures 5.21 to 5.23 plot the horizontal displacements at 3 m (1/4 of the span), 6 m (midspan) and 9 m (3/4 of the span). It can be seen that different traveling fire sizes show different characteristics along the length of the floor. There is significant horizontal cyclic displacements for the traveling fire scenarios which increase contrary to the fire sizes and that are not seen under parametric fires especially for the locations at midspan and at 3/4 of the span. For the first location (1/4 span), the 4% fire size reaches the biggest maximum positive horizontal displacement while larger fire sizes reach the biggest maximum negative horizontal displacement. For the other two locations, there is mainly positive horizontal displacement, and smaller fire sizes reach the maximum horizontal displacement.

Due to the fact that a distributed plasticity approach is used in this study and thus each element has five fiber sections along its length with each fiber having its own

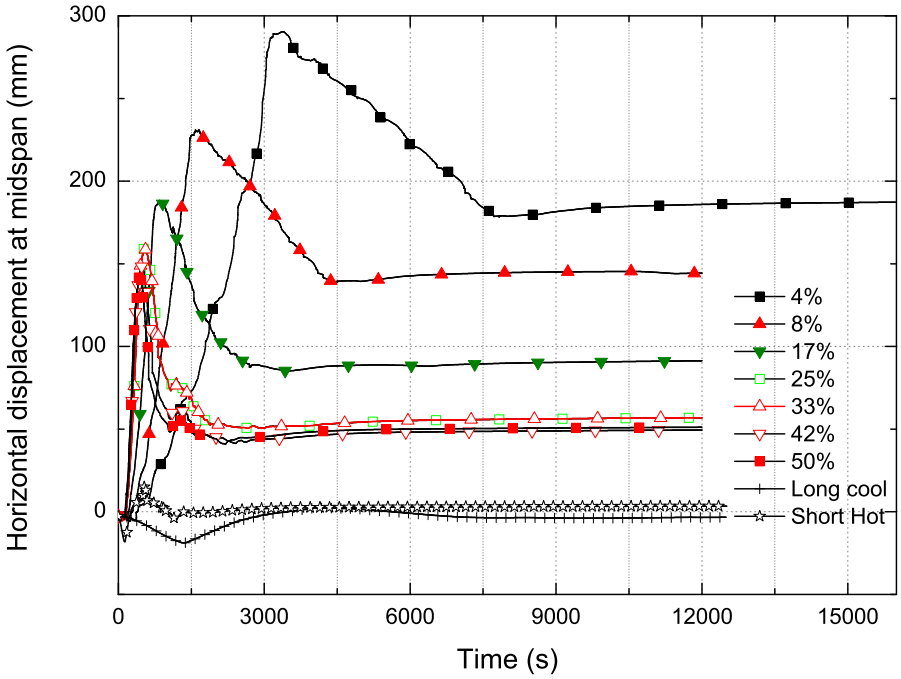

Figure 5.22: Horizontal displacement at midspan (negative and positive displacements indicating outward and inward movement respectively)

stress strain relationship history, the plastic deformation of the elements is a more flexible qualitative measure or indicator of damage. The plastic deformation of the steel beam at different locations (1/4 of the span, midspan and 3/4 of the span) is plotted in Figures 5.24-5.26 respectively. The plastic deformation presented here follows Eurocode material definition and thus includes creep implicitly. This assumption has been challenged as an explicit inclusion of creep may give a more accurate presentation. However, creep is a type of plastic deformation and it is outside the scope of this thesis to study this matter in depth. The emphasis is on the differences between certain locations according to different fire scenarios.

It can be seen that severe plastic deformation occurs along the length of the floor. The plastic deformation is not uniform as it was seen when plotting horizontal displacements. However, contrary to the horizontal displacements, the most

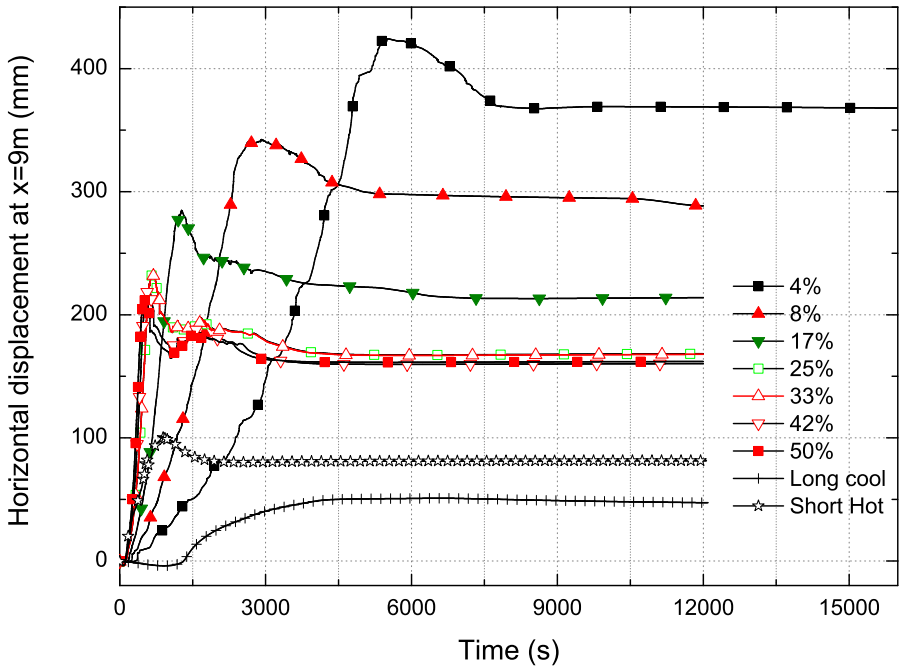

Figure 5.23: Horizontal displacement at 3/4 of the span (negative and positive displacements indicating outward and inward movement respectively)

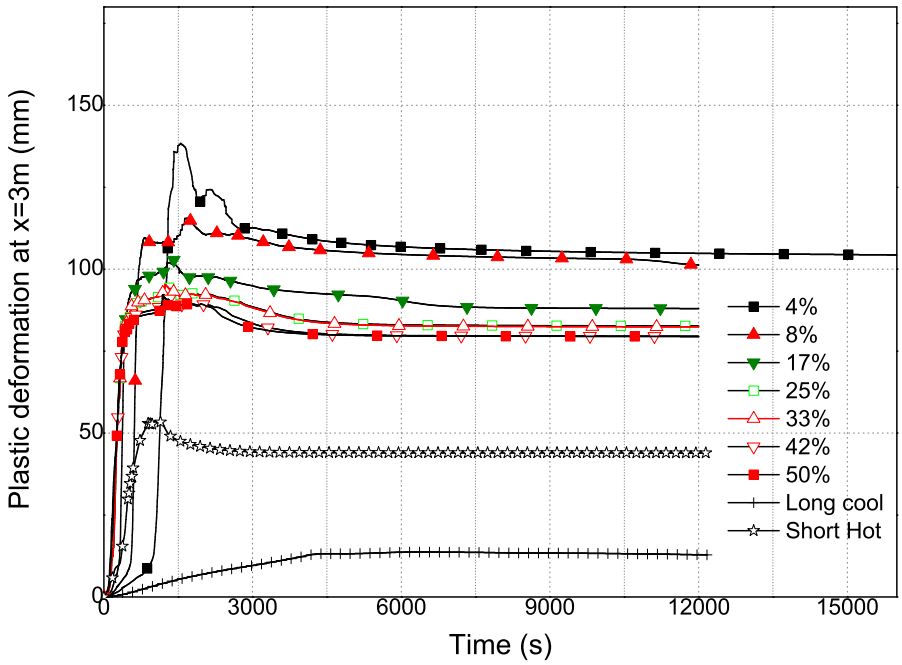

Figure 5.24: Plastic deformation of the steel beam at 1/4 of the span

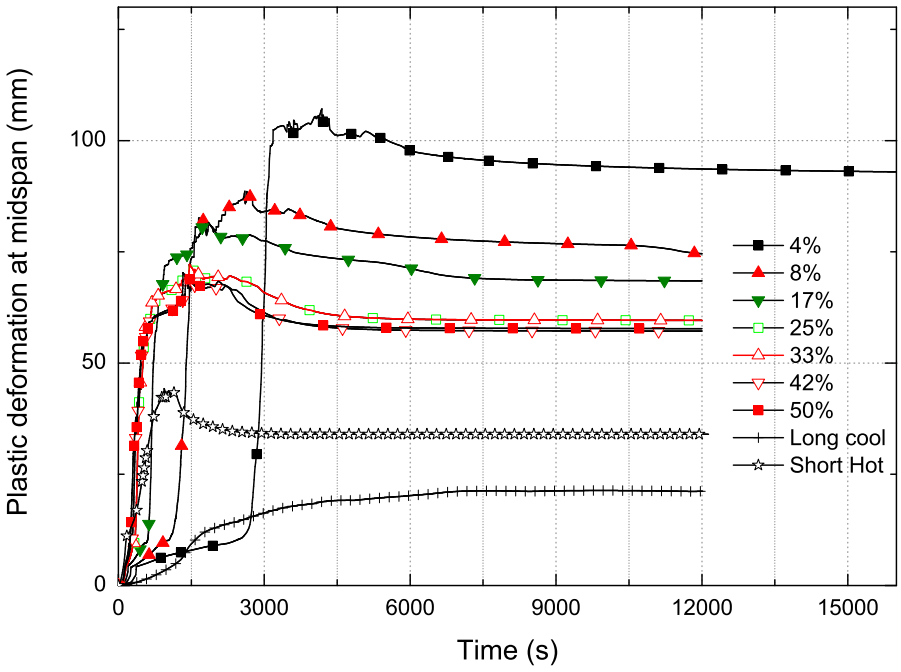

Figure 5.25: Plastic deformation of the steel beam at midspan

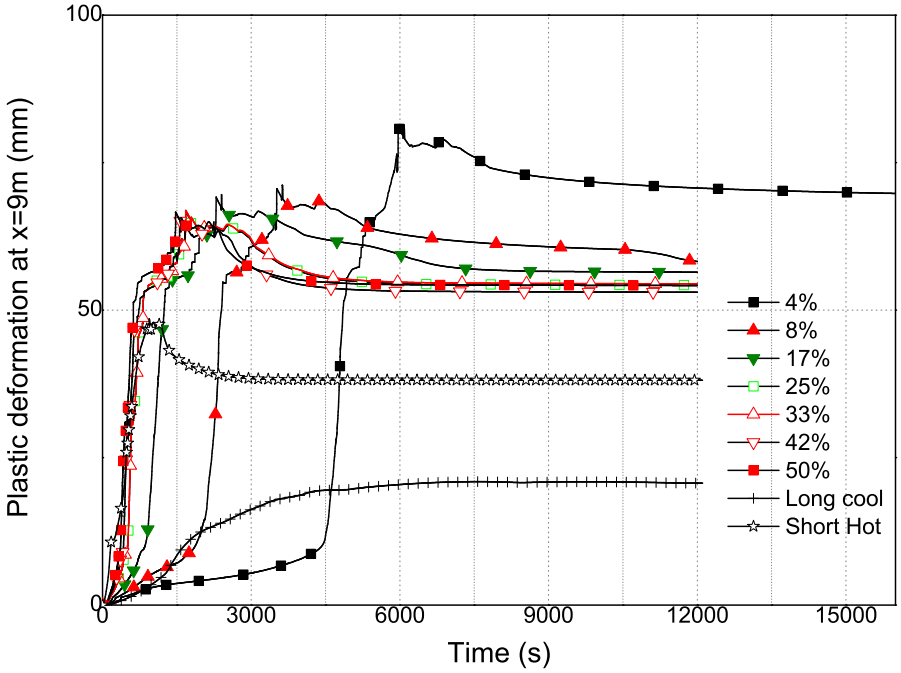

Figure 5.26: Plastic deformation of the steel beam at 3/4 of the span

onerous plastic deformation here occurs at the place of fire origin (on the west side of the floor). This is more firmly seen for the smaller traveling sizes. This is explained because as fire travels the elements subjected to near-field heating yield and also expand against their neighboring elements on the east that are just subjected to less intense far-field heating. This process generates even higher stresses for the near field elements especially for travelling fires of smaller sizes where it takes longer time for neighboring elements to reach similar temperatures.

Moreover, previous research during Cardington experiments [1] illustrated that deflections depend on the total strains and arise from thermal expansion strains. Thus high deflections commonly seen in fire were not strictly associated with mechanical strains and thus damage to the structures. The results demonstrate that these findings do not hold for non-uniform traveling fires when comparing different sizes between them, however for the same fire size the less deflected size on the west has higher plastic deformation than the more deflected east part of the floor.

These analyses can also provide guidance in the context of local failure and repair after a fire, although this work is not getting into detail on this aspect. This information is also useful to insurers that are interested in performance-based criteria when determining possible structural damage levels in fire in order to quantify insurance premiums. Further research will be required to examine these behaviors in other structural layouts such as trusses where possible buckling of a diagonal may take place or cellular beams.

5.5 Conclusions

The traveling fire methodology for structural fire design has been implemented in the OpenSees software framework. A case study has been carried out to examine both the thermal and structural responses of a composite structure in traveling fires. This case study is examined on a generic tall building which represents all typical characteristics found in modern construction.

The following are some of the major findings from the thermal analysis: (1) Traditional thinking of fire severity in light of "equal area" concept seems to be invalid for traveling fires. Fire temperature curves at symmetric locations were supposed to have identical fire severity according to the "equal area hypothesis" but lead to temperature differences up to 102% at these locations in the composite floor. (2) Traveling fires of larger sizes lead to lower times to reach critical steel temperature. (3) Traveling fires of smaller sizes produces higher peak temperatures in the concrete slab. (4) Thermal gradients are created in the upper regions of the beam due to the presence of neighboring concrete slab, and larger fires produce higher thermal gradients. (5) Large through-depth thermal gradients are observed in concrete slab. Smaller fire sizes tend to produce smaller gradients but higher temperatures at locations further away from the fire origin.

For the structural response of the building examined in this work, traveling fires produced higher midspan deflections than the parametric fires with travelling fires of smaller sizes producing the most onerous responses (in terms of deflection), although later in time. However, it should be noted that deflection alone is not the only criterion as it does not necessarily imply failure of the structure. The membrane forces in the floor were also monitored for all the cases. The composite

floor was initially in compression and then snapped into tension where steel was taking most of the axial forces for the rest of the time. The results showed that the parametric fires resulted in higher compressive and tensile forces compared to the traveling fire scenarios. Higher and cyclic horizontal displacements were also seen for the traveling cases that were not seen in the uniform parametric fires. Moreover, higher plastic deformations were observed for the traveling fires compared to the homogeneous parametric fires that could be an indicator of higher damage. Contrary to the findings for a concrete structure where travelling fires of medium size burning areas (e.g. 25%) were identified as the most severe scenarios [77], the highest plastic deformations were observed for fires of smallest sizes for the composite building in this work, and in particular in places with smaller deflections than the adjacent parts. This also implied that deflections may not always be an accurate representation of damage as seen during the Cardington tests [1].

The results of this study challenge the usual assumption that uniform post-flashover fires are always more conservative. Traveling fires which are non-homogeneous fires are seen to produce different structural behaviour which could not be predicted using uniformly burning fire models. Consequently, taking into account that post-flashover fire models like the parametric fires are unrealistic in large compartments, designers should examine the response of open plan tall buildings using a traveling fire methodology to address any potential vulnerabilities that may arise. Hence designers are advised to perform a parametric analysis by varying the fire sizes and ensure robustness for each scenario according to the predicted behaviour. This approach is similar to that in earthquake engineering where the near field and the far field earthquakes have different characteristics in terms of resulting structural performance and

any of them can be more onerous depending on the structure type. It should be mentioned here that this study was concentrated on a structural form of a conventional and generic tall building. It would be interesting also to examine the effect of these traveling fires in different and larger structural layouts where they could potentially have an even bigger influence.

Finally, this work also shows the capability of OpenSees as a flexible platform to perform advanced structural fire analysis by integrating fire, heat transfer and structural models.

Chapter 6

Conclusions and future work

6.1 Conclusions

Given the recent shift from prescriptive design approaches to performance-based approaches for structural fire design, it is essential to accurately quantify the thermal responses of structures in fire as well as to develop an advanced thermal analysis tool for the structural fire research community. This research has focused on the development, validation and application of methodologies for accurate predictions of thermal responses of structures in fire using numerical modelling. Conclusions from this work are summarised in the following discussions.

This work first explored the problem of radiative heat transfer from fire to structural members with cavity geometry (Chapter 3), which is a coupled heat transfer process by heat conduction in the member and radiation in the cavities. A numerical approach is proposed to address this coupled phenomenon, where

heat conduction is solved by the FEM and radiative heat transfer in smoke-filled cavities is solved by the FEDOM. The RTE solver using the FEDOM is verified with benchmark tests with analytical solutions and the coupled procedure is validated with experimental data from standard fire tests.

With satisfactory performance from the validation test, the proposed methodology is then used to model heat transfer in unprotected steel I-sections (with symmetrical cavities) which are exposed to uniformly heating environment in post-flashover fires. Results from the numerical modelling quantitatively highlighted the the effects of section geometry (characterized by cavity aspect ratio and section factor) on radiative heat exchange to the structural members. For example, the average net radiative heat flux for the inner surfaces can be as low as 48% of that for the outer surfaces for a steel I-section with cavity aspect ratio 0.59 and material emissivity 0.8. The presence of hot smoke in cavities demonstrated a different mechanism by augmenting radiative heat transfer by emission to the inner surfaces, with net heat fluxes increasing with smoke opacity.

The proposed approach was also used to examine the one-way coupling methodology which neglects the radiative heat exchange in the cavities. Results showed that the conventional approach could underpredict steel temperatures, particularly for steel members with large section factors and filled with optically thin smoke. This illustrated the importance of the self-radiating mechanism of I-sections in optically thin circumstances but the one-way approach could not take this into account. These findings also suggested that, in order to accurately predict the fire imposed heat fluxes to certain structural members, it is essential to adopt an advanced methodology such as the one proposed in this research to address the coupled heat transfer by conduction and radiation.

Central to the whole project, the open source OpenSees platform was chosen towards the development of an advanced numerical tool for modelling "structures-in-fire" for the structural fire engineering community. A thermal analysis framework for this purpose has been developed in OpenSees by adding a new fire module and a heat transfer module (Chapter 4). The development work followed the object-oriented design paradigm and thus is consistent with the ethos of OpenSees such as flexibility and extensibility. The fire module has incorporated some of the frequently used empirical fire models to determine the fire imposed boundary conditions, and the software design allows the inclusion of other more advanced fire models (or perhaps some middleware) to be readily achieved in the future. The heat transfer module adopted the finite element method (FEM) to solve heat conduction in structures and it is able to handle both the material non-linearities and arbitrary geometry. The performance of the developed framework has been tested through a series of benchmark problems with analytical solutions as well as measured data from large scale fire tests.

Using the developed thermal analysis framework, different types of fire scenarios can be covered and heat transfer in structures can be modelled using both two-dimensional and three-dimensional finite elements. Therefore, the performance of structures in fire can be modelled in conjunction with the modified module for structural analysis which is presented elsewhere. Moreover, the thermal analysis framework also provides methods that facilitates preparing temperature data for structural analysis using the fibre-based elements.

With confidence gained in the validation work for the thermal analysis framework, the extended OpenSees was used to investigate the thermal and structural responses of a composite structure to travelling fires (Chapter 5), which are more

physically realistic fire scenarios in large compartments and represent a paradigm shift for structural fire design. The latest effort in traveling fire methodology [6] has been implemented in the OpenSees framework for the case studies. The travelling fire methodology divides the whole floor area into the near field (burning area) and the far field at any time, and it generates spatially and temporally varying boundary conditions which are physically more realistic and can not be obtained from the conventional post-flashover fire models. The fire size (normally expressed in percentage of the floor area) in this methodology is normally varied parametrically in order to determine the "worst" scenario.

Contrary to the findings for a concrete structure where travelling fires of medium size burning areas (e.g. 25%) were identified as the most severe scenarios [77], results from the thermal analysis in this research showed that traveling fires of larger sizes are more detrimental to steel beams in terms of more rapid heating rate, while those with smaller sizes are more onerous to concrete slabs in light of higher peak temperatures. The results also showed that fires of large sizes tends to produce higher through-depth thermal gradients in the steel beam sections particularly in neighbouring regions with the concrete slab. Smaller fires produce lower thermal gradients but with higher temperatures in the concrete slab particularly at locations far from the fire origin. The subsequent structural analysis suggested that travelling fires produced higher deflections and higher plastic deformations in comparison with the uniform parametric fires, particularly with smaller fire sizes producing more onerous results. The work presented in Chapter 5 is the first effort to examine both the thermal and structural behaviour of a composite tall building in travelling fires. The results seems to be more physically convincing and they challenge the conventional assumption that the post-flashover fires are always more conservative for structural fire design.

The last chapter of this work also demonstrated the potential of the extended OpenSees framework to investigate structural fire performance by integrating fire, heat transfer and structural models. It acts as a advanced numerical platform where fire engineers and structural engineers are able to collaborate in order to utilise the most recent development in the two fields. Given its deliberately designed software structure and open-source nature, there is a strong potential for this framework to be accepted by the structural fire research community for performance-based structural fire design.

6.2 Future work

6.2.1 Enhancement of OpenSees

The thermal analysis framework hitherto developed for OpenSees has incorporated a rage of empirical fire models for determining fire imposed boundary conditions. Further research should be considered to link it with a CFD package as a general way to establish the fire environment and obtain essential field variables (such as gas temperature, convective heat transfer coefficient, radiative heat flux/intensity) at structural surfaces in the heat transfer model. FireFOAM, which has been developed based on the open-source CFD toolbox OpenFOAM (`http://www.openfoam.com`), is an ideal option for this purpose. OpenFOAM shares many merits of OpenSees such as the use of object-oriented programming in C++ and massive parallelization. FireFOAM is currently under active development to include fire related sub-models [136, 137], and a recent

study showed that FireFOAM is able to accurately capture the main characteristics (such as the mean cross-stream velocities and puffing frequency) of a turbulent buoyant helium plume [138].

However, as discussed in Section 2.5.4, the coupling between heat transfer (HT) modelling and CFD modelling should address the problems associated with significant differences in time and length scales, and spatial discretisation schemes in the two approaches. It is highly desirable to develop a middleware program that processes the results from CFD modelling and automatically maps the field variables onto the surfaces of a three-dimensional heat transfer model. In some cases (e.g. an unprotected steel I-section column exposed to localised fires), such a program should include a RTE solver in order to account for the directional radiative intensities from the CFD modelling and to address the radiative heat exchange in structural cavities as discussed in Chapter 3. Similar to the HT-CFD linking, it is also needed to develop a middleware program that maps the temperatures from a three-dimensional heat transfer model using solid elements to structural models made up of a combination of beam-column elements and plate/shell elements. This would result in a fully automated software workflow for modelling the interaction of fire, heat transfer and structural response which is graphically illustrated in Figure 6.1.

6.2.2 Travelling fires

In Chapter 5, the thermal and structural analysis was performed based on the assumption that only one floor of the tall building was on fire. In some cases fire may also travel vertically from one floor to another therefore it is possible to

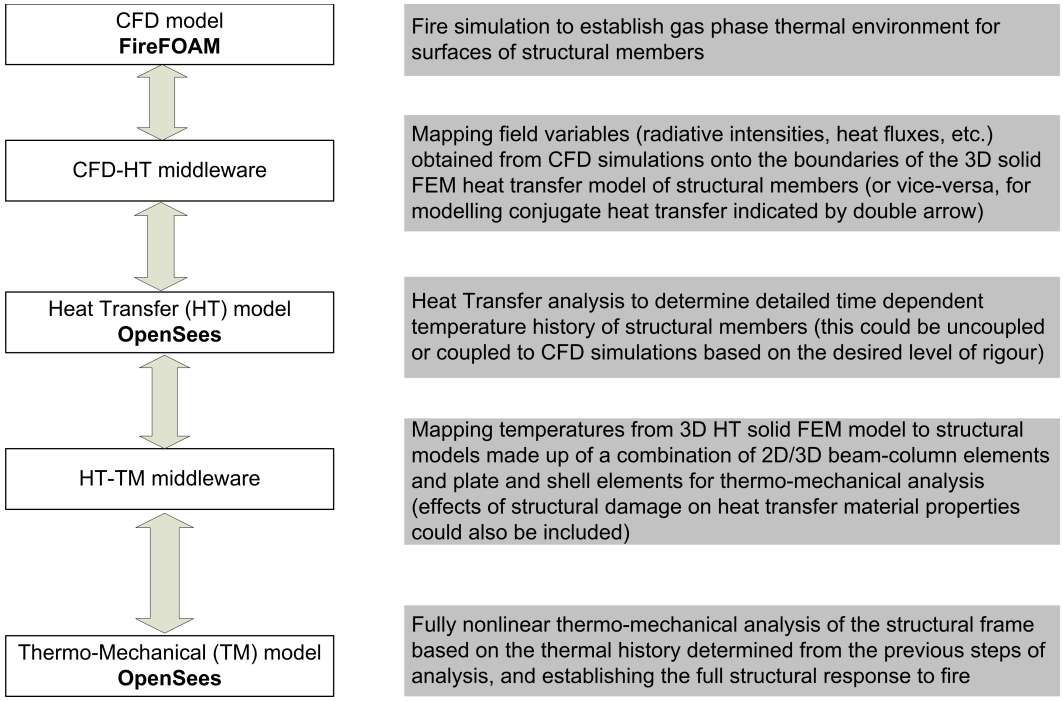

Figure 6.1: Proposed enhancement of OpenSees framework for modelling structures in fire

have travelling fires on multiple floors which has been witnessed in the accidental fires in WTC buildings. A parametric study would be of value for investigating the structural behaviour of a tall building under multi-floor fires by considering different travelling speeds in the vertical direction with also including different fire sizes and different horizontal travel directions.

In addition, the travelling fire model currently implemented in OpenSees also needs further improvement. As discussed in [74], the current implementation relies on the empirical Alpert ceiling jet model to estimate the far field temperatures, and this would limit its application to buildings with simple floor geometry (e.g. a rectangular floor without core) and simple fire travelling paths (e.g. straight fire). Although this kind of linearly travelling fires represent significant improvement compared with the parametric fires, it seems that most fires in reality would

depart from this linearly type therefore more sophisticated implementations of the travelling fire methodology should be developed.

Using CFD modelling would be one of the options to improve the current methodlology. However, this approach still requires a deterministic model to predict the travelling paths of fire, which amounts to predicting fire spread over solid fuels that involves several other aspects such as heat feedback from the gas phase and pyrolysis of the solid fuel. Field quantities such as accumulated net incident heat flux [139] or radiant heat flux [140] may be used as the ignition criteria in modelling fire spread. However it seems computationally challenging to fully address such a coupled problem with gas phase combustion and solid phase pyrolysis over a large floor area (e.g. over 1000 m^2). Another possible approach may be to use stochastic models [141, 142, 143] to determine the most possible travelling paths then use CFD as a deterministic model to establish the resultant thermal environment.

References

[1] A. Usmani, J. Rotter, S. Lamont, A. Sanad, M. Gillie, Fundamental principles of structural behaviour under thermal effects, Fire Safety Journal 36 (8) (2001) 721–744.

[2] A. Usmani, Y. Chung, J. Torero, How did the WTC towers collapse: a new theory, Fire Safety Journal 38 (6) (2003) 501–533.

[3] A. Law, J. Stern-Gottfried, M. Gillie, G. Rein, Structural engineering and fire dynamics: Advances at the interface and Buchanan's challenge, in: IAFSS 2011: 10th International Symposium on Fire Safety Science, 2011, pp. 1563–1576.

[4] V. Kodur, M. Garlock, N. Iwankiw, Structures in fire: State-of-the-art, research and training needs, Fire Technology 48 (4) (2012) 825–839.

[5] J. Stern-Gottfried, G. Rein, Travelling fires for structural design–Part I: Literature review, Fire Safety Journal 54 (2012) 74–85.

[6] J. Stern-Gottfried, G. Rein, Travelling fires for structural design-Part II: Design methodology, Fire Safety Journal 54 (2012) 96–112.

[7] A. Usmani, J. Zhang, J. Jiang, Y. Jiang, I. May, Using Opensees for structures in fire, Journal of Structural Fire Engineering 3 (1) (2012) 57–70.

[8] S. Dembele, R. Rosario, J. Wen, Investigation of glazing behavior in a fire environment using a spectral discrete ordinates method for radiative heat transfer, Numerical Heat Transfer, Part B: Fundamentals 52 (6) (2007) 489–506.

[9] S. Dembele, R. Rosario, Q. Wang, P. Warren, J. Wen, Thermal and stress analysis of glazing in fires and glass fracture modeling with a probabilistic approach, Numerical Heat Transfer, Part B: Fundamentals 58 (6) (2010) 419–439.

[10] T. Harmathy, Fire safety design and concrete, Longman Scientific & Technical, 1993.

[11] BS EN 1992-1-2. Eurocode 2: Design of concrete structures - Part 1-2: General rules - Structural fire design (2004).

[12] T. Lie, et al., Structural fire protection, Vol. 78, American Society of Civil Engineers, 1992.

[13] BS EN 1993-1-2. Eurocode 3: Design of steel structures - Part 1-2: General rules - Structural fire design (2005).

[14] V. Kodur, M. Dwaikat, R. Fike, et al., High-temperature properties of steel for fire resistance modeling of structures, Journal of Materials in Civil Engineering 22 (2010) 423.

[15] V. Voller, C. Swaminathan, B. Thomas, Fixed grid techniques for phase change problems: A review, International Journal for Numerical Methods in Engineering 30 (4) (1990) 875–898.

[16] H. Huang, A. Usmani, Finite element analysis for heat transfer: theory and software, Springer-Verlag, 1994.

[17] E. Lemmon, Multidimensional integral phase change approximations for finite element conduction codes, in: Numerical methods in heat transfer, Wiley-Interscience, Chichester, 1981, pp. 201–213.

[18] A. Buchanan, Structural design for fire safety, Wiley, 2001.

[19] BS EN 1991-1-2:2002. Eurocode 1: Actions on structures - Part 1-2: General actions - Actions on structures exposed to fire (2005).

[20] A. Jowsey, Fire imposed heat fluxes for structural analysis, Ph.D. thesis, The University of Edinburgh (2006).
URL `http://www.era.lib.ed.ac.uk/handle/1842/1480`

[21] H. Liang, GeniSTELA-A generalised engineering methodology for thermal analysis of structural members in natural fires, Ph.D. thesis, The University of Edinburgh (2008).

[22] Y. Wang, Steel and Composite Structures: Behaviour and Design for Fire Safety, Taylor & Francis, 2002.

[23] G. Griffin, The modeling of heat transfer across intumescent polymer coatings, Journal of Fire Sciences 28 (3) (2010) 249–277.

[24] M. Bartholmai, R. Schriever, B. Schartel, Influence of external heat flux and coating thickness on the thermal insulation properties of two different intumescent coatings using cone calorimeter and numerical analysis, Fire and materials 27 (4) (2003) 151–162.

[25] X. Dai, Y. Wang, C. Bailey, A simple method to predict temperatures in steel joints with partial intumescent coating fire protection, Fire technology 46 (1) (2010) 19–35.

[26] U. Wickstrom, Calculation of heat transfer to structures exposed to fire - shadow effects, in: InterFlam 2001: 9 th International Fire Science & Engineering Conference, 2001, pp. 451–460.

[27] Z. Wang, Geometric effect of radiative heat exchange in concave structure with application to heating of steel I-sections in fire, International Journal of Heat and Mass Transfer 53 (5) (2010) 997–1003.

[28] J. Franssen, Calculation of temperature in fire-exposed bare steel structures: Comparison between env 1993-1-2 and en 1993-1-2, Fire safety journal 41 (2) (2006) 139–143.

[29] U. Wickstrom, Comments on calculation of temperature in fire-exposed bare steel structures in prEN 1993-1-2: Eurocode 3 - design of steel structures - part 1-2: general rulesstructural fire design, Fire Safety Journal 40 (2) (2005) 191–192.

[30] Y. Jiang, G. Rein, S. Welch, A. Usmani, Modeling fire-induced radiative heat transfer in smoke-filled structural cavities, International Journal of Thermal Sciences (2012).
URL http://dx.doi.org/10.1016/j.ijthermalsci.2012.11.005

[31] W. Grosshandler, Fire resistance determination and performance prediction research needs workshop: Proceedings, Tech. Rep. NISTIR 6890, National

Institute of Standards and Technology, US Department of Commerce (2002).

[32] J. Franssen, Safir: A thermal/structural program for modeling structures under fire, Engineering Journal,AISC 42 (3) (2005) 143–158.

[33] Y. Jiang, A. Usmani, W. S., Development of heat transfer modelling capability in OpenSees for structures in fire, in: Application of Structural Fire Design, 2011, pp. 324–330.
URL https://www.wiki.ed.ac.uk/download/attachments/116789091/ASFE_YJiang_5.pdf

[34] Y. Jiang, P. Kotsovinos, A. Usmani, G. Rein, J. Stern-Gottfried, Numerical investigation of thermal responses of a composite structure in horizontally travelling fires using OpenSees, Procedia Engineering (in press).

[35] J. Reddy, D. Gartling, The finite element method in heat transfer and fluid dynamics, 2nd Edition, CRC, 2010.

[36] J. Winget, T. Hughes, Solution algorithms for nonlinear transient heat conduction analysis employing element-by-element iterative strategies, Computer Methods in Applied Mechanics and Engineering 52 (1-3) (1985) 711–815.

[37] J. Bergheau, R. Fortunier, Finite element simulation of heat transfer, Wiley, 2008.

[38] D. Drysdale, An Introduction to Fire Dynamics, 2nd Edition, John Wiley & Sons, 1999.

[39] S. Welch, A. Jowsey, S. Deeny, R. Morgan, J. Torero, BRE large compartment fire tests–Characterising post-flashover fires for model validation, Fire Safety Journal 42 (8) (2007) 548–567.

[40] A. Buchanan, The challenges of predicting structural performance in fires, in: IAFSS 2008: 9th International Symposium on Fire Safety Science, Vol. 9, 2008, pp. 79–90.

[41] J. Franssen, Improvement of the parametric fire of eurocode 1 based on experimental tests results, in: Proceedings of the 6th International Symposium on Fire Safety Science, 2000, pp. 927–938.

[42] T. Lennon, D. Moore, The natural fire safety conceptfull-scale tests at Cardington, Fire Safety Journal 38 (7) (2003) 623–643.

[43] R. Feasey, A. Buchanan, Post-flashover fires for structural design, Fire Safety Journal 37 (1) (2002) 83–105.

[44] J. Franssen, Designing steel structures for fire safety, CRC, 2009.

[45] A. Bwalya, An overview of design fires for building compartments, Fire Technology 44 (2) (2008) 167–184.

[46] C. Barnett, BFD curve: a new empirical model for fire compartment temperatures, Fire Safety Journal 37 (5) (2002) 437–463.

[47] J. Zehfuss, D. Hosser, A parametric natural fire model for the structural fire design of multi-storey buildings, Fire Safety Journal 42 (2) (2007) 115–126.

[48] N. Pope, C. Bailey, Quantitative comparison of FDS and parametric fire curves with post-flashover compartment fire test data, Fire Safety Journal 41 (2) (2006) 99–110.

[49] Y. Hasemi, Y. Yokobashi, T. Wakamatsu, A. Ptchelintsev, Modelling of heating mechanism and thermal response of structural components exposed to localized fires: A new application of diffusion flame modelling to fire safety engineering, in: Thirteenth meeting of the UJNR panel on fire research and safety, 1996, pp. 237–247.

[50] T. Wakamatsu, Y. Hasemi, K. Kagiya, D. Kamikawa, Heating mechanism of unprotected steel beam installed beneath ceiling and exposed to a localized fire: Verification using the real-scale experiment and effects of the smoke layer, in: Proceedings of the 7th International Symposium on Fire Safety Science, International Association for Fire Safety Science, London, UK, 2002, pp. 1099–1110.

[51] V. Kodur, L. Gu, M. Garlock, Review and assessment of fire hazard in bridges, Transportation Research Record: Journal of the Transportation Research Board 2172 (1) (2010) 23–29.

[52] B. Y. Lattimer, Heat fluxes from fires to surfaces, in: The SFPE Handbook of Fire Protection Engineering, 3rd Edition, National Fire Protection Association, 2002, Ch. 2-14, pp. 269–296.

[53] J. Schleich, L. Cajot, M. Pierre, M. Brasseur, J. Franssen, D. Joyeux, L. Twilt, J. Van Oerle, G. Aurtenetxe, Development of design rules for steel structures subjected to natural fires in large compartments, Tech. Rep. EUR 18868 EN, European Communities (1999).

[54] G. Heskestad, Fire plumes, flame height, and air entrainment, in: The SFPE Handbook of Fire Protection Engineering, 3rd Edition, National Fire Protection Association, 2002, Ch. 2-1, pp. 1–17.

[55] R. Alpert, Calculation of response time of ceiling-mounted fire detectors, Fire Technology 8 (3) (1972) 181–195.

[56] R. L. Alpert, Ceiling jet flows, in: The SFPE Handbook of Fire Protection Engineering, 3rd Edition, National Fire Protection Association, 2002, Ch. 2-2, pp. 18–31.

[57] S. Deeny, T. Stratford, Stability of RC structure under non-uniform thermal exposure, in: Structures in Fire: Proceedings of the Sixth International Conference, DEStech Publications, Inc, 2010, pp. 270–277.

[58] J. G. Quintiere, Compartment fire modeling, in: The SFPE Handbook of Fire Protection Engineering, 3rd Edition, National Fire Protection Association, 2002, Ch. 3-5, pp. 162–170.

[59] S. Olenick, D. Carpenter, An updated international survey of computer models for fire and smoke, Journal of Fire Protection Engineering 13 (2) (2003) 87–110.

[60] J. Cadorin, J. Franssen, A tool to design steel elements submitted to compartment fires - OZone V2. Part 1: pre-and post-flashover compartment fire model, Fire Safety Journal 38 (5) (2003) 395–427.

[61] J. Cadorin, D. Pintea, J. Dotreppe, J. Franssen, A tool to design steel elements submitted to compartment fires - OZone V2. Part 2: Methodology and application, Fire Safety Journal 38 (5) (2003) 429–451.

[62] J. Cadorin, On the application field of OZone V2, Rapport interne Nº M&S/2002-003 University of Liege.

[63] K. Remesh, K. Tan, Performance comparison of zone models with compartment fire tests, Journal of Fire Sciences 25 (4) (2007) 321–353.

[64] X. Zhang, G. Hadjisophocleous, An improved two-layer zone model applicable to both pre-and post-flashover fires, Fire Safety Journal 53 (2012) 63–71.

[65] V. Novozhilov, Computational fluid dynamics modeling of compartment fires, Progress in Energy and Combustion science 27 (6) (2001) 611–666.

[66] J. Franssen, Structures in fire: yesterday, today and tomorrow, in: IAFSS 2005: 10th International Symposium on Fire Safety Science, 2005, pp. 21–35.

[67] S. Welch, S. Miles, S. Kumar, T. Lemaire, A. Chan, FIRESTRUC - integrating advanced three-dimensional modelling methodologies for predicting thermo-mechanical behaviour of steel and composite structures subjected to natural fires, in: IAFSS 2008: 9th International Symposium on Fire Safety Science, 2009, pp. 1315–1326.
URL `http://www.era.lib.ed.ac.uk/handle/1842/2699`

[68] K. Prasad, H. Baum, Coupled fire dynamics and thermal response of complex building structures, Proceedings of the Combustion Institute 30 (2) (2005) 2255–2262.

[69] D. Duthinh, K. McGrattan, A. Khaskia, Recent advances in fire-structure analysis, Fire Safety Journal 43 (2) (2008) 161–167.

[70] N. Tondini, O. Vassart, J. Franssen, Development of an interface between CFD and FE software, in: Proceedings of the 7th International Conference on Structures in Fire, ETH Zürich, 2012, pp. 459–468.

[71] R. Gann, A. P. Hamins, K. B. McGrattan, G. W. Mulholland, H. E. Nelson, T. J. Ohlemiller, W. M. Pitts, K. R. Prasad, Reconstruction of

the fires in the world trade center towers, Tech. Rep. NIST NCSTAR 1-5, National Institute of Standards and Technology, US Department of Commerce (2005).

[72] G. Rein, X. Zhang, P. Williams, B. Hume, A. Heise, A. Jowsey, B. Lane, J. Torero, Multi-story fire analysis for high-rise buildings, in: InterFlam 2007: 11th International Fire Science & Engineering Conference, 2007, pp. 605–616.
URL http://www.era.lib.ed.ac.uk/handle/1842/1980

[73] J. Stern-Gottfried, A. Law, G. Rein, M. Gillie, J. Torero, A performance based methodology using travelling fires for structural analysis, in: 8th International Conference on Performance-Based Codes and Fire Safety Design Methods, 2010.

[74] J. Stern-Gottfried, Travelling fires for structural design, Ph.D. thesis, The University of Edinburgh (2011).
URL http://www.era.lib.ed.ac.uk/handle/1842/5244

[75] J. Sandström, X. Cheng, M. Veljkovic, U. Wickström, T. Heistermann, Travelling fires for cfd, in: IAFSS 2011: 10th International Symposium on Fire Safety Science, 2011, pp. 1479–1488.

[76] K. McGrattan, B. Klein, S. Hostikka, J. Floyd, Fire dynamics simulator (version 5), technical reference guide, Tech. Rep. NIST Special Publication 1019-5, National Institute of Standards and Technology, US Department of Commerce (2007).

[77] A. Law, J. Stern-Gottfried, M. Gillie, G. Rein, The influence of travelling fires on a concrete frame, Engineering Structures 33 (5) (2011) 1635–1642.

[78] C. Röben, M. Gillie, J. Torero, Structural behaviour during a vertically travelling fire, Journal of Constructional Steel Research 66 (2) (2010) 191–197.

[79] P. Kotsovinos, Y. Jiang, A. Usmani, Effect of vertically travelling fires on the collapse of tall buildings, International Journal of High-Rise Building (invited submission).

[80] Z. Wang, K. Tan, Radiative heat transfer for structural members exposed to fire: An analytical approach, Journal of Fire Sciences 26 (2) (2008) 133–152.

[81] J. Howell, R. Siegel, M. Menguc, Thermal Radiation Heat Transfer, 5th Edition, CRC Press, 2010.

[82] J. Ghojel, A new approach to modeling heat transfer in compartment fires, Fire Safety Journal 31 (3) (1998) 227–237.

[83] J. Ghojel, M. Wong, Heat transfer model for unprotected steel members in a standard compartment fire with participating medium, Journal of Constructional Steel Research 61 (6) (2005) 825–833.

[84] F. Incropera, D. DeWitt, Fundamentals of Heat and Mass Transfer, 5th Edition, John Wiley & Sons, 2001.

[85] J. Zhao, L. Liu, Second-order radiative transfer equation and its properties of numerical solution using the finite-element method, Numerical Heat Transfer, Part B: Fundamentals 51 (3-4) (2007) 391–409.

[86] W. Fiveland, Discrete-ordinates solutions of the radiative transport equation for rectangular enclosures, Journal of Heat Transfer 106 (1984) 699–706.

[87] A. Sanchez, T. Smith, Surface radiation exchange for two-dimensional rectangular enclosures using the discrete-ordinates method, Journal of Heat Transfer 114 (2) (1992) 465–472.

[88] W. Fiveland, Comparison of discrete ordinates formulations for radiative heat transfer in multidimensional geometries, Journal of thermophysics and heat transfer 9 (1) (1995) 47–54.

[89] BS 4-1. Structural steel sections - Part 1:Specfication for hot-rolled sections (2005).

[90] C. Abecassis-Empis, P. Reszka, T. Steinhaus, A. Cowlard, H. Biteau, S. Welch, G. Rein, J. Torero, Characterisation of Dalmarnock fire Test One, Experimental Thermal and Fluid Science 32 (7) (2008) 1334–1343.

[91] K. McGrattan, J. Floyd, G. Forney, H. Baum, S. Hostikka, Improved radiation and combustion routines for a large eddy simulation fire model, in: IAFSS 2003: 7th International Symposium on Fire Safety Science, 2003, pp. 827–838.

[92] R. Viskanta, M. Mengüç, Radiation heat transfer in combustion systems, Progress in Energy and Combustion Science 13 (2) (1987) 97–160.

[93] V. Solovjov, B. Webb, An efficient method for modeling radiative transfer in multicomponent gas mixtures with soot, Journal of heat transfer 123 (2001) 450 – 457.

[94] C. Tien, K. Lee, A. Stretton, Radiation heat transfer, in: The SFPE Handbook of Fire Protection Engineering, 3rd Edition, National Fire Protection Association, 2002, Ch. 1-4, pp. 73–89.

[95] J. Widmann, Evaluation of the Planck mean absorption coefficients for radiation transport through smoke, Combustion Science and Technology 175 (12) (2003) 2299–2308.

[96] D. Wainman, B. Kirby, Compendium of UK Standard Fire Test Data: Unprotected Structural Steel-1, British Steel Corporation, Swinden Laboratories, 1988.

[97] J. Quintiere, M. Di Marzo, R. Becker, A suggested cause of the fire-induced collapse of the World Trade Towers, Fire safety journal 37 (7) (2002) 707–716.

[98] J. Chang, A. Buchanan, P. Moss, Effect of insulation on the fire behaviour of steel floor trusses, Fire and Materials 29 (4) (2005) 181–194.

[99] V. Kodur, M. Garlock, N. Iwankiw, National workshop on structures in fire: State-of-the-art, research and training needs, Tech. Rep. NIST GCR 07-915, National Institute of Standards and Technology, US Department of Commerce (2007).

[100] M. Fowler, K. Scott, UML distilled: a brief guide to the standard object modeling language, Addison-Wesley Longman Publishing Co., 2000.

[101] F. McKenna, Object-oriented finite element programming: frameworks for analysis, algorithms and parallel computing, Ph.D. thesis, University of California, Berkeley (1997).

[102] F. McKenna, M. Scott, G. Fenves, Nonlinear finite-element analysis software architecture using object composition, Journal of Computing in Civil Engineering 24 (1) (2010) 95–107.

[103] J. Franssen, D. Pintea, J. Dotreppe, Considering the effects of localised fires in the numerical analysis of a building structure, Fire Safety Journal 42 (6) (2007) 473–481.

[104] D. Gawin, F. Pesavento, B. Schrefler, Modelling of hygro-thermal behaviour of concrete at high temperature with thermo-chemical and mechanical material degradation, Computer methods in applied mechanics and engineering 192 (13) (2003) 1731–1771.

[105] `https://www.wiki.ed.ac.uk/display/opensees/UoE+OpenSees`.

[106] C. Geuzaine, J. Remacle, Gmsh: A 3-D finite element mesh generator with built-in pre-and post-processing facilities, International Journal for Numerical Methods in Engineering 79 (11) (2009) 1309–1331.

[107] C. Geuzaine, J.-F. Remacle, Gmsh Reference Manual, for Gmsh 2.6 (2012).

[108] E. Gamma, Design patterns: elements of reusable object-oriented software, Addison-Wesley Professional, 1995.

[109] F. McKenna, OpenSees: A framework for earthquake engineering simulation, Computing in Science & Engineering 13 (4) (2011) 58–66.

[110] A. Usmani, Understanding the response of composite structures to fire, Engineering Journal, AISC 42 (2) (2005) 83.

[111] A. Usmani, S. Lamont, Key events in the structural response of a composite steel frame structure in fire, Fire and Materials 28 (2-4) (2004) 281–297.

[112] S. Lamont, A. Usmani, M. Gillie, Behaviour of a small composite steel frame structure in a long-cool and a short-hot fire, Fire Safety Journal 39 (5) (2004) 327–357.

[113] M. de Berg, O. Cheong, M. Van Kreveld, M. Overmars, Computational geometry: algorithms and applications, Springer-Verlag, 2008.

[114] S. Michael, KD tree nearest neighbor and range search, `http://www.mathworks.com/matlabcentral/fileexchange/7030-kd-tree-nearest-neighbor-and-range-search`, [Online; accessed Feb-2012] (2008).

[115] B. Kirby, The behaviour of a multi-storey steel framed building subject to fire attack-experimental data, Tech. rep., British Steel plc, Swinden Technology Centre (1998).

[116] The behaviour of multi-storey steel framed buildings in fire-a european joint research programme, Tech. rep., British Steel plc, Swinden Technology Cntre (1999).

[117] H. Carslaw, J. Jaeger, Conduction of Heat in Solids, 2nd Edition, Oxford Science Publications, Oxford University Press, London, 1959.

[118] K. Krabbenhoft, L. Damkilde, M. Nazem, An implicit mixed enthalpy–temperature method for phase-change problems, Heat and mass transfer 43 (3) (2007) 233–241.

[119] A. Nallathambi, E. Specht, A. Bertram, Computational aspects of temperature-based finite element technique for the phase-change heat conduction problem, Computational Materials Science 47 (2) (2009) 332–341.

[120] S. Lamont, A. Usmani, D. Drysdale, Heat transfer analysis of the composite slab in the Cardington frame fire tests, Fire Safety Journal 36 (8) (2001) 815–839.

[121] M. Spearpoint, Predicting the temperatures of steel members in the Cardington fire tests using the THELMA finite element model, Fire technology 37 (2) (2001) 109–128.

[122] BS EN 1994-1-2:2005. Eurocode 4: Design of composite steel and concrete structures - Part 1-2: General rules Structural fire design (2005).

[123] R. Tenchev, L. Li, J. Purkiss, Finite element analysis of coupled heat and moisture transfer in concrete subjected to fire, Numerical Heat Transfer: Part A: Applications 39 (7) (2001) 685–710.

[124] J. Franssen, Numerical determination of 3D temperature fields in steel joints, Fire and materials 28 (2-4) (2004) 63–82.

[125] J. Stern-Gottfried, G. Rein, L. Bisby, J. Torero, Experimental review of the homogeneous temperature assumption in post-flashover compartment fires, Fire Safety Journal 45 (4) (2010) 249–261.

[126] E. Ellobody, C. Bailey, Structural performance of a post-tensioned concrete floor during horizontally travelling fires, Engineering Structures 33 (6) (2011) 1908–1917.

[127] S. Lamont, B. Lane, G. Flint, A. Usmani, Behavior of structures in fire and real design-a case study, Journal of Fire Protection Engineering 16 (1) (2006) 5–35.

[128] J. Milke, V. Kodur, C. Marrioon, Appendix a: Overview of fire protection in buildings, in: World Trade Center Building Performance Study: Data

collection, preliminary observations, and recommendations, Federal Emergency Management Agency, 2002, pp. A1–A28.

[129] G. Flint, Fire induced collapse of tall buildings, Ph.D. thesis, The University of Edinburgh (2005).

[130] S. Quiel, M. Garlock, Parameters for modeling a high-rise steel building frame subject to fire, Journal of Structural Fire Engineering 1 (2) (2010) 115–134.

[131] D. Kent, R. Park, Flexural members with confined concrete, Journal of the Structural Division 97 (7) (1971) 1969–1990.

[132] H. Hilber, T. Hughes, R. Taylor, Improved numerical dissipation for time integration algorithms in structural dynamics, Earthquake Engineering & Structural Dynamics 5 (3) (1977) 283–292.

[133] M. Garlock, S. Quiel, Plastic axial load and moment interaction curves for fire-exposed steel sections with thermal gradients, Journal of structural engineering 134 (6) (2008) 874–880.

[134] J. Rotter, A. Sanad, A. Usmani, M. Gillie, Structural performance of redundant structures under local fires, in: InterFlam 1999: 8th International Fire Science & Engineering Conference, Vol. 99, 1999, pp. 1069–1080.

[135] T. Lin, Y. Yang, C. Huang, Inelastic nonlinear behavior of steel trusses cooled down from a heating stage, International Journal of Mechanical Sciences 52 (7) (2010) 982–992.

[136] Y. Wang, P. Chatterjee, J. de Ris, Large eddy simulation of fire plumes, Proceedings of the Combustion Institute 33 (2) (2011) 2473–2480.

[137] Z. Chen, J. Wen, B. Xu, S. Dembele, Large eddy simulation of fire dynamics with the improved eddy dissipation concept, in: IAFSS 2011: 10th International Symposium on Fire Safety Science, 2011, pp. 795–808.

[138] G. Maragkos, P. Rauwoens, B. Merci, Application of FDS and FireFOAM in large eddy simulations of a turbulent buoyant helium plume, Combustion Science and Technology 184 (7-8) (2012) 1108–1120.

[139] M. Aksit, P. Mackie, P. Rubini, Coupled radiative heat transfer and flame spread simulation in a compartment, in: Proceedings of the 3rd International seminar on Fire and Explosion Hazards, Windermere, UK, 2000.

[140] C. M. Gutierrez, M. OŃeill, W. Jeffrey, Final report on the collapse of the World Trade Center Towers, Tech. Rep. NIST NCSTAR 1, National Institute of Standards and Technology, US Department of Commerce (2005).

[141] R. Almeida, E. Macau, Stochastic cellular automata model for wildland fire spread dynamics, in: Journal of Physics: Conference Series, Vol. 285, IOP Publishing, 2011, pp. 1–9.

[142] H. Cheng, G. Hadjisophocleous, Dynamic modeling of fire spread in building, Fire Safety Journal 46 (4) (2011) 211–224.

[143] G. Ramachandran, Stochastic models of fire growth, in: The SFPE Handbook of Fire Protection Engineering, 3rd Edition, National Fire Protection Association, 2002, Ch. 3-15, pp. 381–401.

Appendix A

Interface for GmshBuilder class

GmshBuilder is a subclass of ***HTModelBuilder***, and it is provided to aid the creation of a complicated finite element model in a more efficient manner. The **GmshBuilder** object first reads mesh information generated by Gmsh (a powerful finite element mesh generator) and then creates the finite element components according to the mesh and adds them to the heat transfer domain. Methods are provided to specify different types of boundary conditions on the finite element model. The interface of this class is shown below.

```
class GmshBuilder : public HTModelBuilder
{
  public:
  //associate GmshBuilder with HeatTransferDomain and link it
  //with the file containing mesh information generated by Gmsh
  GmshBuilder(HeatTransferDomain& theDomain, const char* filename);
  ~GmshBuilder();

  //read mesh information, create finite element objects
  //(HeatTransferElements, HeatTransferNodes, etc.) and add them
  //into the HeatTransferDomain
  int BuildModel(void);

  //impose the same convection boundary conditions for all the
```

```
15  //boundaries
16  int setConvectionBC(double h, double Tf);
17  //impose convection boundary condition for boundaries with a
18  //specified tag
19  int setConvectionBC(double h, double Tf, int tag);
20
21  //impose the same radiation boundary conditions for all the
22  //boundaries
23  int setRadiationBC(double epsilon, double sigma, double alpha,
        double qir);
24  //impose radiation boundary condition for boundaries with a
25  //specified tag
26  int setRadiationBC(double epsilon, double sigma, double alpha,
        double qir, int tag);
27
28  int setDirichletBC(double T, int tag);
29
30  //set boundary conditions generated by parametric fires
31  //as given in EC 1
32  int setParametricFireConvcBC(ParametricFireEC1*  themodel, double
        h, int tag);
33
34  int setParametricFireRadBC(ParametricFireEC1*  themodel, double
        epsilon, double sigma, double alpha, int tag);
35
36  //set boundary conditions generated by the Hasemi localised
37  //fires as given in EC 1
38  int setLocalisedFireBC(double crd1, double crd2, double crd3,
        double D, double Q, double H, int centerLineTag, int tag);
39
40  //set user defined transient boundary conditions
41  int setUDFFireConvcBC(UserDefinedFire* themodel, double h, int tag
        );
42  int setUDFFireRadBC(UserDefinedFire* themodel, double epsilon,
        double sigma, double alpha, int tag);
43  int setUDFFlux(UserDefinedFire* themodel, int tag);
44
45  //set boundary conditions by Alpert ceiling jet
46  //model (localised fire)
47  int setAlpertFireConvcBC(AlpertCeilingJetModel* themodel, double h
        , int tag);
48  int setAlpertFireRadBC(AlpertCeilingJetModel* themodel, double
        epsilon, double sigma, double alpha, int tag);
49
50  //set boundary conditions generated by the linearly travelling
51  //fire methodology propsoed by Rein and Stern-Gottfried
52  int setLinearTravellingFireBC(AlpertCeilingJetModel* themodel,
        double pos1, double pos2, double Lmax, double h, double Ta,
        double Tf, double epsilon, double sigma, double alpha, int
        DirectionFlag, int tag);
53
54  int createBoundaryPattern(void);
55  int createFireImposedPattern(FireModel* themodel);
56  void removePattern(int tag);
57
```

```
58   protected:
59
60   private:
61
62   int** PhysicalID;
63   int** ConnectivityBC;
64   int** ConnectivityDomain;
65   int** BoundaryEleID;
66   int numFluxBC;
67   int numPatterns, numNearFieldPattern, numFarFieldPattern;
68   int TotalElements, NumBoundaryEle, NumDomainEle, NUMPhysicalNames;
69   const char* fileName;
70   bool travellingStamp, TravelStop;
71 };
```

Appendix B

Heat transfer analysis classes

Heat transfer classes implement the non-linear solution algorithms, and they operate on the finite element components held in the **HeatTransferDomain** to render solutions of a heat transfer problem. Relationships between classes are shown in Fig. B.1 using the UML notations.

HT_TransientAnalysis is a subclass inheriting from ***HeatTransferAnalysis*** class and its instance is associated with several objects of other classes to perform a transient analysis. The architecture of this analysis system is essentially the same as that of OpenSees. A **HT_DOF_Number** object employing algorithms based on graph theory numbers all the degrees-of-freedom in the domain with the aim of reducing the bandwidth of the tangent matrix. A **HT_DOF_Group** object keeps a reference to a **HeatTransferNode** object in the domain and deals with the mapping between degrees-of-freedom and global equation numbers. Similarly, a **HT_FE_Element** is linked to a ***HeatTransferElement*** in the domain

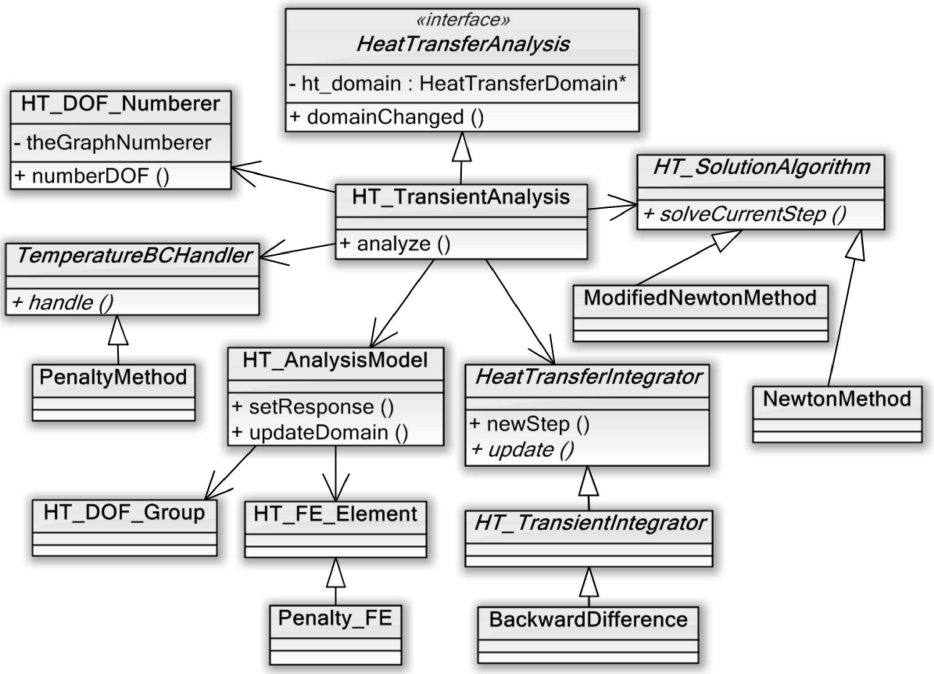

Figure B.1: Heat transfer analysis classes for performing the solution algorithms

and it provides methods to set and retrieve equation numbers for degrees-of-freedom relevant to that element. It also provides methods to return elemental residual vectors and tangent stiffness matrices. A **HT_AnalysisModel** holds all the **HT_DOF_Group**s and **HT_FE_Element**s in an analysis and also provides methods to update the state of the domain. ***HeatTransferIntegrator*** class provides methods to assemble the system of equations by adding elemental contributions. Subclasses of ***HT_TransientIngetrator*** provide methods to set the solution predictor and updater for a transient problem. **BackwardDifference** implements the time-integration algorithm shown in Eq. (2.23) with α being set one, which removes the need of computing initial temperature derivatives of the system. ***TemperatureBCHandler*** is an abstract class, which provides interfaces for imposing the Dirichlet boundary condition on the global system of equations. Its subclasses provide the implementation details, such as using

penalty method. ***HT_SolutionAlgorithm*** implements the algorithms such as the Newton-Raphson method to solve the non-linear system of equations. Using these classes in conjunction with the existing solver classes in OpenSees, stand-alone executable applications can be produced to address general heat conduction problems. In addition, it is also possible to integrate these classes into the main application of OpenSees and allows users to run heat transfer analyses with scripting languages such as Tcl.

Appendix C

A list of classes for the thermal analysis framework

Table C.1: A complete list of classes developed/modified for the thermal analysis framework in OpenSees

Classification	Class name	Modified from	Brief description
Domain	HeatTransferDomain	Domain	For holding all the FE components
Element	HeatTransferElement	Element	Abstract class
	QuadFour	\	2D four-noded quad
	QuadEdight	\	2D eight-noded quad
	BrickEight	\	3D eithg-noded brick
Node	HeatTransferNode	Node	Store temperatures
Temperature BC	TemperatureBC	SP_Constraint	Specify temperature boundary conditions
Flux BC	HeatFluxBC	\	Abstract class
	Radiation	\	Specify radiation boundary conditions
	Convection	\	Specify convection boundary conditions
	PrescirbedSurfFlux	\	Specify net heat flux values
Pattern	BoundaryPattern	LoadPattern	Define transient behaviour of boundary conditions
	FireImposedPattern	\	Define fire imposed transient boundary conditions
Material	HeatTransferMaterial	\	Abstract class
	CarbonSteelEC3	\	Provide temperature dependent material properties for steel as given by EC 3
	NWConcreteEC2	\	Provide temperature dependent material properties for normal weight concrete as given by EC 2
	LWConcreteEC4	\	Provide temperature dependent material properties for light weight concrete as given by EC 4
	SteelASCE	\	Provide temperature dependent material properties for steel given by ASCE manual
	SimpleMaterial	\	Accept user given material infomation

Continued from Table C.1

Classification	Class name	Modified from	Brief description
Fire models	FireModel	\	Abstract class
	ParametricFireEC1	\	Define parametric fires as given in EC 1
	StandardFiresEC1	\	Define standard fires as given in EC 1
	AlpertCeilingJetModel	\	Define localised fires using Alpert ceiling jet model
	HasemiLocalisedFireEC1	\	Define localised fires using Hasemi model
	UserDefinedFire	\	Provide user defined fire boundary conditions (with either temperature or flux)
Analysis	HeatTransferAnalysis	Analysis	Abstract class
	HT_TransientAnalysis	TransientAnalysis	\
	HT_AnalysisModel	AnalysisModel	\
	HT_DOF_Group	DOF_Group	\
	HT_FE_Element	FE_Element	\
	Penalty_FE	PenaltySP_FE	\
	HeatTransferIntegrator	IncrementalIntegrator	Assemble global system of equations, specify time integration schemes etc.
	HT_TransientIntegrator	TransientIntegrator	
	BackwardDifference	\	
	HT_DOF_Numberer	DOF_Numberer	\
	HT_ConvergenceTest	ConvergenceTest	\
	CTestNormTempIncr	CTestNormDispIncr	\
	CTestNormResidual	CTestNormUnbalance	\

Continued from Table C.1

Classification	Class name	Modified from	Brief description
Analysis	HT_SolutionAlgorithm	SolutionAlgorithm	\
	LinearAlgorithm	Linear	\
	NewtonMethod	NewtonRaphson	\
	ModifiedNewtonMethod	ModifiedNewton	\
	HT_FE_EleIter	FE_EleIter	\
	HT_DOF_GrpIter	DOF_GrpIter	\
	TemperatureBCHandler	ConstraintHandler	Enforce temperature BCs in the system of equations
	PenaltyBC_Handler	PenaltyConstraintHandler	
Model builder	HTModelBuilder	ModelBuilder	Abstract class
	GmshBuilder	\	Read Gmsh mesh information and create objects for the finite element model
Recorder	HTRecorder	Recorder	Record nodal temperatures
Interface class	HTSTRCInterface	\	Prepare temperature data for structural analysis
Iterators	AllTempBCIter	SingleDomAllSP_Iter	Low level classes for accessing components in the HeatTransferDomain
	BoundaryPatternIter	LoadPatternIter	
	HeatFluxBCIter	HeatFluxBCIter	
	HT_ElementIter	ElementalLoadIter	
	HT_NodeIter	NodeIter	
	TempBCIter	SP_ConstraintIter	